DEFECT ENERGETICS IN THE ALLOY SEMICONDUCTORS

A Thesis Submitted
in Partial Fulfilment of the Requirements
for the Degree of

DOCTOR OF PHILOSOPHY

by
AMITA DAS

to the

DEPARTMENT OF PHYSICS

INDIAN INSTITUTE OF TECHNOLOGY KANPUR

FEBRUARY 1990

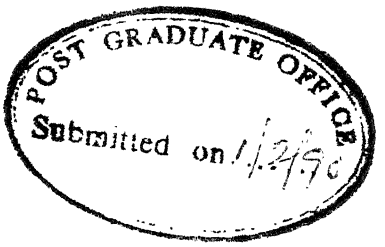

CERTIFICATE

Certified that the work contained in this thesis entitled " **DEFECT ENERGETICS IN THE ALLOY SEMICONDUCTORS** " has been carried out by Ms Amita Das under my supervision and the same has not been submitted elsewhere for a degree.

Vijay Singh

(DR VIJAY A.SINGH

THESIS SUPERVISO

Kanpur

February 1, 1990

ACKNOWLEDGEMENT

I would like to express my deep sense of gratitude towards my thesis supervisor Dr Vijay A.Singh for his very patient and fruitful guidance during the course of my research work. I thank him for introducing me to the rich field of Disordered Systems and also for suggesting the thesis problem. Despite his very busy schedule, he was always willing to spare from his precious and restricted time and to share his rich and varied knowledge with me.

I feel greatly indebted to him, my thesis supervisor , as also to all those able and dedicated teachers, who taught me Physics with great clarity and helpful understanding, creating in me an abiding interest for the subject which ultimately resulted in the urge to explore the frontiers of Physics. Their lectures and my discussions with them will always remain vivid in my memory.

I also thank Dr Vijay A.Singh, Hajra, Shiuli and Kanika for helping me with the painstaking work of proof reading.

Amita Das

CONTENTS

CONTENTS

SYNOPSIS

"DEFECT ENERGETICS IN THE ALLOY SEMICONDUCTORS"

A Thesis Submitted

in Partial Fulfilment of the Requirements

For the degree of

DOCTOR OF PHILOSOPHY

by

AMITA DAS

to the

Department of Physics

Indian Institute of Technology - Kanpur

January 12, 1990

The alloy semiconductors are extensively employed in various electronic devices. They offer a possibility of engineering the material parameters of a semiconductor, notably the band gap and the electron mobility.

Point defects however are invariably present in such semiconductors. These defects could be native: vacancy and anti-site; or foreign: donor, acceptor, transition metal atom etc. In some cases they are responsible for device degradation whereas

in others they are deliberately introduced to serve a specific objective.

The main thrust of this thesis is the study of defect energetics in III-V alloy semiconductors. The alloy semiconductors (e.g. $Ga_{1-x}Al_xAs$ or Si_xGe_{1-x}) are substitutionally disordered and may be viewed as a generalization of the ordered III-V (e.g. GaAs) or group IV (e.g. Si) semiconductors. We concern ourselves with developing a formalism for defect energetics in such disordered hosts as well as conducting calculations for some typically important defect centers. It is possible to specialize the framework we develop to study defect energetics in ordered semiconductors. In a few instances we take advantage of this flexibility and calculate and comment on defect centers in Si and GaAs. Equally significant is the issue whether interpretation and analysis of experiments for ordered systems can be extended to alloy and other disordered semiconductors in an unmodified fashion. We address this issue in the context of Deep Level Transient Spectroscopy (DLTS). We also discuss a complementary technique : Paired Temperature Spectroscopy (PATS).

As noted earliar, the host system $Ga_{1-x}Al_xAs$ for instance, is substitutionally disordered with the cation site being randomly occupied by Ga or Al atom. We employ the sophisticated Coherent Potential approximation (CPA) to describe the host electronic structure: We present examples of the CPA in a classical context. A new derivation of the Weiss molecular field result is presented[1].

A deep level in the forbidden gap of a semiconductor may arise in the presence of a point defect. We present model single band Hamiltonians. We analyse the scalar version of the Koster Slater equation which serves to locate the deep level. Further, with the help of the Hellmann - Feynman theorem we calculate total energy changes due to the presence of point defects[2].

We develop an approximate version of CPA for the realistic multiband systems. This enables us to make quantitative predictions for defects in several alloy semiconductors and in particular we discuss a donor related level in $Ga_{1-x}Al_xAs$ (DX center)[3]. In our calculations we have viewed this defect as a simple donor, which gives rise to a deep level on account of the disorder in the host structure. Our results compare well with the experiments.

We have also studied helium like impurities (impurities having two excess valence electrons than the host) in the context of Effective Mass Theory (EMT). The chemical shift of the level has been obtained by introducing a cavity. Inside the cavity the excess electrons behave as in free atoms; outside, the semiconductor matrix dominates. We apply this formalism to a number of defects (i) chalcogen impurities in silicon (ii) DX center viewed as a negatively charged donor (iii) EL2 center in GaAs viewed as an anti-site defect. Our results are in considerable agreement with the experiments[4].

Finally, we have concentrated on the analysis of experiments

such as Deep Level Transient Spectroscopy (DLTS) and Paired Temperature Spectroscopy (PATS). These are used extensively for the determination of activation energies of the defect levels. We point out that the expression used to get the value of activation energy is valid only for ordered systems. This might result in a systematic discrepancy between the actual and the extracted value of the activation energy[5,6]. We have also focussed on the effect of disorder on the M-center, a metastable defect in InP and its alloys[7].

References

1. "Simple Illustrations of the Coherent Potential Approximation". Amita Das and Vijay A. Singh. Submitted Am.J.Phys (1990).

2. "Electronic Structure of Defects in the Alloy Semiconductors: The Weak Scattering Approximation". Amita Das, Kajoli Banerjee and Vijay A.Singh. Submitted Journal of Physics: Condensed Matter (1990).

3. "DX Center: A Coherent Potential Approximation Based Approach". Amita Das and Vijay A.Singh. Submitted Phys. Rev. B (1990).

4. "Many Electron Effects in the Effective Mass Theory for Helium like Impurities". Amita Das and Vijay A. Singh. Submitted J.Appl. Phys (1990).

5."Deep Level Transient Spectroscopy (DLTS) Analysis of Defect Levels in Semiconductor Alloys". Amita Das, Vijay A. Singh and D.V. Lang. Semicond. Sci. Technol 3 1177-1183 (1988).

6. "Paired Temperature Spectroscopy: A Novel Method to Characterize Traps in Semiconductors". Raj.K.Singh, Vijay A.Singh, James W. Corbett and Amita Das. J.Phys.C: Solid State Phys 19 2177-2187 (1986).

7. "Transient Spectroscopy and Disorder". Vijay A.Singh and Amita Das. Radiation effects (1989).

CHAPTER 1 : INTRODUCTION

1.1: Preliminary remarks

Semiconductors play an important role in technology. There exists a great variety of them ranging from elemental to alloy and even amorphous semiconductors. Members of the group IV in the periodic table, like Ge and Si are semiconductors. The elemental semiconductors have been known for some time and are well studied.

The compound semiconductors offer a wider choice of materials with differing characteristics such as band gap, lattice parameter, electron mobility etc. The popular compound semiconductors are the III - V or II - VI types. These are the compounds of elements of group III and V (for example GaAs) and group II and VI (for example CdTe) respectively. The relationship between the band gap and the lattice parameter of some of these compounds is presented in figure 1.1 .

The alloys of the above mentioned elemental and compound semiconductors also have semiconducting properties and are known as alloy semiconductors. Similar to the compound semiconductors, the alloy semiconductors can also be classified on the basis of the periodic table: the III-V alloys ($Ga_{1-x}Al_xAs$, $Ga_{1-x}In_xAs_{1-y}P_y$), the II-VI alloys ($Hg_{1-x}Cd_xTe$) and the group IV alloys ($Si_{1-x}Ge_x$). Another mode of characterising them is by the

presence of the number of constituents: binary ($Si_{1-x}Ge_x$), ternary ($Ga_{1-x}Al_xAs$), and quaternary ($Ga_{1-x}In_xAs_{1-y}P_y$) alloys. These alloys offer an opportunity of engineering several material parameters, the magnitude of the fundamental gap being one of them. It is possible to tune the band gap of an alloy semiconductor by varying the concentration of its components. As shown in figure 1.1 the band gap of AlAs is 2.2 eV and that of GaAs is about 1.5 eV. By varying x, the concentration of Al in $Ga_{1-x}Al_xAs$ one can in principle tune the band gap from 1.5 eV to 2.2 eV. Moreover, unlike amorphous semiconductors (e.g. a-Si:H), where it is very difficult to control and regulate the content of hydrogen, in these alloys the concentration and the distribution of the alloying species can be precisely controlled by using sophisticated growth techniques.

These materials find widespread applications in various optoelectronic devices. $GaAs_{1-x}P_x$ is used in light emitting diodes, $Ga_{1-x}Al_xAs$ in heterojunction lasers and $Hg_{1-x}Cd_xTe$ in infra red detectors. Further the improvement in growth techniques such as MBE (molecular beam epitaxy) or MOCVD (metallorganic chemical vapour deposition) during the last decade has made it possible to grow these alloys into superlattices and quantum structures. Such structures are important both technologically and from the point of view of physics. These structures consist of alternating thin layers of different semiconducting materials. The material with large band gap acts as a quantum barrier. The height

of the barrier can be monitored with the help of alloy semiconductors. Thus, these structures lead one to probe the quantum regime experimentally.

The main problem which is encountered in growing high quality heterojunctions and superlattices is that the materials of the various layers should be properly lattice matched to avoid strain in the structure. This severely constrains the choice as can be seen from figure 1.1 . Except for the pairs GaAs and AlAs, and GaSb and AlSb, for all other pairs of compounds the lattice parameter is very poorly matched. Hence the importance of alloys like $Ga_{1-x}Al_xAs$ and $Ga_{1-x}Al_xSb$ which are free from the strains of lattice mismatch, cannot be overemphasized.

The primary thrust of this thesis is the study of point defects in III - V alloy semiconductors. The alloy semiconductor may be regarded as a substitutionally disordered system to a good approximation. For example, $Ga_{0.75}Al_{0.25}As$ posseses an underlying Zinc blende structure. The anion sites are occupied by As atoms while each four-fold coordinated As atom is surrounded on an average by one Al and three Ga atoms. One can obtain the electronic structure by employing a suitable mean field theory for disordered systems. Some of these theories are the Virtual Crystal Approximation (VCA) and the Coherent Potential Approximation (CPA) In section 1.2 we explain the central idea behind the CPA with two simple classical examples.

The presence of point defects in these alloy semiconductors

give rise to very interesting and puzzling physical features, metastability and negative U behaviour are some of these. DX center and some other defects have been discussed in detail in subsequent chapters. Further, unlike amorphous semiconductors, these alloy semiconductors provide a possibility of a controlled study of defect in a disordered host.

From the technological point of view the presence of defects play a crucial role. They are responsible for device degradation (e.g. the dark line defect in the light emitting diodes made of $Ga_{1-x}As_xP$). Point defects in semiconductors also give rise to a deep trap inside the forbidden band gap. These deep traps are important because they act as recombination centers and control the lifetimes of carriers in luminescent devices. They are used to increase the probability of radiative electron hole recombination in light emitting diodes in order to increase the intensity of emitted light. This necessitates that the defect which causes the deep trap must be identified so that measures could be taken to control its concentration in the semiconductor host.

The defect level due to an impurity has been obtained via the Koster-Slater equation in our calculations. In section 1.3 of this chapter we illustrate this formalism by considering a simple example. Section 1.4 contains a preview of the various chapters of this thesis.

1.2 The Coherent Potential Approximation (CPA)

In subsequent chapters we have used the sophisticated Coherent Potential Approximation (CPA) for the description of the disordered (alloy) host. The CPA was introduced in condensed matter physics exactly two decades ago by Paul Soven[1] and David Taylor[2]. Its genesis can be traced back to the last century . A similar methodology was employed by Bruggeman in the 1930's to understand the conductivity of a random mixture of two metals. Soven proposed it as a scheme to understand the electronic structure of random binary metal alloys, while Taylor carried out a similar program for phonons. Since then the random systems have been widely studied and the CPA philosophy has been applied extensively to study all types of elementary excitations e.g. excitons[3], magnons etc.

The objective of the CPA is to provide a description of the average properties of a random mixture. The CPA formalism can be well illustrated by considering two simple classical problems[4].

Let us consider a linear system of 'N' springs, 'N_1' springs of stiffness K_1 each and 'N_2' springs of stiffness K_2 each ($N = N_1+N_2$). Let us assume that such a random system can be truly represented by another linear system of N springs with, stiffness K_{eff} for each spring, as shown in figure 1.2a. The objective of any mean field theory is to express K_{eff} in terms of stiffness of two types of springs K_1, K_2 and their concentration N_1/N and N_2/N respectively. One choice for K_{eff} could be

$$K_{eff} = (N_1/N) K_1 + (N_2/N) K_2 \qquad (1.1)$$

This is known as Virtual Crystal Approximation (VCA) and can be compared to Vegard's law (where the bond length of an alloy is set equal to the sum of individual bond lengths weighted by the concentration of each of its components). Expression (1.1) holds only in restricted cases. Here it holds when K_1 approaches K_2.

Let us suppose that each of the effective springs stretch by an amount x when a tensile force 'F' is applied to the system. Thus

$$x = |F| / K_{eff} \qquad (1.2)$$

or

$$N x = N |F| / K_{eff} \qquad (1.3)$$

Here 'N x' is the total extension of the system and K_{eff} / N is the stiffness of the entire system.

Now we perform a CPA gedanken. We replace one of the effective springs by the first type of spring (figure 1.2b). Let x_1 be the extension of this spring when a force F is applied to it. Hence

$$x_1 = |F| / K_1 \qquad (1.4)$$

In this series combination of springs we notice that the tension is uniform throughout and so the total extension is the sum of individual extensions of each spring when the same force is applied to each of them separately. Thus, the total extension in this case will be

$$X_1 = (N - 1)\, x + x_1 \qquad (1.5)$$

Substituting for x and x_1 from equation (1.2) and (1.4) we get

$$X_1 = (N - 1)|F|/ K_{eff} + |F|/ K_1 \qquad (1.6)$$

We repeat the gedanken with the second type of spring (figure 1.2c). In this case the total extension will be

$$X_2 = (N - 1)|F|/ K_{eff} + |F|/ K_2 \qquad (1.7)$$

If springs of stiffness K_{eff} are a true representation of the collection of these springs, then the average of the extensions X_1 and X_2 should be equal to the total extension of the effective system.

$$N_1X_1/ N + N_2X_2/ N = Nx \qquad (1.8)$$

Substituting for X_1, X_2 and x from the above equations and

simplifying we get the following equation

$$1 / K_{eff} = (N_1/N)\ 1/K_1 + (N_2/N)\ 1/K_2 \qquad (1.9)$$

In the light of the above problem one sees that unlike VCA (where the effective value of a physical parameter is set equal to the arithmetic mean of its components), in CPA one first seeks a physical parameter which is additive. In the above problem, extension by a given force is such a parameter. The effective value of this new parameter (extension) is set equal to the arithmetic mean of its components (equation (1.8)). Knowing the functional dependence of the earlier parameter (spring constant in this case) on this new parameter (extension) one gets the required relation (equation (1.9)). Note that for the parallel combination of springs, extension for each spring is same and the total force applied for a given extension (say unity) is the sum of the forces applied to each spring separately to obtain the same (unit) extension. Thus, the force per unit extension which is nothing but the spring constant, is itself an additive parameter. Hence for this arrangement both CPA and VCA give identical results.

In the above gedanken the substitution of any number of sites at any location will yield identical results. It is, however, not so easy to find such a local additive parameter for every problem.

For problems relating to binary alloys, a similar procedure of replacing them with an effectively ordered structure is

employed. In the single site CPA one site of this effectively ordered structure is removed and replaced by one type of atom. This replacement is treated as an impurity in an ordered medium. The scattering matrix T is evaluated for this new system. In this case the scattering matrix T is additive. Hence the average of this matrix over all possible types of insertions is equated to zero. That yields the CPA equation. It is, however, observed that in this case the results obtained depend on the number of sites replaced. The transfer matrix T depends on the environment and it is not a local property of a particular atom at a particular site. This illustrates the approximate nature of the theory.

The application of the CPA formalism is not constrained to treating alloys and mixtures alone, it can also be applied to yield good approximations to many other physical problems.

Consider the case of Ising spins. The Hamiltonian for this system is given by the equation

$$H = - J \sum_{i \neq j}^{n.n} \sigma_i \sigma_j$$

$$J > 0$$

Let 'm' be the average magnetisation per site for this system. In the Braggs William Approximation the magnetisation 'm' per site is given by the equation

$$m = \tanh \beta J z m$$

where z is the number of nearest neighbours, J is the coupling constant and β is the inverse temperature.

The same expression can be derived in a much simpler way using the concepts of CPA. At a particular temperature some of the spins point up and others point down randomly (figure 1.3a). We substitute this random system by an effective ordered structure where the magnetisation at each site is 'm'(figure 1.3b). Now we focus on a particular site. We replace this site first by an up spin and then by a down spin (figure 1.3c). The change in energy of the two system in these two cases will be

$$\Delta E_{up} = Jzm^2 - Jzm$$
$$\Delta E_{down} = Jzm^2 + Jzm$$

But a spin at a particular site can point up or down with a Boltzmann probability. Hence the thermal average of the change in energy should be zero. So

$$\frac{-\exp(\beta Jzm(1-m))Jzm(1-m) + \exp(-\beta Jzm(1+m))Jzm(1+m)}{\exp(\beta Jzm(1-m)) + \exp(-\beta Jzm(1+m))} = 0$$

The denominator does not blow up because the magnetisation 'm' is finite and we are seeking solutions at non zero temperatures.

Hence the numerator can be equated to zero, which yields

$$(1+m)/(1-m) = \exp(2\beta Jzm)$$

or

$$m = \tanh \beta Jzm$$

which is the same as the Braggs William Approximation.

1.3: Koster Slater Equation

We have mentioned in section 1.1 of this chapter that the deep traps in semiconductors are identified with the help of Koster-Slater equation[5]. This is a determinantal equation:

$$|| \; 1 - \bar{G}_h(E_d) \; \bar{V} \; || = 0$$

Here $\bar{G}_h$ is the host Green's function operator. The impurity potential operator is 'V'. E_d serves to locate the defect level. In general the operators $\bar{V}$ and $\bar{G}_h$ are matrices. In this introductory presentation we take them as scalars.

Green's function can be expressed in terms of the host density of states as follows

$$G_h(z) = \int \frac{n(z')dz'}{(z-z')}$$

where $n(z')$ is the density of states of the host medium.

The methodology of obtaining E_d can be well illustrated by considering the case of a hypothetical semiconductor whose density of states is a sum of two delta functions at energy Γ and $-\Gamma$. Thus,

$$n(z) = \delta(z + \Gamma) + \delta(z - \Gamma)$$

The delta functions at Γ and $-\Gamma$ can be identified with the conduction and the valence bands respectively. Figure 1.4 depicts sush a semicircular DOS.

To obtain the energy level due to an impurity of potential strength 'V' in such a semiconductor we proceed as follows. We first evaluate the host Green's function. Thus, in this case

$$G_h(z) = \int \frac{\delta(z'+\Gamma)dz'}{(z-z')} + \int \frac{\delta(z'-\Gamma)dz'}{(z-z')}$$

$$= 1/(z+\Gamma) + 1/(z-\Gamma)$$

$$= 2z/(z^2-\Gamma^2)$$

Now employing the Koster-Slater equation we get

$$2z/(z^2-\Gamma^2) = 1/V$$

The above equation is a quadratic function in z, the solution of which gives the location of the defect level. Thus,

$$z^2 - 2zV - \Gamma^2 = 0$$

$$E_d = z = V \pm (V^2 + \Gamma^2)^{1/2}$$

When $V << \Gamma$

$$z = V \pm \Gamma (1 + V^2/\Gamma^2)^{1/2}$$

As V approaches zero the defect level tends to $\pm \Gamma$, as is clear from the above equation. Thus as V decreases the defect level shifts towards the band edge, for V zero it coincides with the bands. When $V >> \Gamma$

$$z = V \pm V (1 + \Gamma^2/V^2)^{1/2}$$

From the above equation it is clear that as V^2 increases the term Γ^2/V^2 under the square root sign becomes negligible. Thus as V tends to infinity, from either the positive or the negative side, one of the solutions for z goes to zero, that is the level shifts towards the mid gap as $|V|$ is increased. This phenomenon is known as the pinning of the leveland is illustrated in figure 1.4. There is, however, a second solution for z in this case which is outside the gap and is not of much relevance.

1.4: Summary

The examples presented in the previous sections are intended to delineate the broad conceptual framework of this thesis. In the

following paragraphs we briefly summarize the work presented in the subsequent chapters.

In chapter 2 we present defect energetics calculations for some model disordered hosts. We have chosen two types of model hosts. One of them is the nearest neighbour one dimensional tight binding host and the other is a host that has a semicircular density of states. We have studied disorder in these model systems using CPA. We have also employed the weak scattering limit Nordheim's Correction (NC) for small disorder. The Strong Scattering Limit (SSL) has also been used for large values of the disorder parameter. The total energy changes in these systems due to a point defect has been evaluated using Hellmann Feynman theorem. The general trend of the total energy change with the defect potential is found to be the same in all the three approximations. However the saturation value of the energy change for large positive defect potential is underestimated in NC as well as in SSL as compared to CPA[6].

Chapter 3 contains an approximate form of CPA developed for realistic multiband semiconductors. One of the main results of this chapter is that both the CPA and VCA predict identical values for a vacancy related trap level.

In chapter 4 we have concentrated on a particular defect namely the DX center which is present in $Ga_{1-x}Al_xAs$. This is basically a donor related level. However since it is deep inside the gap it is believed to be a donor complex and not a simple

donor. But there is controversy regarding this assignment. The shallow to deep transition of this defect level when the Al concentration is increased beyond 20% seems to suggest that the defect could be a simple donor, and the disordered environment is responsible for its being deep. This idea has been explored in Chapter 4 by using the Coherent Potential Approximation (CPA) to account for the disorder self consistently. Our results agree with the equilibrium Hall measurement[7].

In Chapter 5 we have developed a formalism for helium like impurities (the defect atom has two valence electron more than the host atom) in the semiconductor matrix. The chemical shift of the impurity atom has been taken into account by considering the impurity to be inside a cavity of radius r_o. The influence of the impurity within this cavity is unscreened by the medium. We have applied this theory to study several classes of defects[8] e.g. (i) chalcogen impurities in silicon (ii) anti-site defect in III-V semiconductors (a popular model for EL2 in GaAs) (iii) DX center (which is viewed by some authors as a negatively charged donor due to its EPR invisibility).

Finally, in Chapter 6 we have focussed on the analysis of experiments. In particular we have concentrated on Deep Level Transient Spectroscopy (DLTS) and Paired Temperature Spectroscopy (PATS) which are employed to find the location of the gap states in semiconductors. We point out that the analysis of the results obtained from DLTS and PATS experiments is based on an

expression which is valid for the ordered semiconductor. For disordered materials the same expression may no longer be valid, leading to a systematic discrepancy[9,10]. In chapter 6 we have also focussed on the effect of disorder on M center, a metastable defect in InP and its alloys[11].

REFERNCES

1. P.Soven, Phys. Rev.156 809 (1967).

2. D.Taylor, Phys. Rev.156 1017 (1967).

3. Onodera and Y.Toyozawa, J. Phys. Soc.24 346 (1968).

4. "Simple Illustrations of the Coherent Potential Approximation" Amita Das and Vijay a. Singh, Submitted Am.J.Phys (1990).

5. G.J.Koster and J.C.Slater, Phys. Rev. 95 1167 (1954).

6. "Electronic Structure of Defects in the Alloy Semiconductors: The Weak Scattering Approximation", Amita Das, Kajoli Banerjee and Vijay A.Singh, Submitted Journal of Physics: Condensed matter (1990).

7. "DX Center: A Coherent Potential Approximation Based Approach", Amita Das and Vijay A.Singh, Submitted Phys. Rev. B (1990).

8. "Many Electron Effects in the Effective Mass Theory for Helium Like Impurities', Amita Das and Vijay A. Singh. Submitted J.Appl. Phys (1990).

9."Deep Level Transient Spectroscopy (DLTS) Analysis of Defect Levels in Semiconductor Alloys", Amita Das, Vijay A. Singh and D.V. Lang, Semicond. Sci. Technol 3 1177-1183 (1988).

10. "Paired Temperature Spectroscopy: A Novel Method to Characterize Traps in Semiconductors", Raj.K.Singh, Vijay A.Singh, James W. Corbett and Amita Das, J.Phys.C: Solid State Phys 19 2177-2187 (1986).

11. "Transient Spectroscopy and Disorder", Vijay A.Singh and Amita Das, Radiation Effects and Defects in Solids, (1989).

FIGURE CAPTIONS

Figure 1.1: A plot of band gap vs. the lattice parameter for some typical III-V compound semiconductors.

Figure 1.2: The gedanken (thought experiment) described in section 1.2, (a) depicts a linear array of effective springs, (b) and (c) represent the act of removing one of the effective springs and replacing it by the springs of the first and the second kind respectively.

Figure 1.3: The gedanken on Ising system described in section 1.2, (a) shows the random arrangement of spins at temperature 'T', (b) shows the effective system which replaces the random arrangement of the spins, (c) depicts the act of removing one of the effective spins and replacing it by an up spin and a down spin respectively.

Figure 1.4: An idealized semiconductor DOS. Both the valence and the conduction band are represented by a δ function of equal strength. The resulting defect level is shown below.

Bandgap and Lattice Constant Values for the III-V Semiconductors

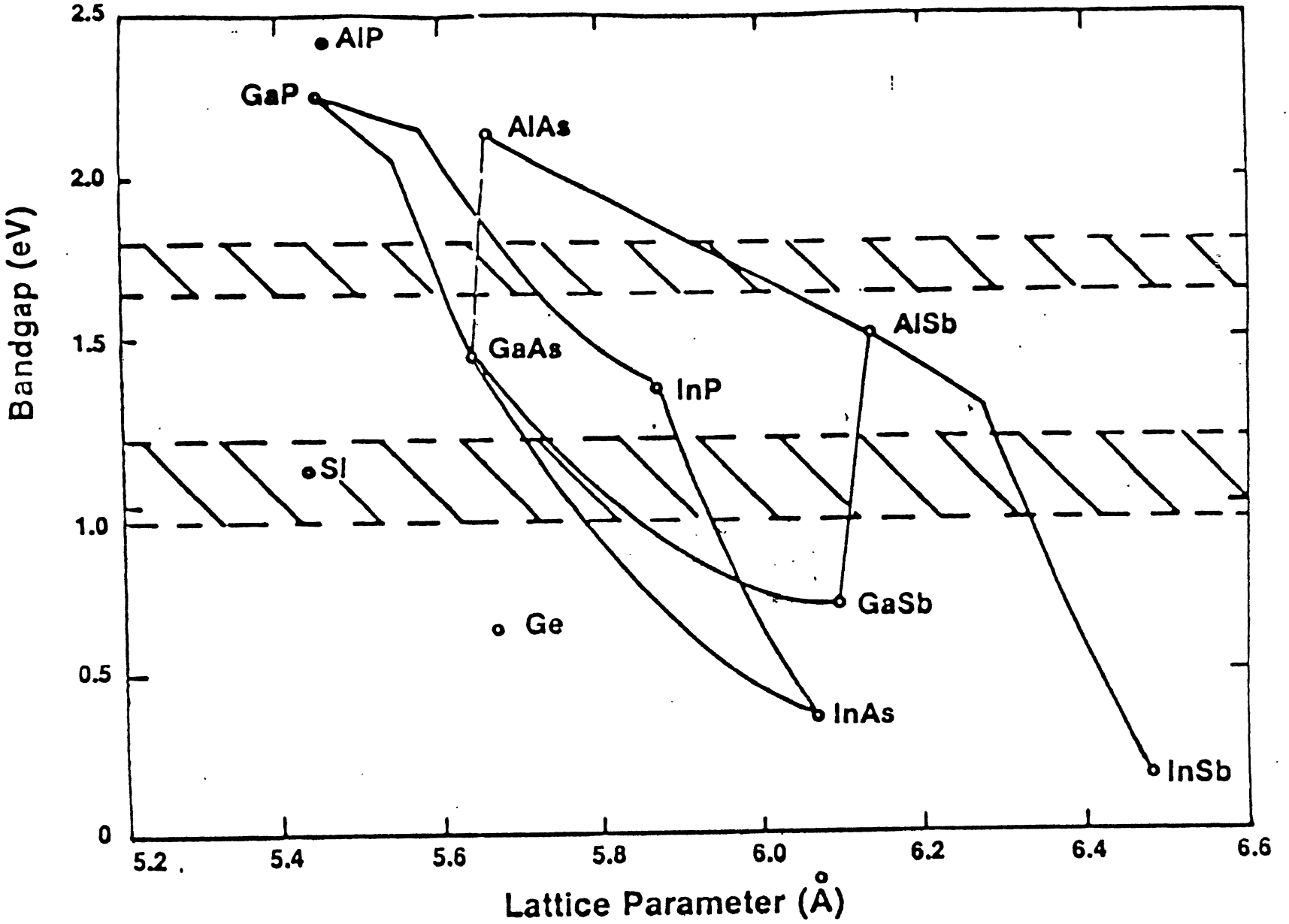

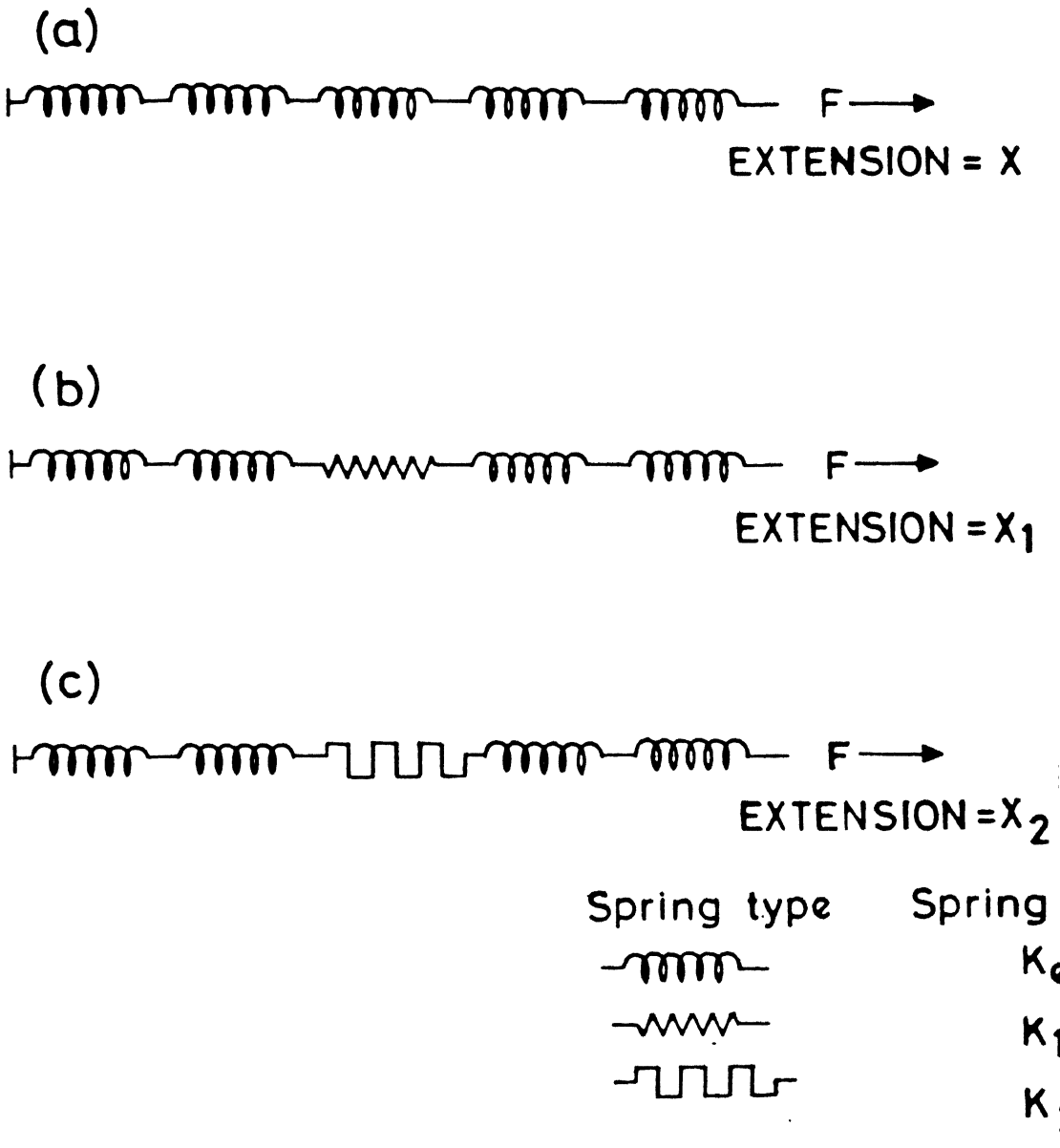
(a)
F
EXTENSION = X
(b)
F
EXTENSION = X_1
(c)
F
EXTENSION = X_2
Spring type
Spring const
K_{eff}
K_1
K_2

FIGURE 1.2

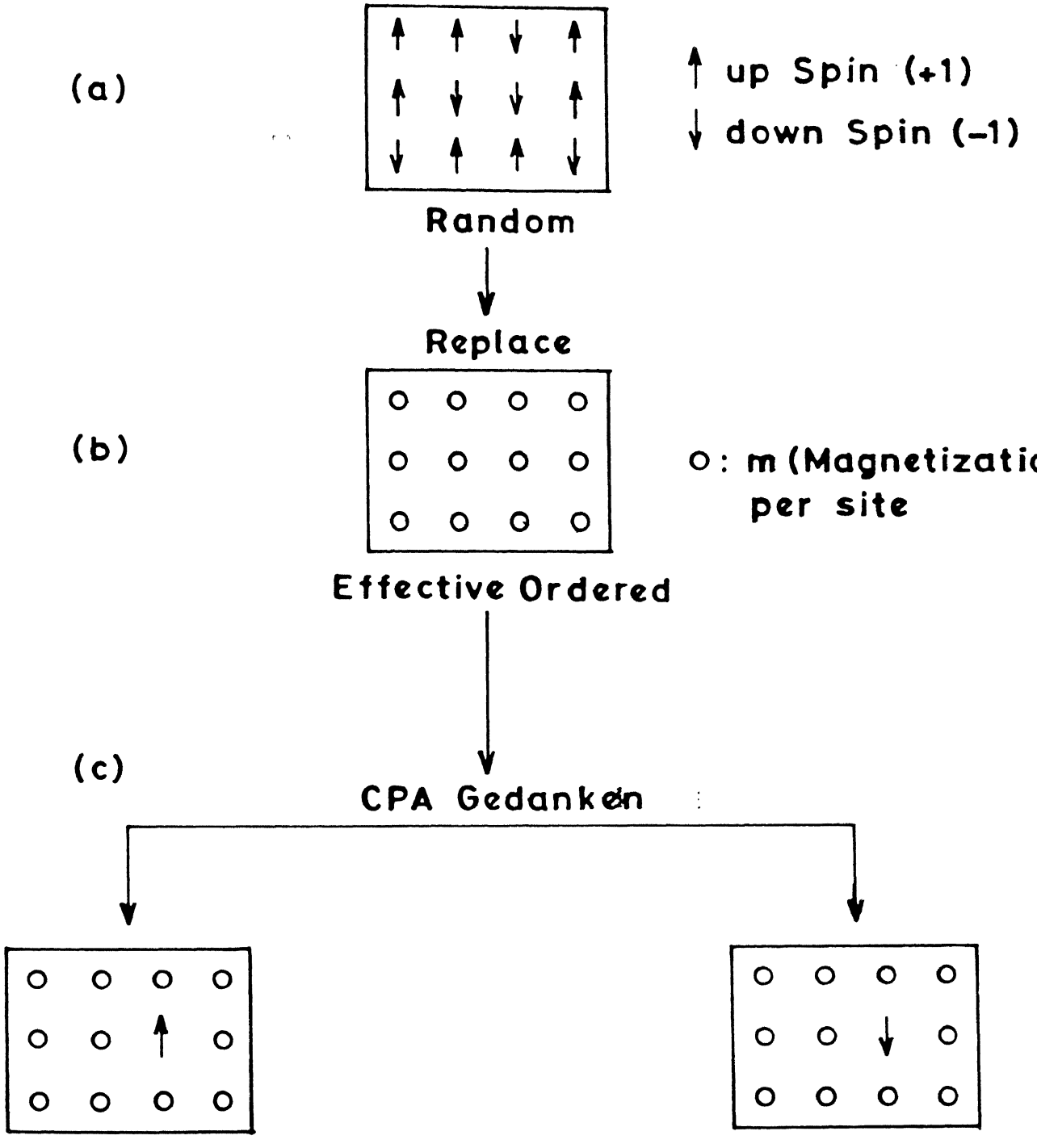
(a)
up Spin (+1)
down Spin (-1)
Random
Replace
(b)
O: m (Magnetizatio
per site
Effective Ordered
(c)
CPA Gedanken

FIGURE 1.3

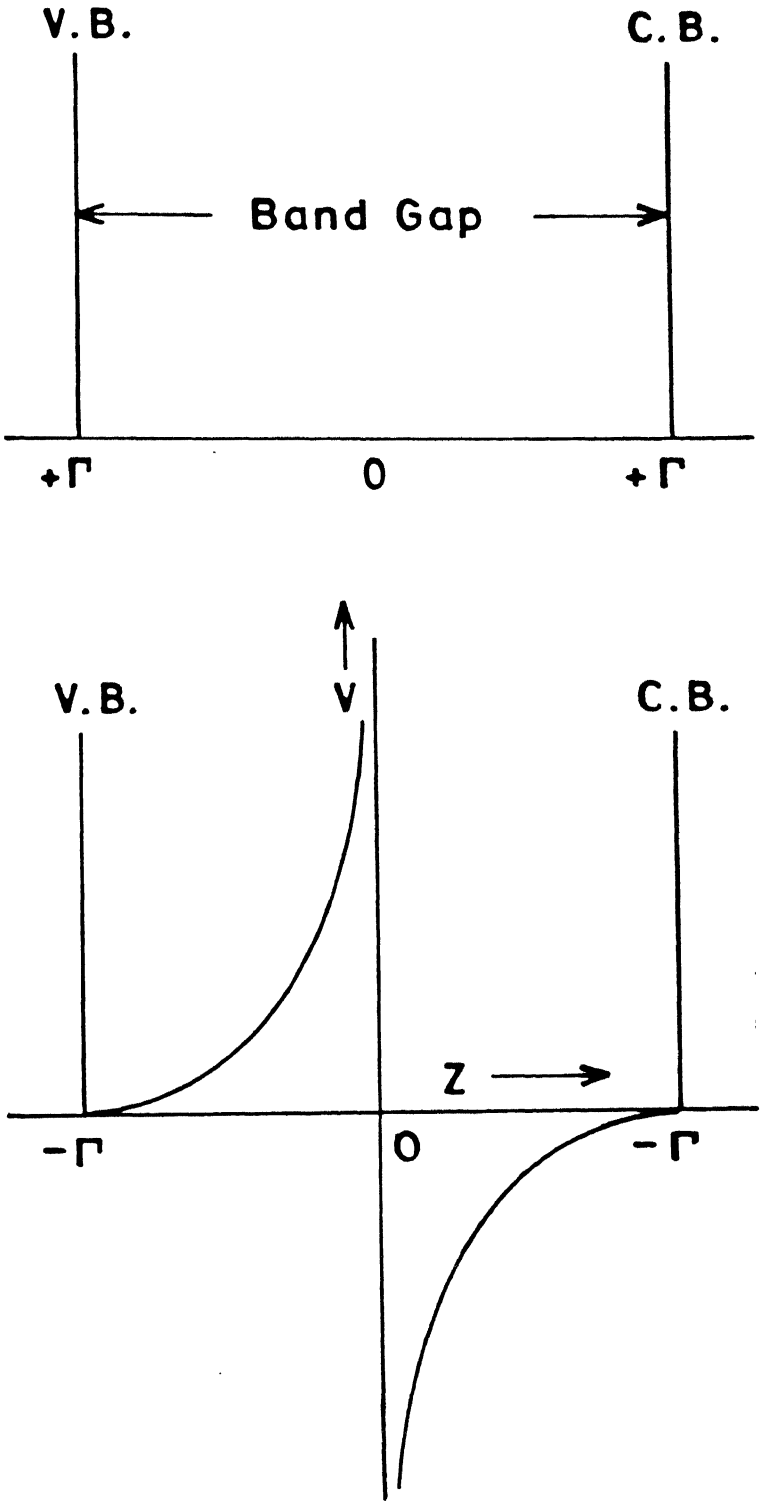

FIGURE 1.4

CHAPTER 2 : DEFECT ENERGETICS:MODEL ANALYSIS

2.1: Preliminary remarks

In this chapter we present an analysis and our results of total energy calculation using Hellmann Feynman theorem for a substitutional defect in a model disordered system. This analysis could be useful for the study of those alloys which are substitutionally disordered. A detailed description of the treatment of a realistic alloy semiconductor will be given in subsequent chapters.

The description of the host medium which is disordered, entails the use of mean field theory. There are several mean field theories. A brief recapitulation of these mean field theories could be useful in this context.

Consider a single band, orthogonal, tight binding, Hamiltonian with diagonal disorder due to the presence of two types of atoms A and B.

$$H_D = \sum_m \varepsilon_m |m\rangle \langle m| - t \sum_{m \neq n}^{n.n} |m\rangle \langle n| \qquad (2.1)$$

Here $\varepsilon_m = \varepsilon_A$ with a probability C_A

$= \varepsilon_B$ with a probability C_B

Here C_A and C_B are the concentrations of the two types of atoms.

$|m\rangle$ and $|n\rangle$ denote the Wannier states at the sites m and n respectively. The transfer term connects the nearest neighbours only.

In the mean field approximation ε_m is replaced by a renormalized self energy $\sigma(z)$, where z is the electron energy. H_D then assumes an effective ordered form.

$$\bar{H}_D = \sigma(z) \sum_m |m\rangle \langle m| - t \sum_{m \neq n}^{n.n} |m\rangle \langle n| \qquad (2.2)$$

An ordered Hamiltonian on the other hand has the form

$$H_O = \mu \sum_m |m\rangle \langle m| - t \sum_{m \neq n}^{n.n} |m\rangle \langle n| \qquad (2.3)$$

Here μ is independent of the electron energy z . Since μ is just a constant in this case, the zero of the energy can always be set such that μ is zero. Hence

$$\bar{H}_D = H_O + (\sigma(z) - \mu) \sum_m |m\rangle\langle m|$$

or

$$\bar{H}_D = H_O + \sigma(z) \sum_m |m\rangle\langle m| \qquad (2.4)$$

The diagonal part of the Green's function at the site labelled zero is

$$F_O(z) = \langle 0| \; 1 / (z - H_O) \; |0\rangle = 1/N \sum_k (1/(z - \varepsilon(k)) \qquad (2.5)$$

$$F(z) = \langle 0| \; 1/(z-H) \; |0\rangle = 1/N \sum_{k} (1/(z-\varepsilon(k)-\sigma(z)) \qquad (2.6)$$

Here $\varepsilon(k)$ is the energy eigenvalue of the ordered system. It is clear from equations (2.5) and (2.6) that the diagonal part of the ordered and disordered Green's function are related by the following equation

$$F(z) = F_{o}(z-\sigma(z)) \qquad (2.7)$$

The self energy $\sigma(z)$ is given in the various mean field approximations as follows:

(i) The Virtual Crystal Approximation (VCA): In the VCA $\sigma(z)$ is defined as the simple average

$$\sigma(z) = C_{A} \; \varepsilon_{A} + C_{B} \; \varepsilon_{B} = \bar{\varepsilon} \qquad (2.8)$$

(ii) The Coherent Potential Approximation (CPA): In the more sophisticated CPA it is obtained by the following self consistent equation

$$\sigma(z) = \bar{\varepsilon} - (\varepsilon_{A} - \sigma(z)) \; F(z) \; (\varepsilon_{B} - \sigma(z)) \qquad (2.9)$$

There are two limiting cases of CPA which are of interest to us

(a) The strong scattering limit (SSL) where

$$\sigma(z) = \bar{\varepsilon} + C_A C_B u^2 / (z-\varepsilon') \qquad (2.10)$$

Here $\varepsilon' = C_A \varepsilon_B + C_B \varepsilon_A$

& $u = (\varepsilon_A - \varepsilon_B)/ 2t$

In the SSL u is presumed to be large

(b) The weak scattering limit, Nordheim's Correction (NC)[1]

$$\sigma(z) = \bar{\varepsilon} + C_A C_B u^2 F_{VCA}(z) \qquad (2.11)$$

Here $F_{VCA}(z) = F_o(z - \bar{\varepsilon})$

The density of states (DOS) is related to the imaginary part of the Green's function. Hence the DOS of the system can be known from the knowledge of the Green's function.

If a single site impurity is added to a medium the potential term in the Hamiltonian changes. The impurity potential is defined as the difference between the total Hamiltonian with impurity and the host Hamiltonian.

$$V_{imp} = H - H_h \qquad (2.12)$$

This impurity potential perturbs the host electronic structure. It may give rise to a defect level inside the band gap. The conditions for the presence of the defect level inside the band

and its location will be discussed in section 2.2. The perturbation of the host DOS and the presence of a defect level in the gap results in changes in total electronic energy. In section 2.3 we discuss a formalism to calculate the total energy changes using Hellmann Feynman theorem. Section 2.4 contains the results of the calculation of total energy changes in two types of model disordered systems.

2.2: Determination of the Defect Level in the Gap.

Consider the ordered, one dimensional, tight binding, Hamiltonian of equation (2.3) in which one atom of different species replaces one of the parent atoms. This atom is then referred to as a substitutional impurity. The Hamiltonian of the system can be written using equation (2.12) as

$$H = H_h + V_{imp}$$

Here V_{imp} is the impurity potential and H_h is the host Hamiltonian. Assuming that the substitutional impurity is neutral and unrelaxed, we obtain

$$V_{imp} = |1\rangle\ (\varepsilon - \varepsilon_o)\langle 1| = |1\rangle\ V\ \langle 1| \qquad (2.13)$$

Here '1' is the defect site. Since we have assumed the impurity to be unrelaxed, that is, there is no rearrangement of neighbouring

atoms. Hence there is no change in the off-diagonal term of the Hamiltonian. The Green's function of this system is given by (Economou 1979)[2]

$$G(z) = 1/(z - H)$$

$$= 1/(z - H_h - V_{imp})$$

or $$G(z) = G_h(z) + G_h(z)\, V_{imp}\, G(z)$$

where $$G_h(z) = 1/(z-H_h)$$

$G_h(z)$ is the host crystal Green's function. Defining the scattering matrix T as

$$T = V_{imp}/\ (1 - G_h(z)\ V_{imp})$$

It can be shown that

$$G(z) = G_h(z) + G_h(z)\ T\ G_h(z)$$

T can also be written in an expanded form

$$T = V_{imp} + V_{imp}\ G_h(z)\ V_{imp} + \ldots.$$

$$= V|1><1| + V^2|1><1|G_h(z)|1><1| + \ldots$$

$$= |1>V<1|\ /\ (1 - G_h(1,1,z))$$

where

$$G_h(l,l,z) = \langle l|G_h(z)|l\rangle$$

Hence

$$G(z) = G_h(z) + G_h(z)|l\rangle V\langle l|G_h(z)/(1 - G_h(l,l,z))$$

The poles of the Green's function give the energy levels. From the above equation we see that the impurity Green's function is the sum of two terms. The first term is the host Green's function and the second term is a function of the impurity potential. The poles of the second term give additional levels over and above the host crystal levels, at say E_p which is given by the solution of the following equation.

$$1 - V\, G_h(l,l,E_p) = 0$$

or

$$G_h(l,l,E_p) = 1/V \qquad (2.14)$$

The above equation is known as the Koster Slater[3] equation for the single band case. It is, however, not necessary that E_p should always be outside the band. We may have a host DOS such that for a small value of the impurity potential there is no solution of equation (2.14) outside the band. This situation is labelled as resonant. Inside the band the Green's function is complex and the T matrix could be written as

$$T = V\ |l\rangle\langle l|\ /\ (1 - V\, G_h^R(l,l,E_p) - iV\, G_h^I(l,l,E_p))$$

The superscripts R and I indicate the real and imaginary part of the Green's function. Further,

$$G_h^R(1,1,E_p) = 1/V$$

yields the resonance state inside the band gap.

It is observed that for some host DOS there is a threshold value of impurity potential. For values of defect potential larger than the threshold a level appears in the gap. It is easy to see from the K-S equation that for the threshold to be zero the real Green's function just outside the band edge should be infinite.

2.3: Determination of Total Energy Changes

The gap level by itself does not present the complete picture of a defect in a semiconductor. The total change in energy is evaluated not merely by considering the gap level, but also the perturbation of the host density of states and the location of the fermi level (z_f). This total energy is related to the heat of solution.

In this section we present the formalism to employ the Hellmann Feynman theorem to obtain the total energy change when the defect is introduced into a model disordered host.

The Hellmann Feynman[4] theorem states that if $H(\lambda)$ be a hermitian operator, which depends on the real parameter λ, and

$|\psi(\lambda)\rangle$ a normalized eigenvector with eigen-value $E(\lambda)$ then

$$\frac{d}{d\lambda} E(\lambda) = \langle \psi(\lambda) | \frac{d}{d\lambda} H(\lambda) | \psi(\lambda) \rangle \qquad (2.15)$$

The total energy of the system is given by

$$E = \int_{-\infty}^{Ef} \omega \, \rho(\omega) \, d\omega \qquad (2.16)$$

where $\rho(\omega)$: density of states

: # of states per unit energy

But $\rho(\omega)$ can be expressed in terms of the Green's function

$$\rho(\omega) = 1/\pi \sum_i Im \, G_{ii}(\omega)$$

Here $G_{ii}(\omega)$ is the diagonal part of the Green's function The total energy changes can be expressed as

$$\Delta E = - \sum 1/\pi \int_{-\infty}^{Ef} \omega \, Im \left\{ \left[G_{imp}(\omega) \right]_{ii} - G^{h}_{ii}(\omega) \right\} d\omega \qquad (2.17)$$

Here $(G_{imp})_{ii}$ is the diagonal part of the Green's function of the

host with the impurity atom and $G^{h}_{ii}(\omega)$ is that of the host medium. If the host medium is ordered then $G_{ii}(\omega)$ is same for all 'i's because of translational invariance. For disordered host the medium is not translationally invariant, however, as mentioned in section 2.1 the medium can be replaced by an effective ordered system. Thus for this case too the diagonal host Green's function will have the same value for all sites.

Since the impurity atom is located at a particular site, $(G_{imp})_{ii}$ is site dependent. Thus one needs to evaluate $(G_{imp})_{ii}$ for every site separately, which is not easy. This difficulty is overcome by taking recourse to the Hellmann Feynman theorem. The Hamiltonian of the host system is

$$H_h = \sigma \sum_m |m\rangle \langle m| + t \sum_{m \neq n}^{n.n} |m\rangle \langle n|$$

and that with an impurity is

$$H = \sigma \sum_m |m\rangle \langle m| + t \sum_{m \neq n}^{n.n} |m\rangle \langle n| + (\varepsilon - \sigma) |l\rangle\langle l|$$

$$= \sigma \sum_m |m\rangle \langle m| + t \sum_{m \neq n}^{n.n} |m\rangle \langle n| + V |l\rangle\langle l|$$

Here the Hamiltonian depends on the parameter V, the impurity potential. Using Hellmann Feynman theorem one gets the following equation as shown by Villaseñor et al[5]

$$\frac{d}{dV}\left(E_{imp} - E^{h}\right) = \int_{-\infty}^{Ef} \langle\psi|l\rangle \langle l|\psi\rangle \, d\omega$$

$$= \int_{-\infty}^{Ef} |\langle\psi|l\rangle|^{2} \, d\omega$$

$$= \int_{-\infty}^{Ef} \rho_{l}(\omega,V) \, d\omega \qquad (2.18)$$

$\rho_{l}(\omega,V)$ is the local density of states at the impurity site and is given in terms of the diagonal part of the impurity Green's function as follows

$$\rho_{l}(\omega,V) = -1/\pi \; \mathrm{Im} \; (G_{imp}(\omega,V))_{ll}$$

The evaluation of the diagonal part of the impurity Green's function at the defect site is straightforward. It is given by the expression

$$(G_{imp}(z))_{ll} = G^{h}_{ll}(z) \left\{ 1 + V \, G^{h}_{ll}(z)/(1 - V \, G^{h}_{ll}(z)) \right\}$$

Integrating equation (2.18) with respect to the impurity potentia the total energy change can be easily obtained.

2.4: Results for Total Energy Change in Two Model Cases

We investigate the effect of various mean field

approximations on the total energy change for two types of model disordered hosts.

(i) The first model is that of one dimensional tight binding system . In this case the diagonal part of the Green's function is given by

$$F(z) = ((z-\sigma(z))^2 - 1)^{-1/2} \qquad (2.19)$$

(ii) The second model is that of a realistic three dimensional semicircular density of states where

$$F(z) = 2\,((z-\sigma(z)) \pm (z-\sigma(z))^2 - 1)^{1/2}) \qquad (2.20)$$

Our calculations are for a 50-50 alloy. We will focus on two different physical situations, one in which the atoms of the alloy are chemically very different from each other, and the other in which they are almost similar. These situations are characterized by large and small values of the disorder parameter 'u'. The disorder parameter 'u' is defined as the difference between the diagonal energies of the two atoms divided by the off diagonal term 't'.

$$u = (\varepsilon_A - \varepsilon_B) / 2t$$

We next present results for the change in total electronic energy due to a single site impurity in the above mentioned model disordered hosts.

In Figure 2.1 we predict the change in electronic energy as a function of the defect potential for various band fillings for the realistic semicircular host . The Fermi level is denoted by z_f. Note that z_f = 0 corresponds to the half filled band, z_f = 2.5 (-2.5) correspond to approximately three quarter (one quarter) filled bands . Note further that V = ε_{imp} . The disordered host is described in the Coherent Potential Approximation . The disorder parameter u is large (= 5.0) . The defect potential (V) perturbs the host band as well as creates a localized level outside the host band. For negative values of the defect potential the localized states appear below the band, consequently lowering the energy . From the figure it is clear that for large negative defect potentials the plot is linear irrespective of the band filling . The position of the defect level is proportional to V for large V .This being the dominant contribution to the energy , accounts for the linearity of the plot at large defect potentials. The level characteristic are the same for positive V , this time however the level being above the band, it is left unoccupied. Consequently we expect ΔE to approach a saturation value as V is increased .

Figure 2.2 represents the same plot as that of figure 2.1 with identical parameters, except that now the disordered host is

described by employing the Nordheim's correction . The general behaviour of the curve is similar to figure 2.1 (e.g linearity at large negative values of V and saturation at large positive V). The saturation occurs at approximately the same value of V as that in figure 2.1 . However the saturation value of ΔE is considerably lowered (approximately 15%) as compared with the results in figure 2.1.

In Figure 2.3 we have used the strong scattering limit to describe the host . The general trend of the curve is similar to that of CPA . However, the saturation value for large positive V is once again underestimated as in the Nordheim's correction.

A similar analysis was repeated for the same model host which was weakly disordered (e.g. u = 0.8). The results obtained by employing Nordheim's Correction were found to be in very good agreement with the CPA.

In figure 2.4 and 2.5 we investigate the effect of two mean field theories: CPA and NC respectively on the defect energy in a one dimensional host .The value of the disorder parameter is chosen to be the same as in figure 2.1 and 2.2 (u = 5.0) The overall behaviour is similar to figures 2.1 - 2.3 (e.g. linearity at large negative values of V and saturation of ΔE at large positive values of V). We notice however that the Nordheim's Correction severely underestimates the saturation energy ΔE for large positive V .In the strong scattering limit the results seem to improve, but nevertheless saturation value differ considerably

from the Coherent Potential Approximation .

For weakly disordered one dimensional host (u = 0.8) the results obtained by using Nordheim's Correction was found to agree very closely with the Coherent Potential description.

The results of this chapter have been presented in detail in Reference 6.

REFERENCES

1. L. Nordheim, Ann.Phys 9 607 (1931).

2. E.N.Economou, "Green's Functions in Quantum Physics" (Springer Verlag) (1971).

3. G.J.Koster and J.C.Slater, Phys. Rev. 95 1167 (1954).

4. R.P.Feynman, Phys.Rev. 56, 340 (1939).

5. P.Villaseñor Gonzälez and J. Urias, Solid State Commun. (1988).

6. "Electronic Structure of Defects in the Alloy Semiconductors: The Weak Scattering Approximation". Amita Das, Kajoli Banerjee and Vijay A. Singh. Submitted Journal of Physics: Condensed Matter.

FIGURE CAPTIONS

Figure 2.1: Electronic energy change ΔE vs. the defect potential V for various band fillings . Note that $z_f = 0$ corresponds to a half filled band . The model considered is the realistic three dimensional host .

Figure 2.2: Parameters and the model is the same as figure 2.1 except that the Nordheim's Correction is used to describe the host. Note the general similarity of the figures 2.1 and 2.2.

Figure 2.3: Electronic energy change ΔE vs. the defect potential V for various band fillings . Parameters and the model used is same as figure 2.1 except that the Strong Scattering Limit is used to describe the host .Note that there is no improvement over the Nordheim's result.

Figure 2.4: Plot of electronic energy vs. the defect potential for various band fillings for a one dimensional host . The host is described by the Coherent Potential Approximation.

Figure 2.5: Same as figure 2.4 except that the host is described by the Nordheim's correction . Note that NC proves to be a very poor approximation.

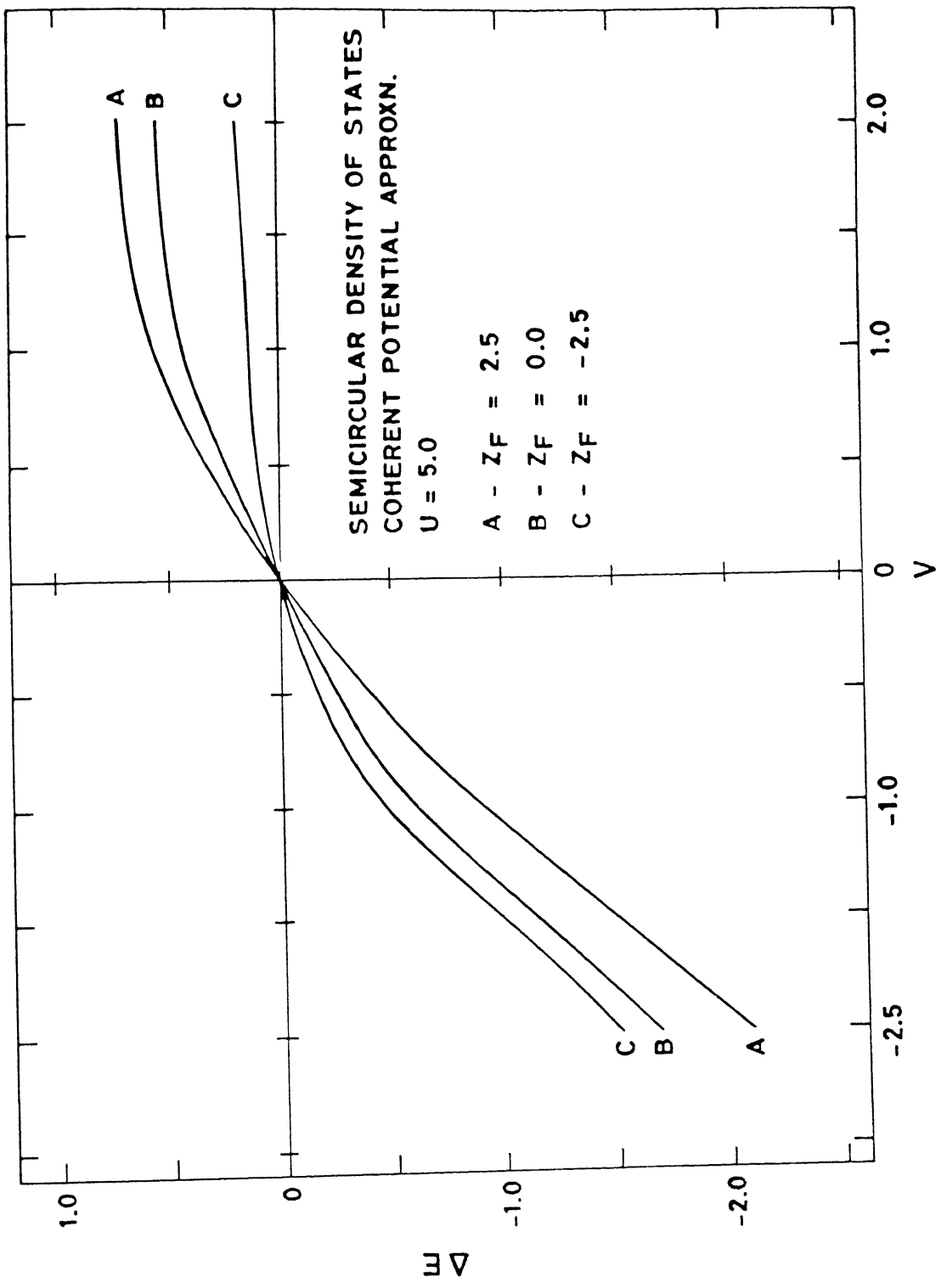
SEMICIRCULAR DENSITY OF STATES
COHERENT POTENTIAL APPROXN.
U = 5.0
A - Z_F = 2.5
B - Z_F = 0.0
C - Z_F = -2.5
A
B
C
ΔE
V
1.0
0
-1.0
-2.0
2.0
1.0
0
-1.0
-2.5

FIGURE 2.1

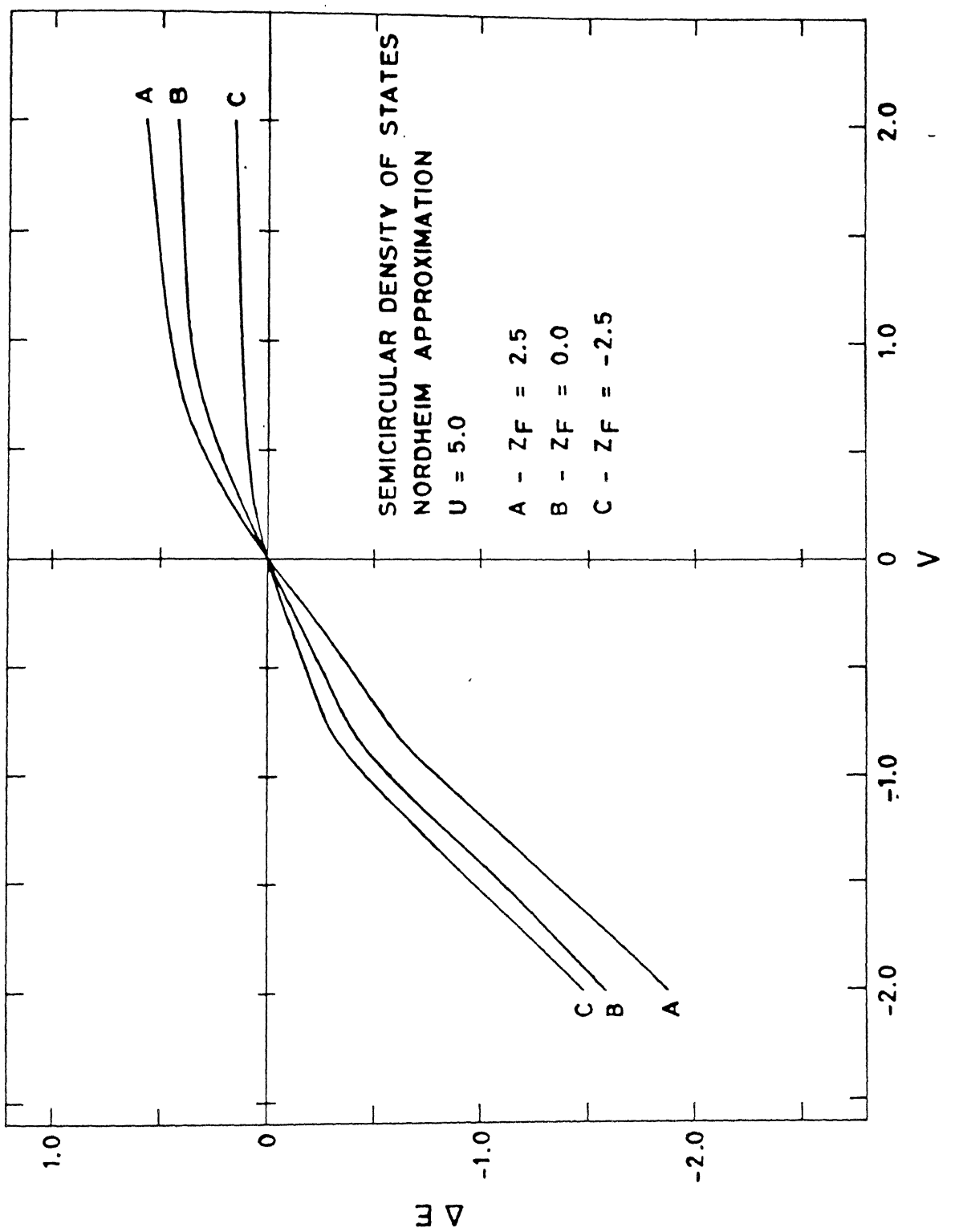
SEMICIRCULAR DENSITY OF STATES
NORDHEIM APPROXIMATION
U = 5.0
A - ZF = 2.5
B - ZF = 0.0
C - ZF = -2.5
A
B
C
ΔE
V
1.0
0
-1.0
-2.0
2.0
1.0
0
-1.0
-2.0

FIGURE 2.2

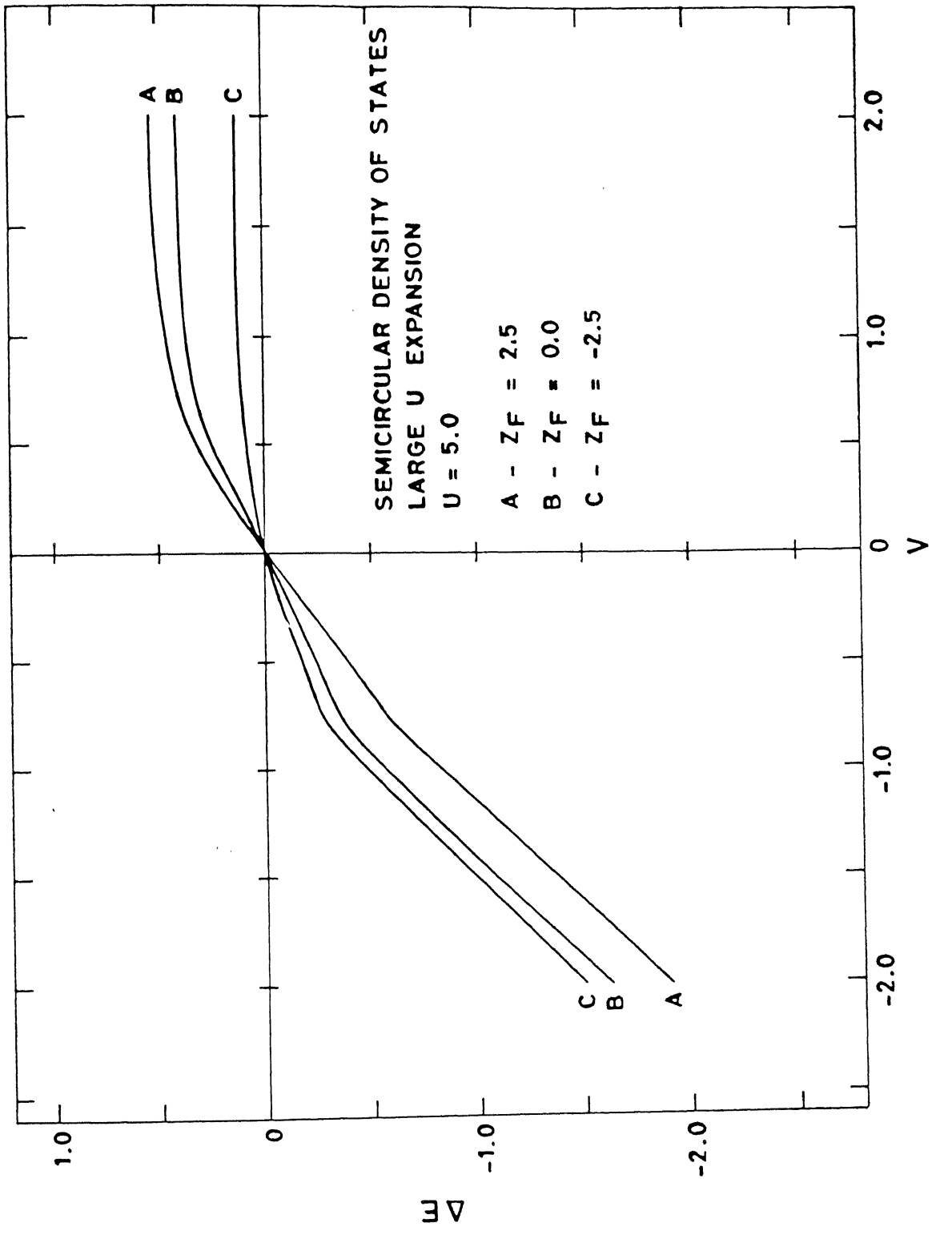
SEMICIRCULAR DENSITY OF STATES
LARGE U EXPANSION
U = 5.0
A - Z_F = 2.5
B - Z_F = 0.0
C - Z_F = -2.5
A
B
C
ΔE
V
1.0
0
-1.0
-2.0
2.0
1.0
0
-1.0
-2.0

FIGURE 2.3

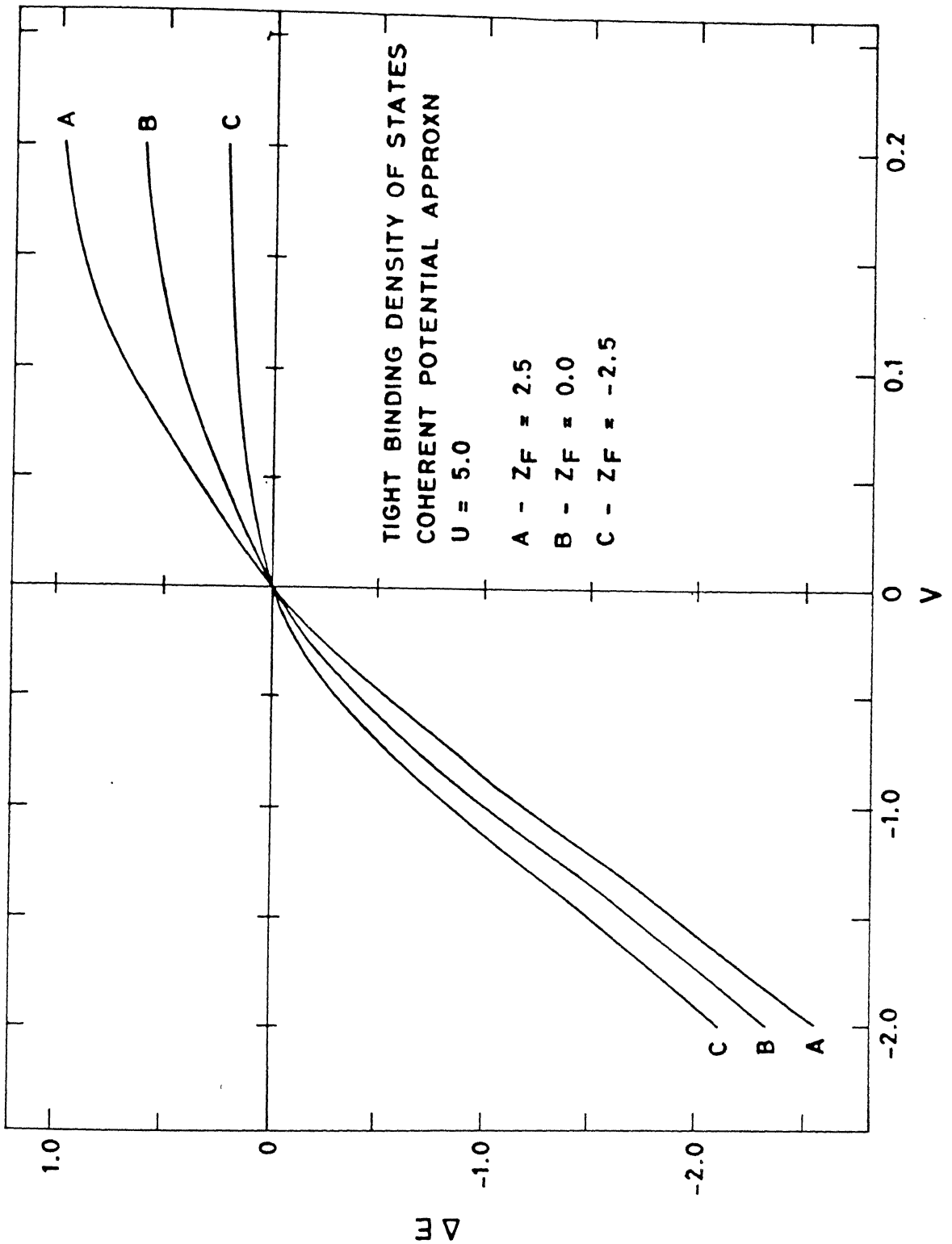
TIGHT BINDING DENSITY OF STATES
COHERENT POTENTIAL APPROXN
U = 5.0
A - Z_F = 2.5
B - Z_F = 0.0
C - Z_F = -2.5
A
B
C
1.0
0
-1.0
-2.0
Δ m
0.2
0.1
0
-1.0
-2.0
V

FIGURE 2.4

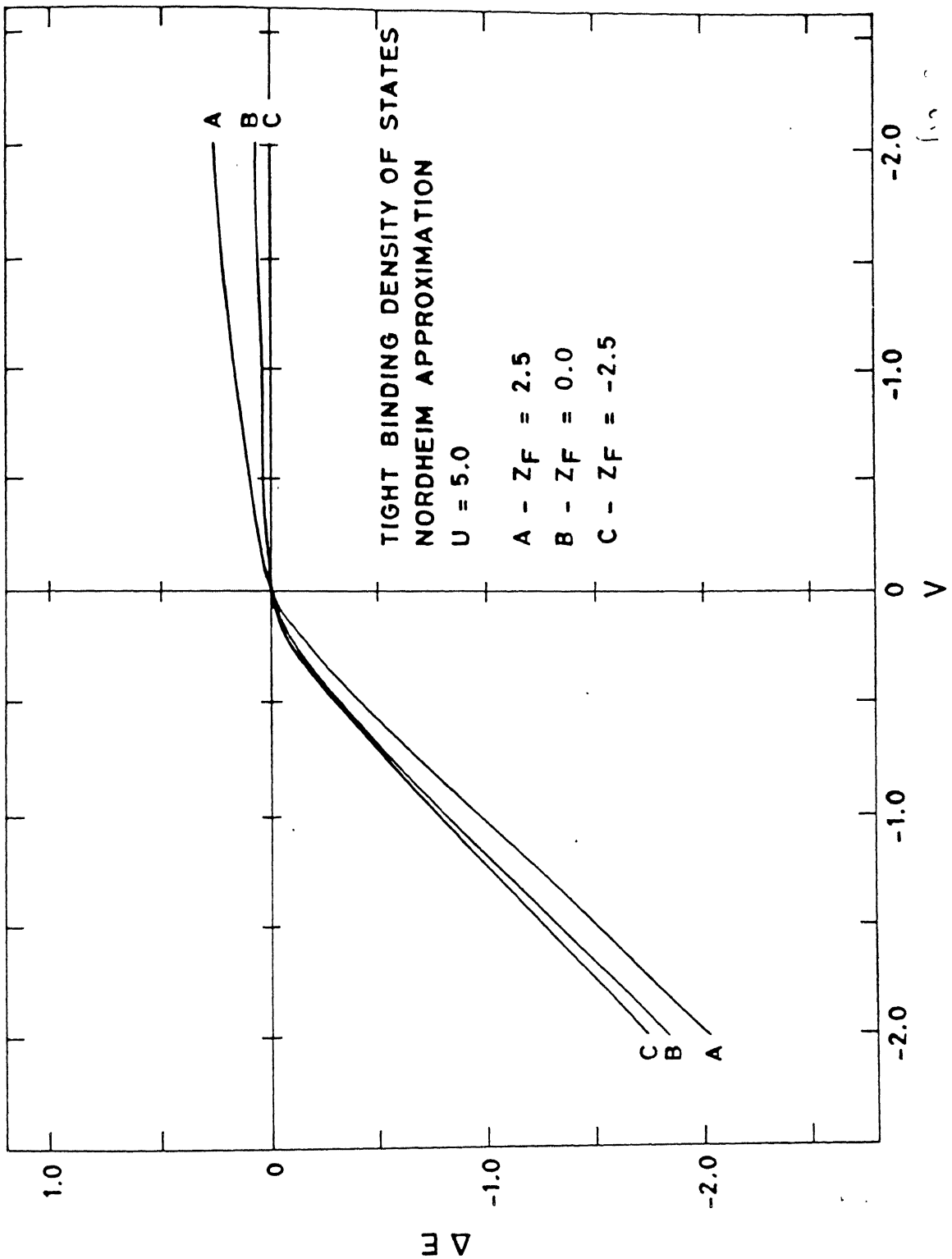
TIGHT BINDING DENSITY OF STATES
NORDHEIM APPROXIMATION
U = 5.0
A - Z_F = 2.5
B - Z_F = 0.0
C - Z_F = -2.5
A
B
C
ΔE
1.0
0
-1.0
-2.0
V
0
-1.0
-2.0

FIGURE 2.5

CHAPTER 3 : MULTIBAND CPA FOR REALISTIC SEMICONDUCTOR ALLOYS

3.1: Preliminary Remarks

In this chapter we will study defect energetics in realistic semiconductor alloys. We divide the framework necessary to study electronic energetics associated with defects into various stages. The first stage is the determination of the host electronic structure. For this an alloy semiconductor may be regarded as a substitutionally disordered system. For example $Ga_{0.75}Al_{0.25}As$ posseses an underlying zinc-blende structure. Each four-fold coordinated As atom is surrounded on an average by one Al and three Ga atoms. Since the cation site can be occupied by either Al or Ga with probabilities which depend on their respective concentrations, the analysis of chapter 2 can be employed. This disordered structure, in which the occupancy of the cation site is probablistic, can be replaced using MFT by an effective ordered structure in which all cation sites are considered to be equivalent. This replacement is, however, at the cost of several physical characteristics of the original system. In the original disordered system there can be localization effects, which are largely washed out by the effective ordered crystal which replaces it.

A realistic description of a disordered medium could be achieved by very large cluster calculations averaged over all

possible configurations. This method is computationally feasible only for very small cluster sizes, which probably do not do justice to real systems. In our work we have concentrated on the mean field description of the disordered medium.

The second stage is to determine the mean defect level in the gap $Z_d(V)$. Here V is the defect potential. The mean gap level $Z_d(V)$ is then given by the well known Koster Slater equation[1].

In section 3.2 we present the LCAO tight binding scheme to calculate the electronic structure of the host. In section 3.3 we introduce the Coherent Potential Approximation (CPA) formalism and describe the methodology employed to incorporate the CPA for the multiband case. Section 3.4 contains the description of a proposed deep level approximation. Section 3.5 contains results and discussion.

3.2: LCAO Tight Binding Scheme

As noted in the earlier chapter, the host electronic structure should be known in order to predict the presence of gap level due to an impurity. In this section we describe the method adopted to find the host structure.

We employ the empirical tight binding scheme for the evaluation of the host band structure. We write the crystal wave function as a linear combination of Bloch functions $|nb\bar{k}\rangle$ each of which depends on only one type of orbital. Thus our basis set is given by

$$|nb\bar{k}\rangle = N^{-1/2} \sum_{i,b} \exp(i\bar{k}\bar{R}_i + i\bar{k}\tau_b)|nb\bar{R}_i\rangle \qquad (3.1)$$

$|nb\bar{R}_i\rangle$ are the atomic orbitals centered on the N crystal sites. The wavevectors $\bar{k}$ lie in the first Brillouin zone of the reciprocal lattice. The band index is n and b is the sublattice index. The primitive vectors of the (fcc) lattice are

$$A_1 = a/2\ (x + y)$$
$$A_2 = a/2\ (y + z)$$
$$A_3 = a/2\ (x + z)$$

Here 'a' is the lattice constant and x, y, z are unit vectors in the Cartesian system. The primitive vectors of the bcc reciprocal lattice are

$$a_1 = 2\pi/a\ (x + y - z)$$
$$a_2 = 2\pi/a\ (z + y - x)$$
$$a_3 = 2\pi/a\ (x + y + z)$$

For a bcc reciprocal space the k vectors are defined by

$$k = 2\pi/a\ (M_1, M_2, M_3)$$

Here each of the M_1, M_2 and M_3 is less than or equal to unity. Furthermore, they satisfy the condition

$$M_1+M_2+M_3 \leq 3/2$$

The above two conditions on M_i's define the unit cell (the first

Brilloin zone) in k space (bcc type).

The zinc-blende structure comprises of two interpenetrating fcc lattices one for the cation and other for the anion. The index 'b' in equation (3.1) denotes whether the site is an anion site or a cation site. Assuming that the anion positions are given by R_ι's. We define

$$\tau_b = \delta_{b,c}\ a/4\ (1,1,1)$$

to take the cation site into account.

The valence electrons are the ones which participate in the covalent bonding. The compounds with which we will be dealing in our calculations have zinc-blende structure and their valence orbitals comprise of one s and three p shells. The index n in equation (3.1) stands for the s, p_x, p_y, and p_z orbitals. In the basis $|nb\bar{k}\rangle$ the Hamiltonian matrix is of size (8×8). The matrix elements of the Hamiltonian are obtained empirically by matching them to the experimentally obtained band structure at high symmetry points. However, attempts to fit the conduction bands fail. To match the conduction bands two excited s orbitals, one at the anion and the other at the cation site are introduced in the basis set of $|nb\bar{k}\rangle$, thus rendering the Hamiltonian matrix to be of size (10×10).

A representative table of Hamiltonian matrix elements is shown by Harrison It has been assumed that the Hamiltonian couples only the nearest neighbours. The empirical values of the diagonal and the off diagonal terms $E(n,b)$ and $V(n_1b_1,n_2,b_2)$ have been

listed by Vogl[3] et al for several semiconductor elements and compounds.

In the case of semiconductor alloys, there is a substitional disorder either at the anion or cation site (for ternary alloys) and at both sites (for quarternary alloys). We have used the VCA approximation discussed in chapter 2 to determine the input matrix elements of alloys (Ho et al 1983)[4]. The CPA corrections to these is described later in section 3.3.

Consider an alloy of composition $A_xB_{1-x}C_yD_{1-y}$. Let us denote the lattice constant (or bond length) for the compounds AC,AD,BC and BD by d_1, d_2, d_3 and d_4 respectively. The representative diagonal matrix elements of the above four compounds are written as $(AC)_{nn}$, $(AD)_{nn}$, $(BC)_{nn}$ and $(BD)_{nn}$; and the off diagonal terms as $(AC)_{n_1n_2}$, $(AD)_{n_1n_2}$, $(BC)_{n_1n_2}$ and $(BD)_{n_1n_2}$.

The diagonal matrix element of the VCA averaged Hamiltonian for the alloy is given as follows

$$(H)_{nn} = xy\,(AC)_{nn} + x(1-y)(AD)_{nn} + (1-x)y(BC)_{nn} + (1-x)(1-y)(BD)_{nn} \tag{3.2}$$

$$(H)_{n_1n_2} = xy(d_1/d)^2(AC)_{n_1n_2} + x(1-y)(d_2/d)^2(AD)_{n_1n_2} + (1-x)y(d_3/d)^2(BC)_{n_1n_2} + (1-x)(1-y)(d_4/d)^2(BD)_{n_1n_2} \tag{3.3a}$$

where

$$d = xyd_1 + x(1-y)d_2 + (1-x)yd_3 + (1-x)(1-y)d_4 \tag{3.3b}$$

Notice that the above equation respects the inverse square scaling

with the bond length of the off diagonal element of the Hamiltonian as enunciated by Harrison(1980).

Diagonalising the Hamiltonian yields the band structure of the system. We, however, need to find the Green's function of the system. The Green's function can be evaluated by the knowledge of the density of states. The calculation of the density of states from the band structure was premised on the methodology proposed by Lehman and Taut[5] in which the Brilloin zone is divided into tetrahedrons. A detailed description of this scheme is given by Rath and Freeman(1975)[6].

3.3: Multiband CPA Formalism

As mentioned in the earlier chapter the CPA is a better method of treating disorder. We will illustrate in this section the method adopted by us to introduce a CPA description of the disordered host.

We are dealing with substitutional and not positional disorder of the lattice. Hence, the underlying symmetry of the lattice remains the same as that of the tetrahedral group (T_d). The basis functions which we have chosen for our calculations decompose into four irreducible representations of the T_d group, two are of A_1 type (of dimensionality one each) and the remaining two are of the type T_2 (dimensionality three each). A_1 is a totally symmetric representation which is invariant under all group transformations. We will refer to it as an S state. The irreducible representation T_2 has the same transformation

properties as the simple functions x, y, and z under the T_d symmetry operations. The basis functions for this irreducible representation could be chosen as ψ_x, ψ_y, and ψ_z which have an axial symmetry about OX, OY, and OZ cartesian axes respectively. We shall refer to them as P states.

The Hamiltonian expressed in the above symmetry adapted basis will be seperated into two blocks as follows.

$$H = \begin{bmatrix} H_{A_1} & 0 \\ 0 & H_{T_2} \end{bmatrix} \qquad (3.4)$$

H_{A_1} is a matrix of size (2×2) corresponding to two A_1 representations. H_{T_2} corresponds to the two T_2 representations and is of size 6×6. The two representations of the A_1 as well as the T_2 have, as their basis, functions which are centered either at the anion or at the cation site. The Hamiltonian further does not couple the basis functions of T_2, centered at the same site but having axial symmetry about a different axis. Thus H_{T_2} reduces to three (2×2) matrices corresponding to basis functions having symmetry about x, y and z axes respectively. These three sets of matrices however are identical since the tetrahedral structure does not distinguish between the three axial directions.

A disordered Hamiltonian can be broken into a random part 'V' and a configuration independent part W. Thus

$$H = W + V \qquad (3.5)$$

The random part is assumed to be site diagonal hence

$$H = W + \sum_j V_j \tag{3.6}$$

Here 'j' represents the site index. As mentioned in section 3.2 we have chosen W to be our input VCA Hamiltonian, and we will be incorporating the CPA corrections due to the random part $\sum_j V_j$ to this. The random potential can be written as

$$V_j = \sum_m |mR_j\rangle (\varepsilon_j - \bar{\varepsilon}) \langle mR_j| \tag{3.7}$$

Here m stands for a S like state and three P like T_2 states. ε_j takes values ε_A or ε_B depending on whether the atom A or B is occupying the site. $\bar{\varepsilon}$ is the VCA energy defined in the earlier section for W.

The CPA formalism replaces the configuration averaged one electron Green's function by an effective Green's function.

$$G_{eff} = 1/(Z - H_{eff})$$

H_{eff} is defined as

$$H_{eff} = W + \Sigma \tag{3.8a}$$

$$H_{eff} = W + \sum_j \Sigma_j \tag{3.8b}$$

Σ_j is termed as the self energy of the system and is obtained from

the condition such that the single site scattering matrix t_j when averaged over all configurations is zero. Σ can be viewed as a block diagonal matrix, each block is identified by a particular site 'j' and is of size (8×8) for the above mentioned eight states. Furthermore, the translational symmetry of the averaged crystal ensures that each block is identical. Thus Bloch's theorem can be invoked and Σ can be represented in a reduced Bloch space of size (8×8). The tetrahedral symmetry further decomposes Σ into two blocks of A_1 and T_2 representations. We write Σ as

$$\Sigma = \begin{bmatrix} \Sigma_{A_1} & 0 \\ 0 & \Sigma_{T_2} \end{bmatrix}$$

$$\Sigma_{A_1} = \begin{bmatrix} \Sigma_{A_1}^{a} & 0 \\ 0 & \Sigma_{A_1}^{c} \end{bmatrix}$$

where the superscripts 'a' and 'c' stand for anion and cation respectively.

$$\Sigma_{T_2} = \begin{bmatrix} \Sigma_{T_{2x}} & & \\ & \Sigma_{T_{2y}} & \\ & & \Sigma_{T_{2z}} \end{bmatrix}$$

Each of the $\Sigma_{T_{2x}}$, $\Sigma_{T_{2y}}$, $\Sigma_{T_{2z}}$ can be further decomposed into cation

and anion subspaces as has been shown for Σ_{A_1}. The off diagonal elements of Σ have been neglected, which is in spirit with the approximation invoked by Chen and Sher[7].

Symmetry about x, y, and z axis further ensures that

$$\Sigma_{T_{2x}} = \Sigma_{T_{2y}} = \Sigma_{T_{2z}} = \Sigma_{T_2}$$

The CPA equation (see equation 2.9) for this multiband case is a matrix equation of the form

$$\bar{\Sigma}(z) = -(\bar{\varepsilon}_A - \bar{\Sigma}(z))\bar{F}(z)(\bar{\varepsilon}_B - \bar{\Sigma}(z))$$

The above mentioned symmetry reduces it to a set of four coupled scalar equations

$$\bar{\Sigma}_{r,d}(z) = -(\varepsilon_{A_{r,d}} - \bar{\Sigma}_{r,d}(z))\,\bar{F}_{r,d}(z)\,(\bar{\varepsilon}_{B_{r,d}} - \bar{\Sigma}_{r,d}(z)) \qquad (3.9)$$

Here 'r' refers to the symmetry and 'd' to the cation or anion subspaces. These equations are coupled via the Green's function. An approximate method of decoupling the above equations can be devised using the partitioning technique of Löwdin[8].

The component Green's function $F_{r,d}$ can be evaluated from the component density of states as follows.

$$F_{r,d} = \langle j\ r,d\ |G_{eff}|\ j\ r,d\rangle$$

Here 'j' is the site index. Since all sites of the effective system are identical, we can express $F_{r,d}$ as trace over all sites

$$F_{r,d} = 1/N \; Tr \; \langle r,d \mid G_{eff} \mid r,d \rangle$$

$$= \frac{1}{N} \sum_{n,k} \frac{|\langle r,d \mid n,k \rangle|^2}{(z - \Sigma_{r,d} - \varepsilon_n(k))}$$

$$= \left(\frac{\Omega}{N^2(2\pi)^3} \right) \sum_n \int \frac{|\langle r,d \mid n,k \rangle|^2 \; d^3k}{(z - \Sigma_{r,d} - \varepsilon_n(k))}$$

$$= \frac{1}{N} \int \frac{d\varepsilon}{(z - \Sigma_{r,d} - \varepsilon)} \left[\frac{\Omega}{N(2\pi)^3} \sum_n \int |\langle r,d|n,k\rangle|^2 \delta(\varepsilon - \varepsilon_n(\bar{k})) \; d^3k \right]$$

The factor in the square bracket is the component density of states $\rho(r,d)$. Thus

$$F_{r,d} = \frac{1}{N} \int \frac{d\varepsilon \; \rho_{r,d}(\varepsilon)}{z - \Sigma_{r,d} - \varepsilon} \qquad (3.10)$$

Using equations (3.9) and (3.10) the CPA corrections to the Green's function can be determined.

3.4: Point Defects in Multiband Systems

In this section we focus on point defects. These could be

either substitutional impurities or vacancies present in the disordered alloy semiconductors. The description of the host structure has been described in detail in the earlier sections of this chapter.

The defect potential caused by the substitution of an impurity atom for a host atom has the following three distinct contributions (i) a short range central cell potential (ii) a long range Coulomb potential (iii) an electron-lattice interaction caused by the lattice relaxation around the impurity. We will ignore the screened Coulomb potential and assume a simple realistic model in which there is no lattice relaxation. We will deal essentially with the central cell potential which is the difference between the atomic potentials of the impurity and the host atom.

The single site defect can be identified with V_j of equation 3.6. In this case the index 'j' corresponds to a particular site and is not a running index over all sites.

Thus the defect potential can be made block diagonal in this symmetry adapted basis; it contains one (2×2) a_1 symmetry matrix and three (2×2) t_2 symmetry matrices. The three (2×2) P type symmetry matrices will be identical. The defect potential is then

$$V^r_{i,j} = \begin{bmatrix} \varepsilon^r_{c,imp} - \varepsilon^r_{c,host} & V^r_{imp} - V^r_{host} \\ V^r_{imp} - V^r_{host} & \varepsilon^r_{a,imp} - \varepsilon^r_{a,host} \end{bmatrix}$$

'r' represents the symmetry and i & j = {c, a} correspond to cation and anion respectively.

We approximate the atomic energy difference between two atoms in a solid to be similar to the difference between free atoms. We also neglect the off-diagonal elements as they scale as the inverse square of the bond length and we have accounted for these in equations (3.2) and (3.3). Thus, if the impurity is at the cation site then

$$V^{r}_{i,j} = \begin{bmatrix} \varepsilon^{r}_{c,imp} - \varepsilon^{r}_{c,host} & 0 \\ 0 & 0 \end{bmatrix}$$

The bound state energy E_b can be obtained by the solution of the following K-S type equation.

$$1/V_{r,d} = F_{r,d} \qquad (3.11)$$

3.5: Deep Level Approximation

If the defect level is a simple vacancy on a cation or an anion sublattice then the corresponding defect potential is infinity. From equation (3.11) we see that the defect level due to vacancy will then be given by the zeroes of the $F_{r,d}$. Here 'r' denotes the symmetry of the level and 'd' the sublattice which has vacancy as a defect.

Substituting the value of $F_{r,d}$ in equation (3.9)we get the

value of $\Sigma_{r,d}$, which is zero. One thusobserves that for the vacancy level the CPA result is identical to the VCA. This suggests that a perturbation approach to an ultra deep level in alloy semiconductor can be employed. We call this the deep level approximation (DLA). This DLA is obtained from the self consistent CPA equation by retaining first order terms in inverse defect potential (1/V).

The self consistent CPA equation is (dropping the subscript for lattice and symmetry)

$$\Sigma(z_d) = -(\varepsilon_A - \Sigma(z_d))\, F(z_d)\, (\varepsilon_B - \Sigma(z_d))$$

Using the K-S equation

$$F(zd) = 1/V = \delta$$

where δ is a small parameter. Thus

$$\Sigma(z_d) = -(\varepsilon_A - \Sigma(z_d))\, \delta\, (\varepsilon_B - \Sigma(z_d))$$

Retaining first order terms in δ one gets

$$\Sigma(z_d) = -\delta\, \varepsilon_A\, \varepsilon_B$$

Moreover

$$F(z_d) = F_{VCA}(z') \qquad (3.12)$$

where

$$z_d = z' - \Sigma(z_d)$$

or

$$z_d = z' + \delta\, \varepsilon_A\, \varepsilon_B \qquad (3.13)$$

Let z_c be the location of the defect level for the vacancy. Expanding $F_{VCA}(z')$ about $F_{VCA}(z_c)$ one gets on neglecting higher powers

$$F_{VCA}(z') = F_{VCA}(z_c) + (z'-z_c)F_{VCA}'(z_c)$$

We have chosen δ to be sufficiently small hence z' can be assumed to be quite close to z_c. But $F_{VCA}(z_c) = 0$, since z_c is by definition a vacancy level and the VCA result is exact for it. Hence

$$\delta = (z'-z_c)\, F'_{VCA}(z_c) \qquad (3.14)$$

From equation (3.13) and (3.14)

$$z_d = z_c + \delta/F'_{VCA}(z_c) + \delta\, \varepsilon_A\, \varepsilon_B \qquad (3.15)$$

Thus knowing the vacancy level and the slope of the VCA Green's function at the vacancy level the deep defect level for a given defect potential can be directly read from equation (3.15).

3.6: Results

In this section we present some typical results of our defect level calculations[9].

Figure 3.1 depicts the t_2 cation defect level in the fundamental gap of $GaAs_{0.8}Sb_{0.2}$. The cation vacancy level for this system is at 0.33eV above the valence band edge. The agreement between DLA and CPA is excellent near z_{vac}.

Figure 3.2 depicts a similar comparison between the DLA and the CPA for the t_2 anion defect level in the fundamental gap of $Ga_{0.8}Al_{0.2}As$. The DLA results deviate from the CPA as we move away from the vacancy level which is at z_{vac} = 1.35eV. Figure 3.3 shows a t_2 cation level in $Ga_{0.6}Al_{0.4}As$.

As demonstrated in section 3.5, the VCA and CPA give identical results for the vacancy level in an alloy semiconductor. It is worthwhile exploring the differences between the two for a general gap level. It must be noted that when the host energies for the two species are close to each other, then the VCA ought to be satisfactory (small scattering regime). Let us consider the case of $GaAs_{0.8}Sb_{0.2}$. From Vogl[3] parameters Table we observe that the cation p-orbital energy E(p,c) for GaAs and GaSb differ only by 20%. Thus in figure 3.4 , the defect level as charted out in the CPA is almost indistinguishable from the VCA.

When the energy difference between the two species is large we expect CPA and VCA to differ considerably. That is borne out by a plot of figure 3.5 in which the a_1 cation defect is plotted for $Ga_{1-x}Al_xAs$. The energy E(s,c) differs for two systems GaAs and

AlAs in this case by 56%.

In section 3.3 we have proposed a simplified multiband CPA formalism. It is possible to generalize it. An interesting generalisation using the Effective Medium Approximation (EMA) of Roth[9,10] has recently been proposed. Some of the results of this chapter is presented in reference 11.

REFERENCES

1. G.F.Koster and J.C.Slater, Phys. Rev. 95, 1167 (1954).

2. W.A.Harrison, "Electronic Structure and Properties of Solids" (Freeman - San Fransisco) (1980).

3. P.Vogl,H.P.Hjalmarson and J.D.Dow, J. Phys. Chem. Sol. 44 365 (1983).

4. E.S.Ho and J.D.Dow, Phys. Rev. B 27, 1115 (1983).

5. G.Lehmann and M.Taut, Phys. Status Solidi 54, 469 (1972).

6. J.Rath and A.J.Freeman, Phys. Rev. B 11 No 6, 2109-2117 (1975).

7. A.B.Chen and A.Sher, Phys. Rev. B 17, 4726 (1978).

8. P.O.Löwdin, J. Appl. Phys. 33, suppl 1, 251,(1962).

9. L.M.Roth, Phys. Rev. B 9, 2476 (1974).

10. J.E.Hasbun and L.M.Roth, Phys. Rev. B 37, 2829, (1989).

11. "DX Center: A Coherent Potential Approximation Based Approach", Amita Das and Vijay A. Singh. Submitted Phys. Rev.B (1990).

FIGURE CAPTIONS

Figure 3.1: A Plot of the inverse defect potential strength vs. the t_2 cation defect level in the fundamental gap of $GaAs_{0.8}Sb_{0.2}$. The solid and the broken lines show the results obtained by using CPA and DLA respectively. Note that the vacancy level shown by an arrow is predicted at 0.33eV by both the theories.

Figure 3.2: A Plot of the inverse defect potential strength vs. the t_2 anion defect level in the fundamental gap of $Ga_{0.8}Al_{0.2}As$. The solid and the broken lines show the results obtained by using CPA and DLA respectively. Note that the vacancy level shown by an arrow is predicted at 1.35eV by both the theories.

Figure 3.3: A Plot of the inverse defect potential strength vs. the t_2 cation defect level in the fundamental gap of $Ga_{0.6}Al_{0.4}As$. The solid and the broken lines show the results obtained by using CPA and DLA respectively. Note that the vacancy level shown by an arrow is predicted at 0.39eV by both the theories.

Figure 3.4: A plot of defect potential strength vs. the t_2 cation defect level in $GaAs_{0.8}Sb_{0.2}$ as charted out using CPA(——) and VCA (----). The common vacancy level predicted by the theories is shown by an arrow at 0.327eV.

Figure 3.5: A plot of defect potential strength vs. the a_1 cation

defect level in $Ga_{0.4}Al_{0.6}As$ as charted out using CPA(——) and VCA (----). Note there is no vacancy level within the fundamental gap.

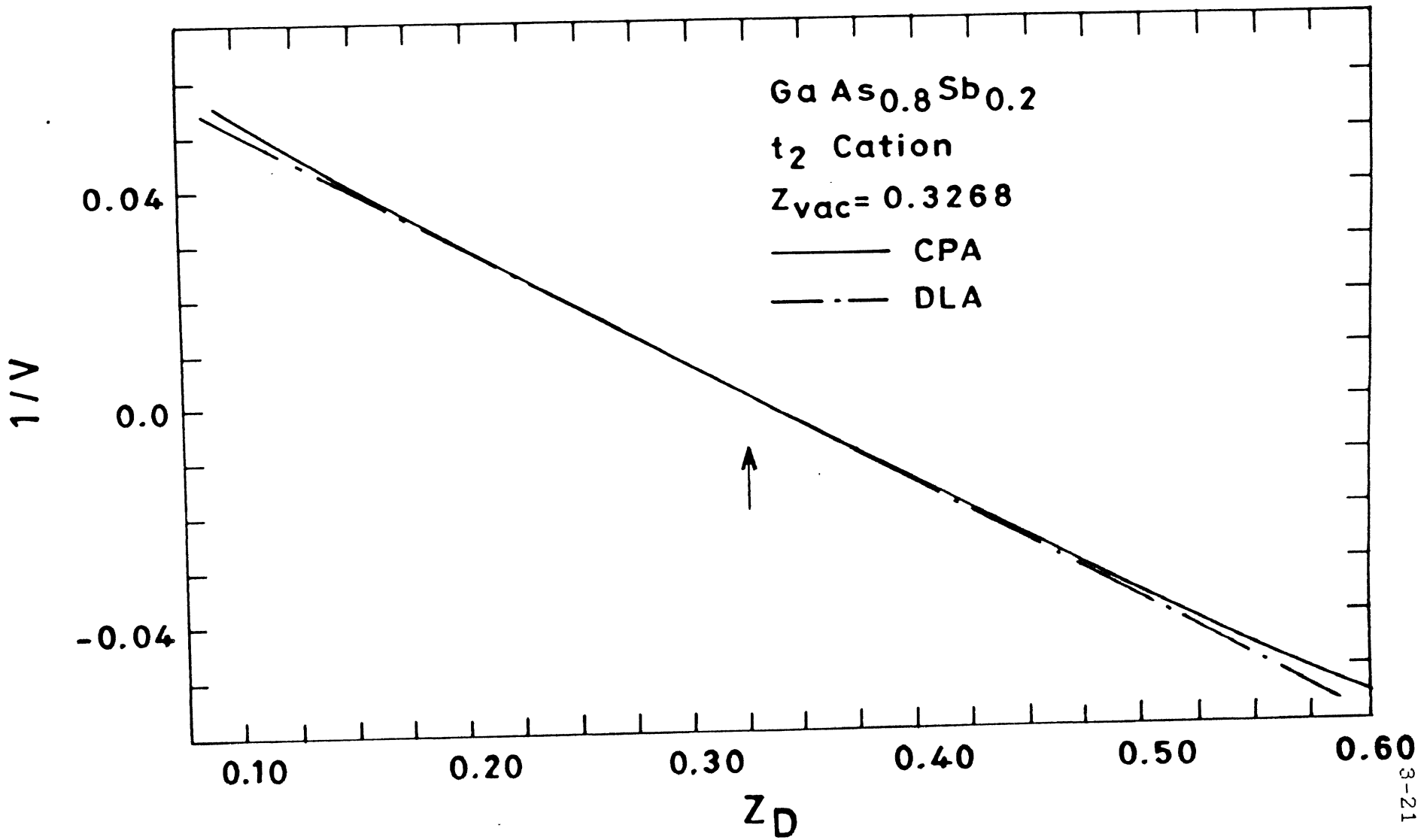
Ga As0.8 Sb0.2
t2 Cation
Zvac= 0.3268
CPA
DLA
0.04
0.0
-0.04
1/V
0.10
0.20
0.30
0.40
0.50
0.60
ZD

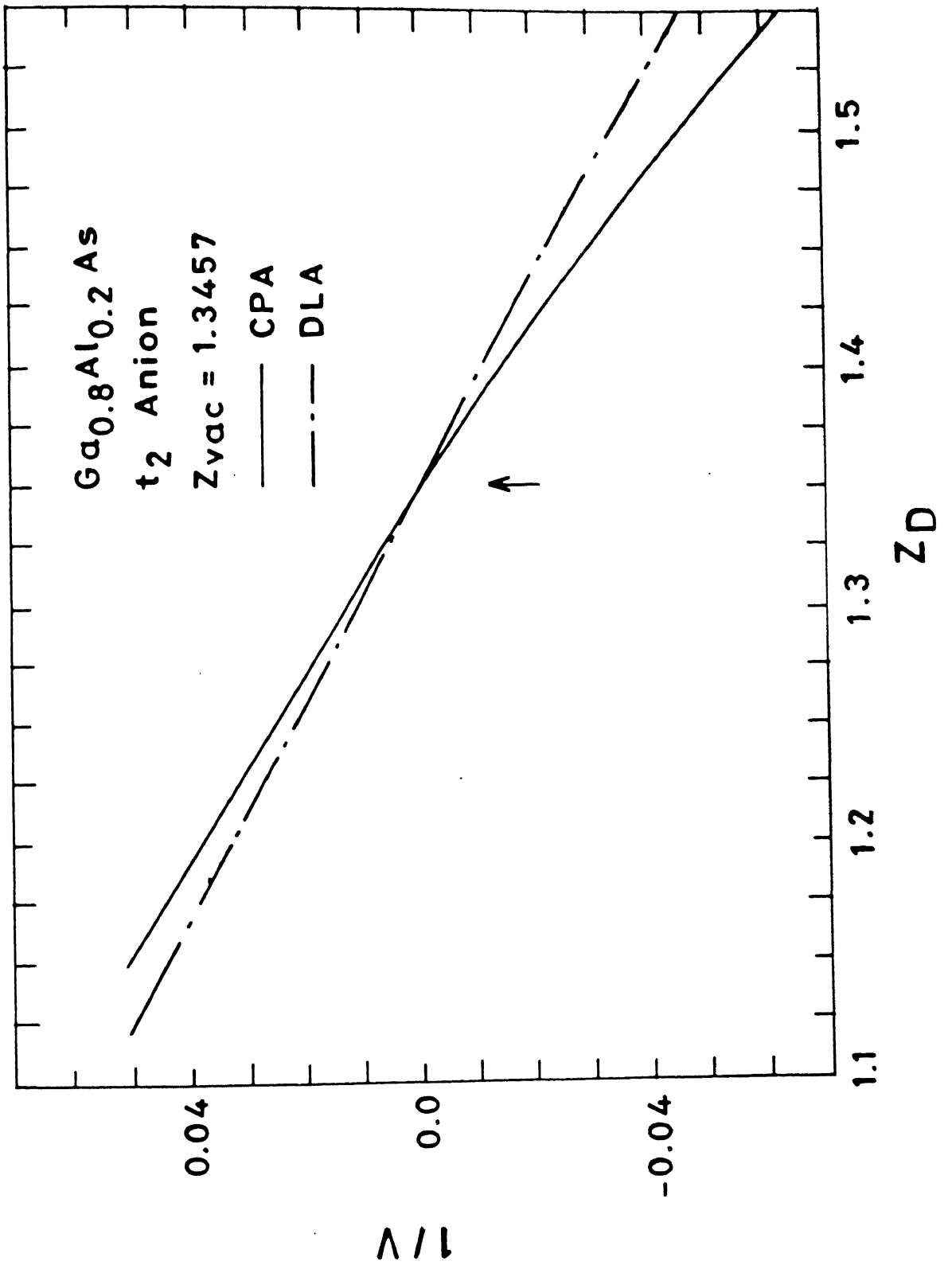
$Ga_{0.8}Al_{0.2}As$
t_2 Anion
Z_{vac} = 1.3457
CPA
DLA
1/V
0.04
0.0
-0.04
1.1
1.2
1.3
1.4
1.5
Z_D

FIGURE 3.2

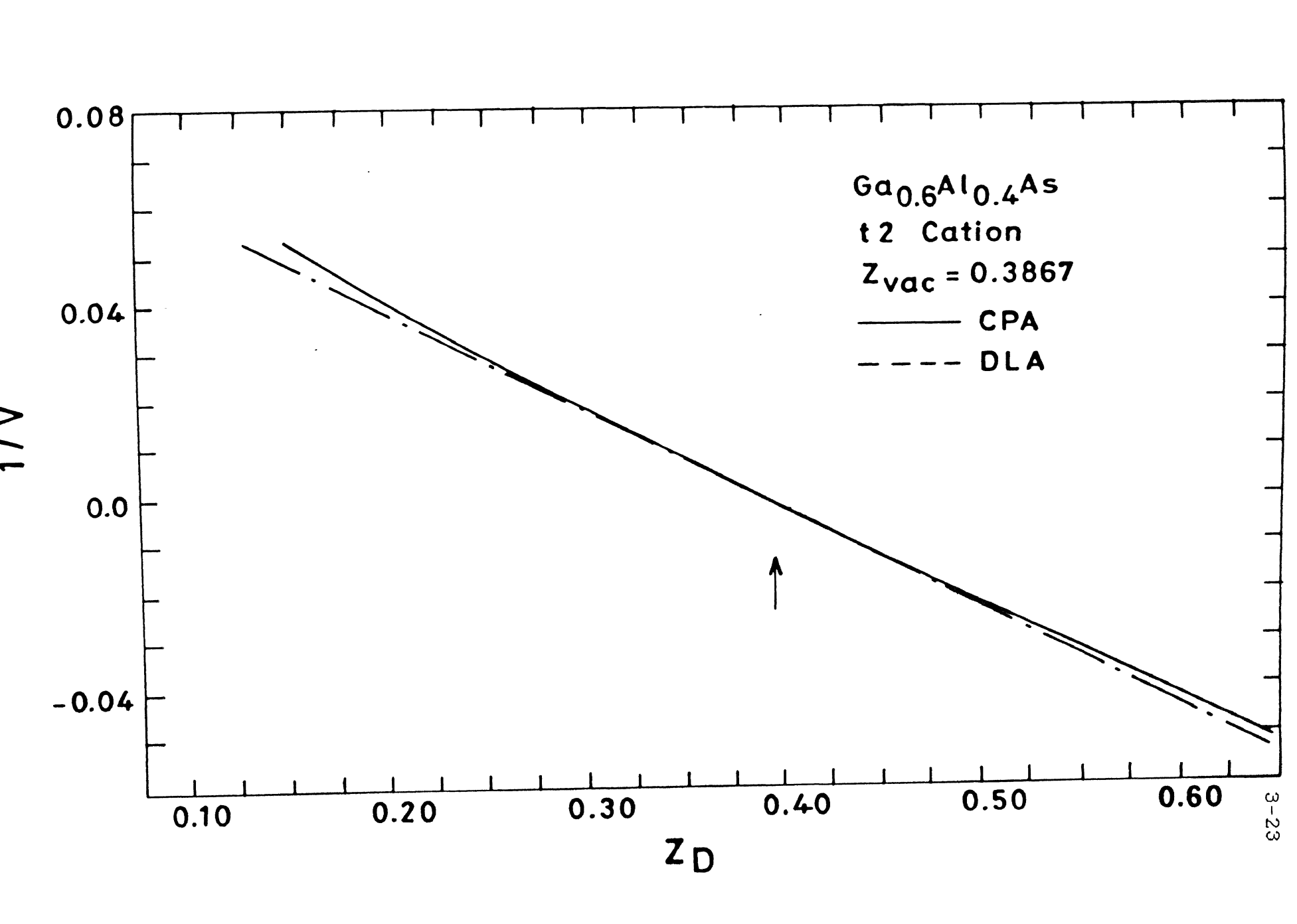
0.08
0.04
0.0
-0.04
1/V
0.10
0.20
0.30
0.40
0.50
0.60
Z_D
$Ga_{0.6}Al_{0.4}As$
t2 Cation
$Z_{vac} = 0.3867$
CPA
DLA
3-23

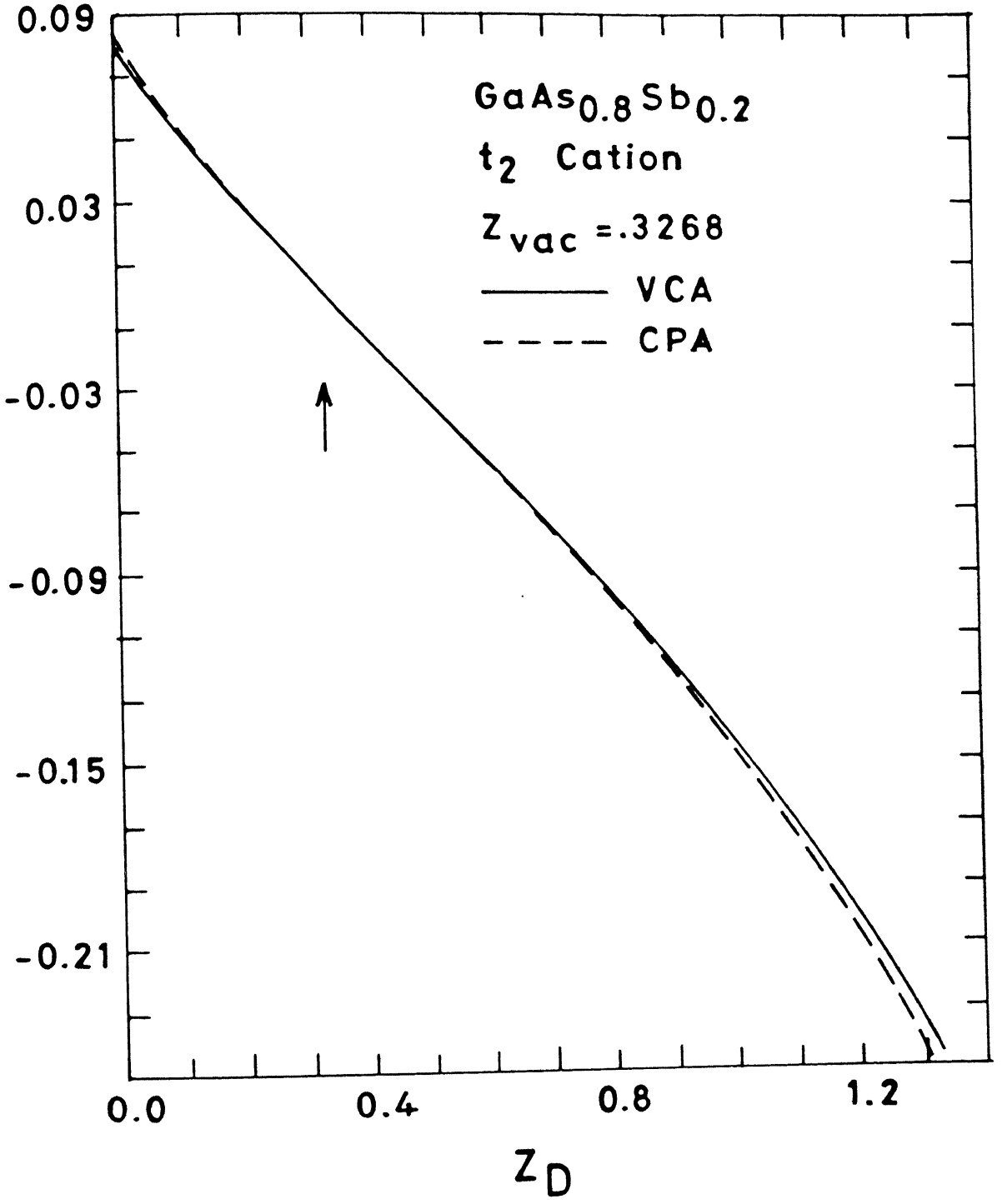
0.09
0.03
-0.03
-0.09
-0.15
-0.21
0.0
0.4
0.8
1.2
Z_D
$GaAs_{0.8}Sb_{0.2}$
t_2 Cation
Z_{vac} =.3268
VCA
CPA

FIGURE 3.4

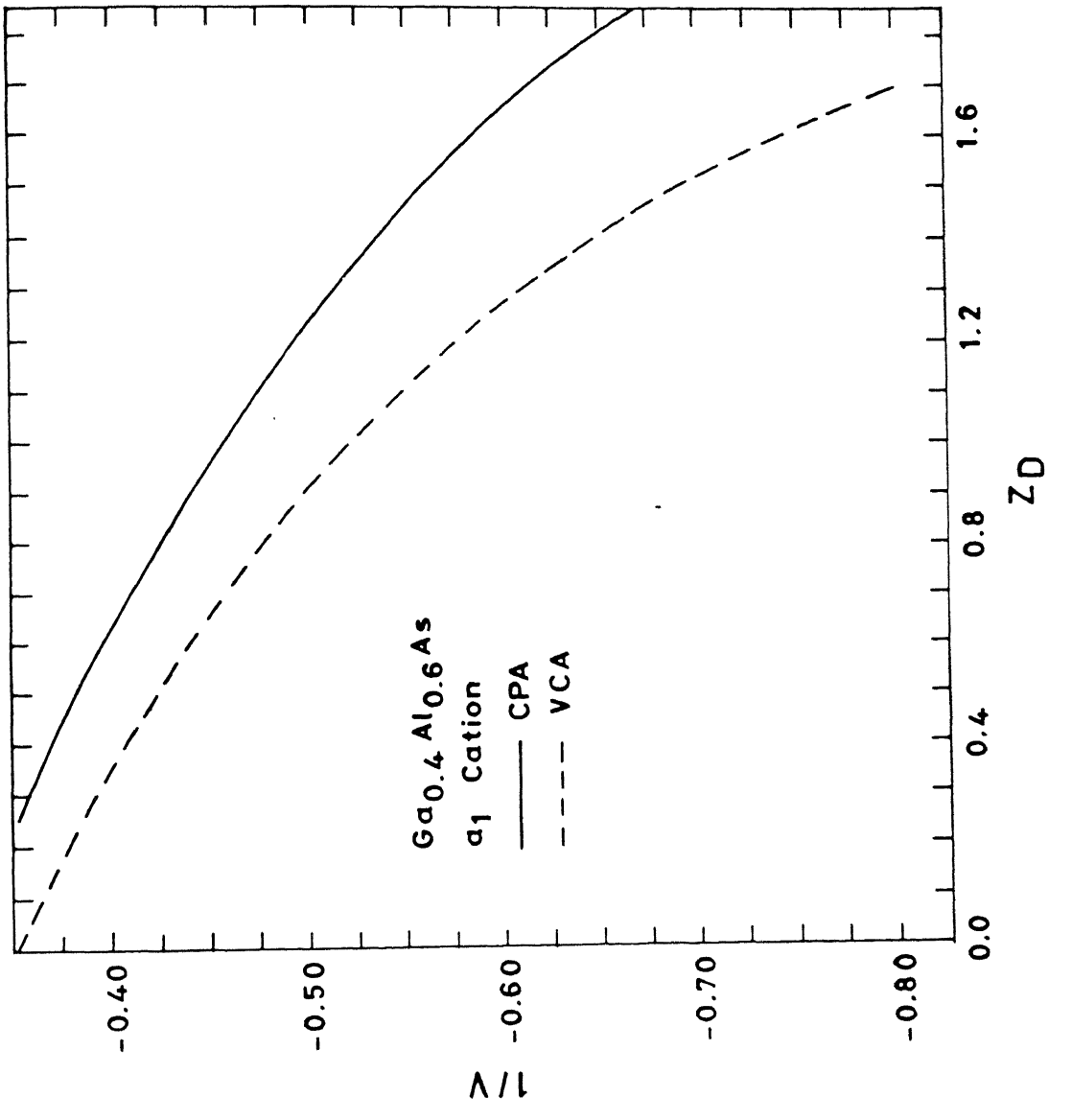
$Ga_{0.4}Al_{0.6}As$
a_1 Cation
CPA
VCA
1/λ
-0.40
-0.50
-0.60
-0.70
-0.80
Z_D
0.0
0.4
0.8
1.2
1.6

FIGURE 3.5

CHAPTER 4 : DX CENTER: SUBSTITUTIONAL DONOR DEFECT IN ALLOY SEMICONDUCTOR

4.1: Introduction

The DX center has attracted the attention of a large number of semiconductor physicists on account of its anomalous properties. The center, present in the alloy semiconductor $Ga_{1-x}Al_xAs$ presents a challenge both from a basic physics and a technological point of view.

The center as its name suggests is related to a donor impurity in $Ga_{1-x}Al_xAs$. Group VI impurities (S,Se,Te) as well as Group IV impurities (Si,Ge,Sn) in $Ga_{1-x}Al_xAs$ give rise to this defect. The concentration of this defect is approximately equal to the donor concentration ($N_{DX} \approx N_{Donor}$) and is independent of the method or condition of epitaxial growth.

The DX center exhibits divergent activation energies when probed thermally and optically, the latter being anomalously large. The energies reported depend also on the time scale over which the experiments are performed. The Hall activation energy E_T is distinct from the Deep Level Transient Spectroscopy (DLTS) activation energy E_e. The former is a slow equilibrium measurement while the latter is a relatively 'fast' non equilibrium process. Further, there is a barrier to capture (E_b) which leads to persistent photoconductivity (ppc) and consequent parasitic effects in the devices. Lang[1] has reviewed some of the salient

experimental features of the DX center recently.

This center has been reported in

(i) $Ga_{1-x}Al_xAs$ ($0.2 \leq x \leq 0.45$)

(ii) GaAs under pressure $\geq$ 20 kbar.

(iii) GaAs under heavy doping ($N_{Donor} > 10^{19}$ per cm^3)

Theories proposed to account for its peculiar characteristics fall into three categories.

(i) The large lattice relaxation model of Lang[2] et al.

(ii) The effective mass theory where the donor is presumed to be coupled to an energetically higher symmetry point (L or X) in the conduction band[3].

(iii) The alloy model where the substitutional disorder in $Ga_{1-x}Al_xAs$ is held to be primarily responsible for its anomalous behaviour[4].

It has been widely conjectured that the DX center is a donor vacancy complex. There is evidence however that the DX center is a simple substitutional donor and not a complex. Mizuta et al[5] have

argued for this model based on Hall effect and DLTS experiments. Morgan[6] has proposed that it is a simple substitutional donor which may be displaced albeit slightly from its normal centered position. Arguments based on coupling to L, X and Γ points all presuppose a substitutional impurity.

Our investigation is limited to this 'substitutional' premise. Within this paradigm we shall present calculations which are non perturbative and which self consistently account for the alloy disorder. The formalism is based on the tight binding Green's function method. It is well suited for cases where the defect is localized.

In section 4.2 we present experimental results with which we hope to compare our calculations. In section 4.3 we present our calculations and provide a discussion. Section 4.4 contains the conclusion.

4.2: Experimental Results

Table 4.1 depicts the thermal Hall energy E_T of the DX center in $Ga_{1-x}Al_xAs$ obtained by various workers. As the concentration of Al species increases, the band gap E_g increases and so does E_T. At $x = 0.45$, there is a cross over from the Γ point to the X point. A key result of the table is the value of $\Delta E_T/\Delta x \approx 700$ meV (Chand et al)[7]. We note in a similar work , Shubert and Ploog[8] quote E_T with a value diminished approximately by a factor of two. There also exists a parallel work on Sn by Basmaji[9] using

magnetoresistence with values of E_T roughly the same as the ones quoted in Table 4.1. No clear evidence of the DX center has been observed for Oxygen and Carbon. The values in Table 4.1 are those in which no hydrostatic pressure has been applied to the sample. The doping is also not excessive. Further there is a small but perceptible chemical trend : E_T for Si is larger than for Sn. Our endeavour will be to understand the trend with respect to the aluminium concentration in the host and also with the chemical characteristics of the donor species.

Table 4.2 gives the DLTS activation energies for Group IV and Group VI donors. A key result of Table 4.2 is the existence of clear chemical trends : the Group VI donors have a const E_e ($\approx$ 300 meV) while the Group IV impurities exhibit a monotonic decrease as we go down the column.

4.3: Theoretical Results

Our calculations are based on the Koster Slater formalism described in Chapter 2. The substitutional disorder on the cation site was taken into account using

(i) The virtual crystal approximation (VCA)

(ii) The single site Coherent Potential Approximation (CPA) as formulated by us.

These are described in earlier chapters.

We devote our attention to two systems: $Ga_{0.7}Al_{0.3}As$ (x=0.3) and $Ga_{0.6}Al_{0.4}As$ (x = 0.4). The band gap for these systems

obtained by using the Vogl[10] tight binding parameters are 1.8 eV and 1.95 eV respectively. These are in agreement with the experimental values quoted in Table 4.1.

The defect potential on the anion site is defined as

$$V_D = V_{ns} - \bar{V}_{as} \qquad (4.1)$$

Here V_{ns} is a shifted s-state ionization potential for the principal quantum number n of the donor species involved : n = 3,4 and 5 for S, Se and Te respectively. These ionization potentials are taken from the tables of Clementi and Roetti[11]. This value is shifted by a relatively constant value to define the zero of energy with respect to the vacuum and not with respect to the top of the valence band. $\bar{V}_{as}$ is simply the average s state anion As potential.

$$\bar{V}_{as} = (1 - x)\, E_{GaAs}(s,a) + (x)\, E_{AlAs}(s,a) \qquad (4.2)$$

The parameters E(s,a) are taken from Vogl[10] et al. Calculations presented are accurate upto 5 meV at best.

In figures 4.1 and 4.2 we plot the a_1 anion defect level as a function of the inverse potential ($1/V_D$). The latter is simply the diagonal Green's function (at the impurity site) as the Koster Slater equation would demand. The VCA and the CPA plots are nearly identical. This result is not surprising since the relevant input

parameters E(s,a) of GaAs and that of AlAs differ by less than 10%. The VCA is a good approximation under such circumstances.

Table 4.3 depicts the calculated impurity levels for the Group VI elements. For Te, the value of $E_C - E_D$ = 120 meV is in the same range as the experimental value of Hall energy E_T = 100 ($\pm$50) meV quoted in Table 4.1. The trend for increasing x is consistent with observation. Further the chemical trend is very weak . There is a reduction of only 15 meV as we go from S to Te. This is in conformity with the DLTS observations in Table 4.2. It is also borne out by Hall measurements[12].

The more interesting observations are for the cation donor species. Si is by far the most extensively studied DX center. We may define the a_1 cation defect potential in a manner analogous to equations (4.1) and (4.2). In figures 4.3 and 4.4 we plot the a_1 cation defect level as a function of inverse defect potential. The VCA and the CPA plots are different. This may be understood by examining the Vogl[10] input parameters E(s,c) of GaAs and AlAs. These differ by 80% .

Table 4.4 depicts the calculated impurity levels for the Group IV elements. The CPA values for Si and Sn are in good agreement with the experimental Hall activation energies E_T reported in Table 4.1. Further the average value of the slope obtained by us is $\Delta(E_C - E_D)/\Delta x \approx$ 700meV. Chand et al report an experimental value of $\Delta E_T/\Delta x$ = 707meV for Si. Moreover the chemical trend of a small but perceptible monotonic decrease in E_T

with increasing Z the atomic number (as we go down Group IV) is also borne out. The VCA results also exhibit this trend, but the absolute values of the activation energies as well as that of the slope $\Delta(E_C - E_D)/\Delta x$ are in poor agreement with the experiments.

4.4: Conclusion

The results of our CPA based calculations mimic the experimental Hall activation energies in terms of (i) Chemical trend as one donor species (S) substitutes another (Sn) (ii) The slope $\Delta E_T/\Delta x$. Both Group IV and Group VI impurities are well accounted for.

Our calculations show that the DX center is a level wlth a_1 symmetry. The calculations for the t_2 symmetry level has also been done and no correlation with the experimental values have been discerned. The work of Hjalmarson and Drummond[13] as well as Oshiyama and Ohnishi[14] also indicate that the DX center has a_1 symmetry. Equipped with this information about the DX state, the phenomenon of ppc (persistent photoconductivity) can be understood on the basis of symmetry arguments alone. $Ga_{1-x}Al_xAs$ is a direct band gap material when the aluminium concentration is less than 45% . So in this range of Al concentration the Γ point constitutes the minimum of the conduction band. The transition matrix element involves an operator which depends on position. This matrix element will be zero for a conduction band edge (Γ point) to DX state (a_1 type). Thus the carriers will have to get excited to a

higher state before they drop to the DX center defect level in the gap, resulting in persistent photoconductivity. However when the Al concentration is increased beyond 45% the X point takes over as the conduction band minimum. The X to a_1 transition is not forbidden and hence there should not be any persistent photoconductivity in this region. This is borne out by experiments[3,7]. This does not however rule out the possibility of a small distortion which has little effect on E_T and E_e, and results in persistent photoconductivity and large E_{opt}[3,7,13,14].

It would be interesting to explore the metastable characteristics of this defect by performing total energy calculations. The methodology using the Hellmann - Feynman theorem within the tight binding framework has been outlined in the second chapter. Pressure dependence also needs to be theoretically investigated. This task is reserved for future.

Further, the DX center has been found to be EPR invisible[15]. In view of this characteristic of the defect a negatively charged donor is plausible. This point is explored in the next chapter where we examine the band model for the DX center.

REFERENCES

1. D.V.Lang in "Deep Centers in Semiconductors" ed. S.T.Pantelides, Gorden and Bread. New York (1986).

2. D.V.Lang and R.A.Logan, Phys Rev Lett. 39 635-639 (1977); D.V.Logan and M.Jaros, Phys Rev B 19, 1015-1030 (1979).

3. A.K.Saxena , J Phys C 13 4323 (1980); Phys Stat Sol b105, 777 (1981)

4. T.N.Theis, B.D.Parker , P.M.Solomon and S.L.Wright, Appl Phys. Lett 49 , 1542, (1986) and references therein.

5. M.Mizuta, M. Tachikawa, H.Kukimoto, S.Minomura, Jpn. J. Appl Phys. 24 (1985)

6. T.N.Morgen Phys Rev B34, 2664-2669 (1986)

7. N.Chand, T.Henderson, J.Klein, W.T.Masselink, and P.Fisher Phys Rev B30, 4481 (1984).

8. E.F.Shubert and K Ploog, Phys Rev B30 7021 (1984)

9. Basmaji S.S.Commun 63 73 (1987)

10. P.Vogl, H.P.Hjalmarson and J.D.Dow 1983 J Phys Chem Sol 44 365.

11. E.Clementi and C.Roetti, Atomic and Nuclear Data Tables, 14 428 (1974).

12. B.M.Arora , Private Commun.

13. H.P.Hjalmarson and T.J.Drummond, Phys. Rev. Lett. 60, 2410 (1988), and Appl.Phys. Lett.48, 656 (1986).

14. A.Oshiyama and S.Ohnishi, Phys. Rev. B 33, 4320 (1986).

15. K.Khachaturyan, E.R.Weber and M.Kaminska (to be published).

TABLE : 4.1

Experimental Hall Energy E_T (meV) in $Ga_{1-x}Al_xAs$ as reported by several workers. Eg is the band gap in eV.

x	E_g (eV)	E_T(meV) Si (1)	E_T(meV) Sn (2)	E_T(meV) Te (3)
0.20	1.67	10	6	-
0.25	1.73	18	20	100 $\pm$ 50
0.30	1.80	66	40	-
0.35	1.86	108	65	-
0.40	1.92	140	120	-
0.45	1.98	150	130	-

References

1. Chand et al Phys Rev B30 4451 (1984).

2. Lifshitz and Jayaraman Phys Rev B21 670 (1980).

3. Lang and Jaros , Phys Rev B19 , 1015 (1979).

TABLE : 4.2

DLTS Activation Energies (eV) in $Ga_{1-x}Al_xAs$

Author	S	Se	Te	Si	Ge	Sn
Kumagai[1] x	0.28 (0.43)	0.28 (0.43)	0.28 (0.434)	0.43 (0.3)	0.33 (0.3)	0.21 (0.3)
Lang-Logan x	-	0.28 (0.4)	0.43 (0.4)	-	-	0.19 (0.4)
Wagner[3]	-	0.32	-	-	-	-
Zhou[4] et al	-	-	-	0.44	-	-
Kunzel[5]	-	-	-	0.41	-	-

References

1. O. Kumagai, H.Kawai, Y.Mo. and K.Kaneko Appl Phys Lett 45 1322-1323 (1984).

2. D.V.Lang, R.A.Logan Phys Rev Lett 39 635 1977; Inst Phys Conf Ser No 43 , 433 (1979)

3. E.E.Wagner J. Appl. Phys 51 5435 (1980).

4. B.L.Zhou Appl Phys A 28 223 (1982).

5. H.Kunzel Appl Phys A32 69 (1983).

TABLE : 4.3

The calculated a_1 anion defect level in $Ga_{1-x}Al_xAs$. The CPA and the VCA are nearly identical, hence only the CPA results are shown.

$\overline{V_{as}}$ = -8.09 eV for x = 0.3, and -8.02 eV for x = 0.4 .

Donor	V_{ns} (eV)	CPA: $E_c - E_D$ x = 0.3(meV)	CPA: $E_c - E_D$ x = 0.4(meV)
S	-21.513	135	145
Se	-21.060	130	135
Te	-20.750	120	130

TABLE : 4.4

The calculated a_1 cation defect levels in $Ga_{1-x}Al_xAs$. Both the CPA and the VCA results are shown. $\overline{V_{cs}}$ = -2.21 eV (x = 0.3) and -2.06eV (x = 0.4).

Donor	(x = 0.3) CPA	(x = 0.3) VCA	(x = 0.4) CPA	(x = 0.4) VCA
Si	70	290	150	400
Ge	55	270	120	390
Sn	40	260	100	370

FIGURE CAPTIONS

Figure 4.1: Plot of inverse defect potential strength vs. the a_1 anion defect level in $Ga_{0.6}Al_{0.4}As$ as obtained by CPA (——) and VCA (----).

Figure 4.2: Similar to figure 4.1 except that the Al concentration in this case is 30% .

Figure 4.3: Similar to figure 4.1 except that in this case the defect is at the cation site.

Figure 4.4: Similar to figure 4.2 but with the defect at the cation site.

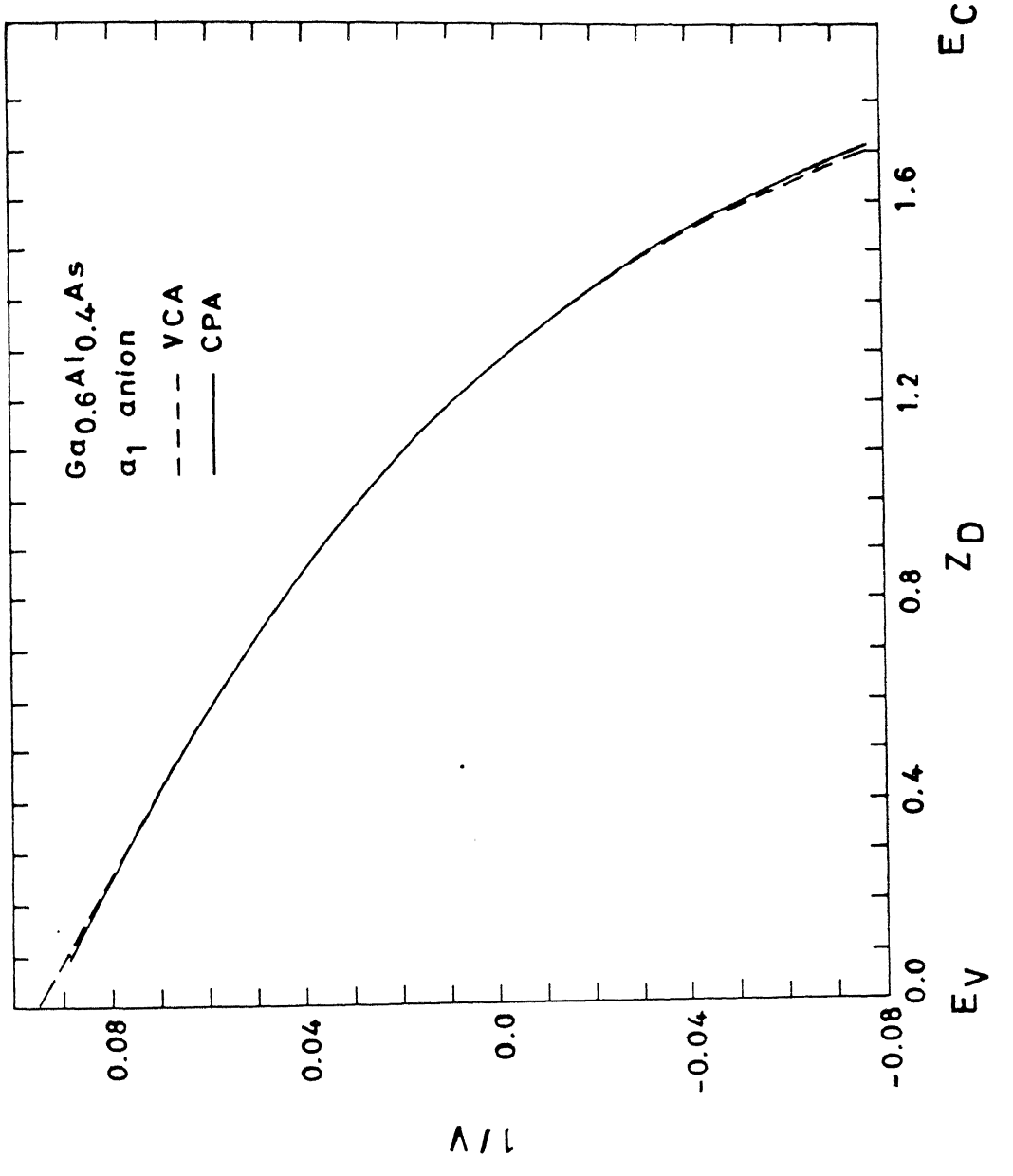
$Ga_{0.6}Al_{0.4}As$
a_1 anion
VCA
CPA
E_C
E_V
Z_D
1/V
0.08
0.04
0.0
-0.04
-0.08
0.0
0.4
0.8
1.2
1.6

FIGURE 4.1

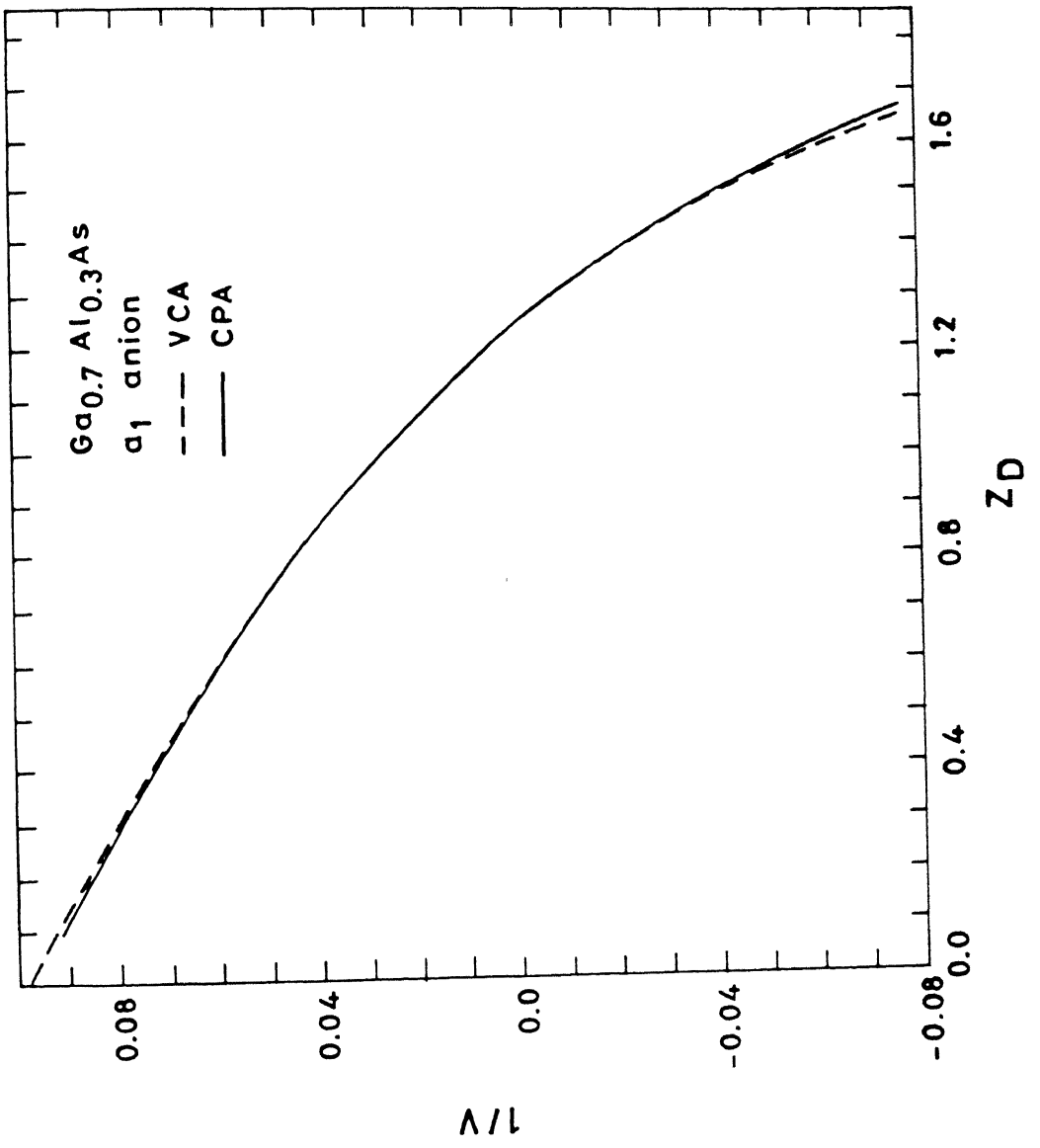
$Ga_{0.7}Al_{0.3}As$
a_1 anion
VCA
CPA
0.08
0.04
0.0
-0.04
-0.08
1/V
0.0
0.4
0.8
1.2
1.6
Z_D

FIGURE 4.2

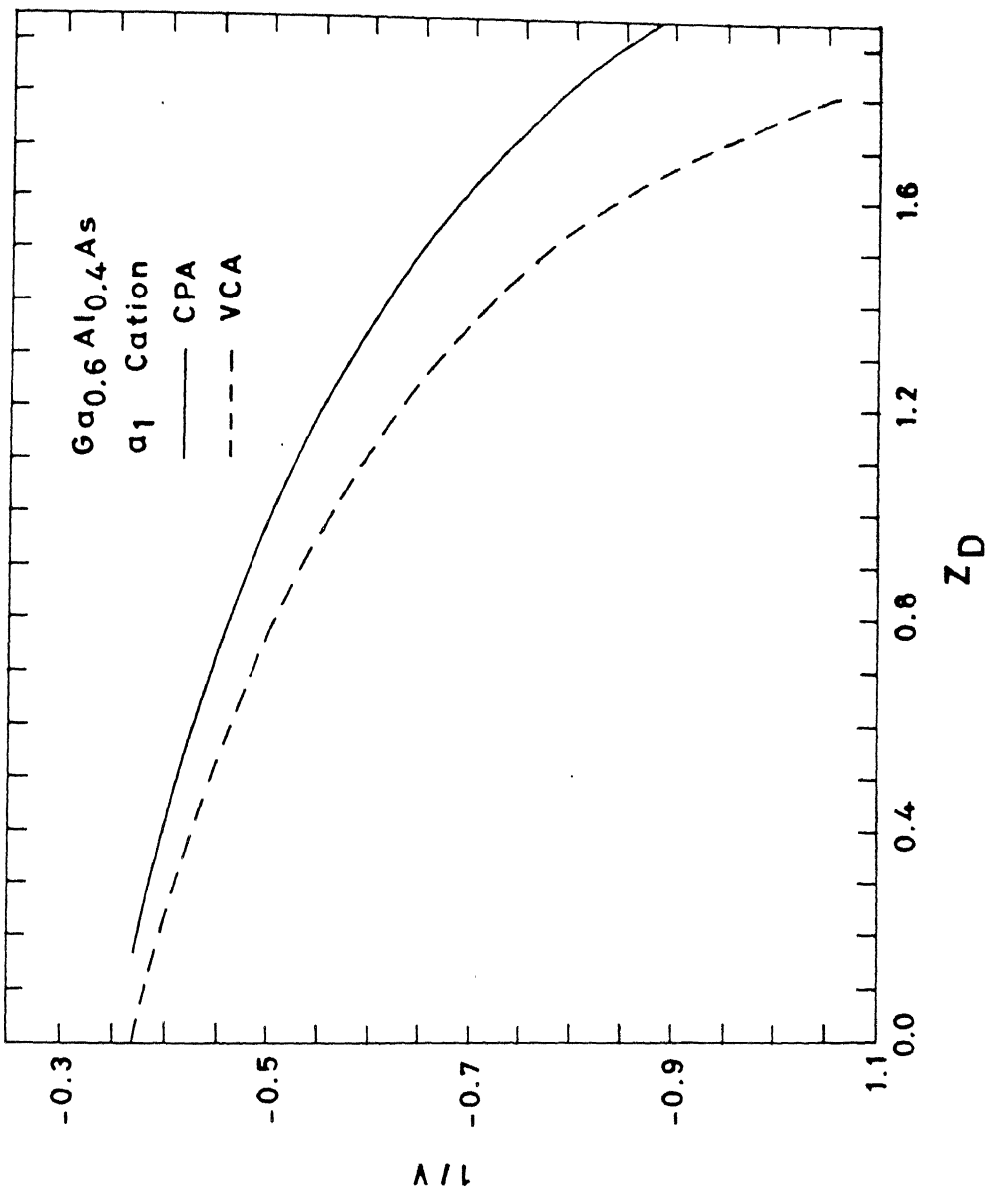

FIGURE 4.3

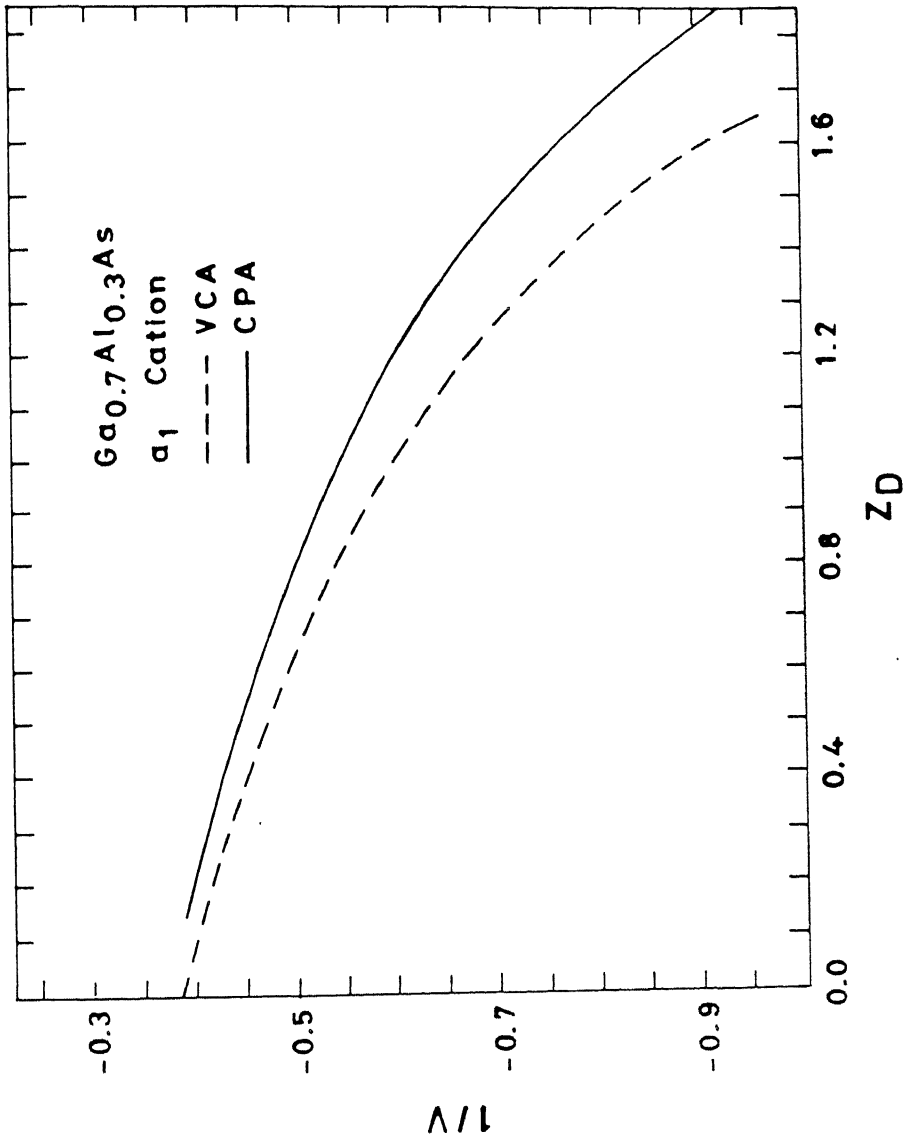

FIGURE 4.4

CHAPTER 5 : MANY ELECTRON EFFECTS IN THE EFFECTIVE MASS THEORY

5.1: Introduction

In this chapter we consider many electron effects in the context of Effective Mass Theory (EMT)[1]. We apply EMT theory for helium like impurities in the semiconductor matrix. This model is relevant to the chalcogens and some noble metal impurities in silicon. The discussion of helium like impurities is also relevant to anti-site defects in III - V semiconductors, a currently popular model for EL2 in GaAs[2]. It is further relevant to the study of DX center in $Ga_{1-x}Al_xAs$ as this defect is presently being viewed by several authors as a negatively charged center[3].

We present here a brief outline of the effective mass formalism. A perfect crystal can be described by an effective one electron Hamiltonian as

$$H_o = T + V_o \tag{5.1}$$

Where

$$T = - \hbar^2/2m_o \nabla^2$$

is the kinetic energy and V_o is the potential energy term, which has the full symmetry of the lattice. The corresponding eigenvalue problem is

$$H_o \psi^o_{nk} = E^o_{nk} \psi^o_{nk}$$

Here k is the wave vector and n is the band index.

A crystal with an isolated defect (dilute doping in semiconductors) can also be described in one electron approximation by a Hamiltonian H

$$H = T + V$$

Here V is the new one electron potential and it may be written as

$$V = V_o + U$$

So

$$H = H_o + U$$

Here U is the defect potential. The eigenvalue problem for an imperfect crystal is

$$H \psi_\nu = E \psi_\nu$$

We will be interested in those energies E_ν which are within the forbidden band gap. These bound state energies will be dealt within the framework of EMT.

Theoretically it is possible to expand the bound state eigen function ψ_ν in terms of all Bloch functions. However, to simplify the task, the effective mass approximation is invoked. Pertaining to a given physical situation it enables us to consider

only a few conduction band states in terms of which the bound state is expressed.

The detailed derivation of the effective mass equation in reciprocal space has been given by several authors[4]. However, the nature of the approximation involved in this theory can be understood by the following simplified model of the defect.

Consider a substitutional donor which has one excess nuclear charge +e relative to the host and one excess valence electron. In view of the great stability of covalent bonding all electrons of the impurity atom except one will be engaged in bonding. This extra electron experiences a potential of the excess nuclear charge +e on the impurity. In vacuum this is exactly the situation of hydrogen atom. However, in a solid some modifications are needed for the Schrödinger equation pertaining to this problem. They are as follows

(i) The nuclear charge +e polarizes the solid, leading to dielectric screening. Thus, the potential experienced by the excess electron is $-e^2/\varepsilon r$ instead of $-e^2/r$. Here ε is the static dielectric constant of the solid.

(ii) In the hydrogen atom the origin of energy is taken to be at infinite separation where the electron becomes free. Here the lowest energy at which the electron becomes free is the bottom of the conduction band E_c. Hence E_c is chosen to be the origin of the energy.

(iii) A free electron in vacuum propagates with its own mass m. However, in a solid the presence of periodic potential influences

this propagation. This is taken into account by introducing the concept of effective mass m^* .

Thus the Schrödinger equation for this excess electron is

$$\left\{ -\frac{\hbar^2}{2m^*}\nabla^2 + \frac{e^2}{\varepsilon r} \right\} \psi = (E - E_c)\,\psi \qquad (5.2)$$

For those impurities which have two excess electrons relative to the host atom the problem is similar to the helium atom. Consequently, the Schrödinger equation for these two excess electrons will be

$$\left\{ -\frac{\hbar^2}{2m^*}(\nabla_1^2 + \nabla_2^2) - \frac{Z'e^2}{\varepsilon r_1} - \frac{Z'e^2}{\varepsilon r_2} + \frac{e^2}{\varepsilon r_{12}} \right\} \psi = (E - E_c)\,\psi \qquad (5.3)$$

Here Z' is the excess nuclear charge. Note that for negatively charged center (as is the case of DX) the excess nuclear charge will not be equal to the excess number of electrons. The above equations are valid for one band with one extremum.

The effective mass equation for a band with several extrema was first derived by Twose (reported by Fritzsche)[5]. If one neglects the intervalley mixing, then each minima can be considered as being independent of others. One obtains the usual effective mass equation for each minima separately with the effective mass tensor corresponding to that particular minima. If however, all the minima are equivalent then the effective mass

tensors corresponding to all the extrema will be identical leading to a degenerate level in the gap. The degeneracy of the level is the same as the number of equivalent minima. This degeneracy is lifted by incorporating the intervalley mixing. There are several ways of incorporating this effect. One such approach is the conventional first order perturbation theory described by Bourgoin and Lannoo[6]. Resca and Resta[7] have shown that in the case of intervalley mixing the effective Schrödinger equation of the envelope wave function associated with the donor is the potential V(r) modulated by a spatial renormalization factor $|\phi(0,r)|^2$. We will be neglecting the intervalley mixing effect in all our calculations.

In section 5.2 we present our formalism for treating helium like impurities. Section 5.3 contains results. Section 5.4 constitutes the conclusion.

5.2: Formalism

A great deal of work has been done on hydrogenic EMT. However, a corresponding effective mass theory for helium like impurities as defined in section 5.1, remains to be explored.

The helium like impurities were first treated by Glodeanu[8] in the framework of EMT. He employed a fitting procedure for Z, the excess nuclear charge to account for the chemical shift observed experimentally. The defect level energy was obtained by a variational treatment of the Hamiltonian. Our endeavour will be to account for the chemical shift in this many body problem. We will

consider the impurity to be surrounded by a sphere of cavity radius r_o. The influence of the impurity within the cavity is unscreened by the medium, hence inside the cavity the electron experiences the unscreened Coulomb potential of the excess nuclear charge. Beyond this cavity the medium dominates and the potential due to excess nuclear charge is only partially experienced by the electron.

The potential energy function can be divided into the following three regions:

$$V_I = - \frac{Ze^2}{\varepsilon_o r_1} - \frac{Ze^2}{\varepsilon_o r_2} + \frac{2Ze^2}{\varepsilon_o r_o} \left[1 - \varepsilon_o/\varepsilon \right] \qquad (5.4)$$

for $r_1 \;\&\; r_2 < r_o$

$$V_{II} = 2\left[-\frac{Ze^2}{\varepsilon_o r_1} - \frac{Ze^2}{\varepsilon\, r_2} + \frac{Ze^2}{\varepsilon_o r_o} \left[1 - \varepsilon_o/\varepsilon \right] \right] \qquad (5.5)$$

for $r_1 < r_o \;\&\; r_2 > r_o$

$$V_{III} = -\frac{Ze^2}{\varepsilon\, r_1} - \frac{Ze^2}{\varepsilon\, r_2} \qquad (5.6)$$

for $r_1 \;\&\; r_2 > r_o$

The above equations give the potential experienced by the electron excluding the interaction term, which will be dealt with later. Here ε_o and ε are the dielectric constant for the vacuum and the medium respectively. The third term in V_I and V_{II} has been added specifically to make the potential continuous at the boundaries of the three regions. Note that this term is a constant. The interaction term $e^2/\varepsilon' r_{12}$ (where $\varepsilon' = \varepsilon_o$ or ε depending on the values of r_1 and r_2) can not be made continuous by a mere addition of a constant term. However, for a given probability charge distribution $|\psi|^2 e$ of a particular electron the potential experienced by the other electron can be made continuous.

The above problem was solved using two types of trial functions. The results in both the cases were found to be in fair agreement with each other.

In the first case the trial function was chosen to be the product of two hydrogen atom wave functions

$$\psi(r_1, r_2) = 1/\pi\,(\eta/a)^3 \exp(-\eta r_1/a) \exp(-\eta r_2/a) \qquad (5.7)$$

Here η is the variational parameter. The electron electron interaction was chosen to be $e^2/\varepsilon_o r_{12}$ when both r_1 and r_2 were less than r_o and $e^2/\varepsilon r_{12}$ otherwise. The potential experienced by one electron due to the probability distribution of the form $|(1/\pi)^{1/2}\,(\eta/a)^{3/2}\exp(-\eta r_1/a)|^2$ of the other electron can be made continuous at the boundary of the cavity by the addition of a term

dependent on 'η' .

The average value of the Hamiltonian in the state $\psi(r_1, r_2)$ is evaluated analytically. Newton Raphson method is employed next, to find the value of the parameter η at which the energy is minimum.

Figure 5.1 exhibits a typical plot of ground state binding energy per electron as a function of the cavity radius r_o. Here ε and m^* are taken to be 10 and 0.5 respectively. The energy level is shallow for small values of r_o. At r_o equal to 1.4 a.u there is a crossover from shallow to deep level. This shallow to deep instability is often encountered in experimental situations (see section 5.3). It may be understood simply: when r_o the cavity radius is relatively large, the electron is in a free atom environment. When r_o is small, the semiconductor matrix dominates. The crossover point r_{oc} is found to be a monotonic increasing function of ε and monotonic decreasing function of m^*. The effective mass of GaAs is less than that of AlAs, and the static dielectric constant of GaAs is more than that of AlAs. This results in lowering of r_{oc} as one goes towards higher concentration of Al in $Ga_{1-x}Al_xAs$.

The behaviour of energy with respect to the cavity radius r_o is similar in spirit to that observed by Bourgoin and Mauger[9] in the context of hydrogenic EMT with a cavity. The above choice of trial function has been employed to arrive at the results of section 5.3.

In the second case the trial function is chosen to be the linear combination of two standard variational solutions for

helium atom immersed in vacuum and in the medium. They are as follows.

$$\phi_1(r_1,r_2) = 1/\pi\ (\eta_1/a)^3\ \exp(-\eta_1 r_1/a)\ \exp(-\eta_1 r_2/a) \qquad (5.8)$$

$$\phi_2(r_1,r_2) = 1/\pi\ (\eta_2/a)^3\ \exp(-\eta_2 r_1/a)\ \exp(-\eta_2 r_2/a) \qquad (5.9)$$

where $\eta_1 = (Z-5/16)$

and $\eta_2 = (Z-5/16)m^* \varepsilon_o/m\ \varepsilon$

The trial function is

$$\psi(r_1,r_2) = C_1\phi_1 + C_2\phi_2 \qquad (5.10)$$

This choice of trial function is similar in spirit to Reiss[10]. He has chosen a similar trial function to solve the problem of hydrogenic EMT with a cavity.

In this case the expansion coefficient is the variational parameter. When r_o is zero the situation is similar to helium atom immersed in the medium with no cavity. In this case C_1 is found to be zero and C_2 is unity. Similarly when r_o is infinity implying that there is no effect of the medium, C_2 is found to be zero and C_1 is unity. For an intermediate value of r_o both terms have non zero coefficients.

In the second method the potential experienced by one electron due to the electron electron interaction term cannot be made continuous for both ϕ_1 and ϕ_2 simultaneously by adding the same constant. Hence, the dielectric constant was taken to be ε

throughout for this particular derivation. The expectation value of the Hamiltonian in the two states ϕ_1 and ϕ_2 can be obtained once again analytically.

Defining

$$H_{11} = \langle \phi_1 | H | \phi_1 \rangle$$
$$H_{22} = \langle \phi_2 | H | \phi_2 \rangle$$
$$H_{12} = \langle \phi_1 | H | \phi_2 \rangle$$
$$H_{21} = \langle \phi_2 | H | \phi_1 \rangle$$
$$\Delta_{21} = \langle \phi_2 | \phi_1 \rangle$$

The ground state energy is obtained from the solution of the following equation.

$$\begin{vmatrix} H_{11} - E & H_{21} - \Delta_{21}E \\ H_{12} - \Delta_{21}E & H_{22} - E \end{vmatrix} \qquad (5,11)$$

Figure 5.2 shows a typical plot for the ground state energy per electron vs. the cavity radius r_o for this particular derivation. The result agrees with that of case 1, implying thereby that an approximate treatment of the interaction term is fairly justified in this context. Small changes in this term do not alter the result drastically.

5.3: Applications

5.3a: Chalcogen Donors in Silicon

The chalcogen donor level in silicon is six fold degenerate. Since the chalcogen occupies a substitutional site, the overall symmetry is tetrahedral (T_d). The symmetry is broken by the central cell potential and is also known as valley-orbit splitting. The six fold degeneracy is thus lifted to a singlet a_1, a triplet t_2 and a doublet e. The singlet a_1 is the lowest. Spin orbit effects further split the t_2 level to Γ_8 (doubly) degenerate and Γ_7 (non - degenerate). Stray fields are responsible for lifting the degeneracy of the doublet states e and Γ_8.

The experimental situation has been exhaustively reviewed by Grimmeiss and Janzen[11]. The chalcogen species S, Se, Te have been known to introduce two distinct levels. The deeper level known as the A-center is now identified with the ionized impurity atom, e.g. S^+, Se^+ or Te^+. The shallower ones, labelled B-center correspond to the neutral species S^o, Se^o, Te^o.

Our calculations will focus on the neutral B-center. Further, only the ground state energy is considered. Table 5.1 depicts the current experimental status of the chalcogen species in Si (excluding Oxygen). For completeness, we also display the energies attributed to chalcogen related defects. Our interest is confined to the second column of Table 5.1. The calculation of excited state energies, for example $(1s - a_1) \longrightarrow (1s - t_2)$ within effective mass theory can be performed.[12] We would, however, first

like to examine the ground state energies within our proposed cavity model described in section 5.2.

In figure 5.3 we plot the double donor level of Si as a function of cavity radius. The cavity radius has been expressed in units of the nearest neighbour distance r_{nn} for silicon (r_{nn}= 4.43 a.u). Figure 5.3 shows that there is very little change in the position of the defect level as the cavity radius is increased upto approximately 0.665 times r_{nn}. This is the region where the medium dominates. Beyond this as one increases the cavity radius, the position of the defect level shifts very rapidly, the energy level curve shows a very steep change and the level becomes deeper.

Our endeavour will be to explain the results of column 2 of table 5.1 within the framework of EMT. We need an appropriate value of the cavity radius for different chemical species that are depicted in table 5.2. One method of determining the cavity radii is to employ the innermost orbitals of the doubly ionized atomic species. We define an average size of the doubly ionized species as

$$\langle r_{av} \rangle = \sum_i \langle r_i \rangle n_i \; / \; \sum_i n_i$$

Where, for sulphur (S^{++}) 'i' is equal to 1s, 2s, 2p, 3s, 3p; for selenium (Se^{++}) 'i' is 1s, 2s, 2p, 3s, 3p, 3d, 4s, 4p; and for Tellurium (Te^{++}) 'i' is 1s, 2s, 2p, 3s, 3p, 3d, 4s, 4p, 4d, 5s, 5p. These radii have n_i as 1 for s, 3 for p and 5 for d. For the outermost valence p-orbital n_i is 1. These radii are tabulated in

table 5.2. Note that these are distinct from the neutral atomic radii. The latter increases with atomic number Z and primarily determines valence based solid state properties. The core radii in table 5.2 are typical of the atom and not of the solid.

The agreement between the calculated and the observed values is fair. For impurities like sulphur, selenium and tellurium, whose core radii are found to be larger than the crossover cavity radius r_{oc}, the error range for the defect energy is found to be large. Due to the steep rise of the defect energy as a function of r_o, a difference of 0.001 a.u in the value of $\langle r_{av} \rangle$ can give rise to a difference of about 0.05 eV in the defect energy. Thus a rounding error for $\langle r_{av} \rangle$ even at the third decimal place gives rise to an error of about $\pm$ 0.05 eV in energy. In this context the results reported for Magnesium are fairly accurate. The energy curve at the core radius of magnesium is fairly steady. Thus minor differences in determining the core radius do not get reflected in the defect level energy.

5.3b: The DX Center: A Negatively Charged Donor

As mentioned in the concluding section of chapter 4 the DX center defect which is found in $Ga_{1-x}Al_xAs$ is EPR invisible. In view of this characteristic it is conjectured that this defect is due to a negatively charged donor[3]. A negatively charged donor will have two electrons in excess to the host atom which it substitutes. Hence, the analysis of section 5.2 is applicable for an investigation of this situation.

We present preliminary results. Figure 5.4 depicts the donor level as the function of cavity radius for $Ga_{0.7}Al_{0.3}As$. The Γ band related donor level is uniformly shallow. The X band donor level is the deepest, being deeper than the L band. There appears to be no unique way of fixing the cavity radius for the negatively charged center. If for the sake of argument we fix the cavity radius at a value of approximately half the nearest neighbour distance (say $r_o \approx 3$a.u) then figure 5.4 predicts a DX level tied to the L band and positioned approximately at 300 meV below the conduction band. There is a shallow level tied to the Γ band. The defect level tied to the X band is inside the valence band. The same value of r_o for GaAs (in figure 5.5) leads to two shallow levels which track Γ and L band respectively. The level due to X band is nevertheless inside the valence band.

In this context it is worthwhile quoting a similar work based on EMT by done Burgoin and Mauger[9] for single electron donors. They have incorporated the multivalley mixing effect of several equivalent minima for X as well as L bands. Due to this intervalley mixing effect the L derived state with a_1 symmetry is found to be deeper than the X derived state of the same symmetry.

We have shown above that a simple cavity model without incorporating the correction due to intervalley mixing can explain the L band tracking of the DX state. Further, the conjecture of it being a negative center, put forward to explain the EPR invisibility is also borne out by our calculations.

5.3c: The EL2 Center: an Anti-site Defect

EL2 is the commonest native deep defect in GaAs. It is called the main electron trap. It is conjectured that it is an anti-site defect namely, arsenic on the cation gallium site (As_{Ga}). Calculations using the Koster Slater equation have reported this defect to be deep.

It is clear, however, that As_{Ga} is a substitutional helium like donor. Hence it is worthwhile applying the analysis of section 5.2 to this problem. Figure 5.4 represents the plot of a double donor level with respect to the cavity radius r_o. We note that the nearest neighbour distance in GaAs is $r_{nn} \approx 5.6$ a.u. A cavity radius of about $r_o \approx 4r_{nn}$ yields a deep level at the mid gap. Thus our calculations show that an effective mass approach to the problem can possibly explain the deep level characteristic of the EL2 level.

5.3d: Double Donor in $Ga_{1-x}Al_xAs$

In this context it is interesting to observe that as we approach AlAs the double donor level becomes deep more readily (e.g at a lesser value of r_o). This can be seen by examining the plot of $Ga_{0.55}Al_{0.45}As$ in figure 5.7 and comparing it with the plot of GaAs in figure 5.6. In figure 5.7 the crossover from shallow to deep defect level starts when the cavity radius is around 7 a.u whereas for pure GaAs it occurs at about 11.4 a.u.

Fixing the cavity radius at a particular value one observes that the donor level gets deeper from the conduction band as the

aluminium concentration is increased from 0.0 to 0.45 (see figure 5.8). For aluminium concentration higher than 0.45 the X band takes over as the minimum of the conduction band. Thus beyond x = 0.45 an analysis relevant to the X band needs to be done to view the trend of the double donor defect level with aluminium concentration. For aluminium concentration less than 45% we see that the same impurity (characterized by a particular cavity radius) will give rise to an increasingly deep level in the environment of increased aluminium concentration. We believe that similar trends will be observed for hydrogenic donor impurities.

5.4: Conclusion

In this chapter we have proposed a simple cavity model Effective Mass Theory for helium atom and have applied it to several problems of interest.

We have studied the chalcogen impurities in silicon and have obtained results which agree well with experimental values. Further the DX center, which is currently being viewed as a negatively charged center due to its EPR invisibility, has also been studied using this methodology. Our results do not rule out such a possibility. However, a firm statement in favour of such a conjecture cannot be made since the cavity radius in this case remains an empirical parameter.

The anti-site defect in GaAs has also been treated. We have found that for a reasonable value of the cavity radius, the theoretical results agree with the experimental values for the EL2

defect center, suggesting thereby that it could be an anti-site defect. We have also shown that the double donor level in $Ga_{1-x}Al_xAs$ will become increasingly deep with increased Al concentration. Similar trends can also be discerned for single donor impurities in $Ga_{1-x}Al_xAs$.

Thus, even a simple theoretical model of helium atom within a cavity can be successfully employed for several semiconductor problems.

REFERENCES

1. J.M.Luttinger and W.Kohn, Phys.Rev. 97, 969 (1955).

2. G.A.Baraff and M.Schluter, Phys. Rev. Lett. 55, 2340 (1985).

3. K.Khachaturyan, E.R.Weber and M.Kaminska, to be published.

4. W.Kohn, Solid State Physics 5, 257 (1957); S.T.Pantelides, Rev. Mod. Phys 50, 797 (1978).

5. H.Fritzsche, Phys. Rev. 125, 1560 (1962).

6. M.Lanoo and J.Bourgoin. "Point defects in Semiconductors-I Theoretical Aspects", Springer Verlag series in Solid State Physics 22.

7. L.Resca and R.Resta, Solid State Commun. 29, 275 (1979).

8. A.Glodeanu, Phys. Stat. Sol. 19, K43 (1967).

9. J.C.Bourgoin and A.Mauger, Appl. Phys. Lett. 53, (9), 749 (1988).

10. H.Reiss, J. Chem. Phys. 25, 681 (1956).

11. H.G.Grimmeiss and E.Janzen, "Deep Centers in Semiconductors," ed S.T.Pantelides, Gorden and Breach Science Publishers 87 (1986).

12. M.Altarelli, Proc 16th Int. Conf. Phys. of Semiconductors Montpellier 22 (1981). Ed M.Averous, North-Holland Amsterdam (1983).

13. A.G.Milnes Deep Impurities in Semiconductors Wiley, N.Y (1973)

TABLE 5.1

Ground state binding energies in eV of chalcogen isolated substitutional atoms (D), chalcogen pairs (D_2) and chalcogen related defects (D_c).

DEFECT	D^o	D^+	D_2^o	D_2^+	D_c^o	D_c^+
S	0.32	0.61	0.19	0.37	0.11 0.16	
Se	0.31	0.59	0.21	0.39	0.12	0.21
Te	0.20	0.41				

REFERENCE

H.G.Grimmeiss and B.Skerstom, Phys. Rev. B 23, 1947 (1981).

TABLE 5.2

The core radii $\langle r \rangle_{av}$ of the chalcogen impurities and of Mg in atomic units. The calculated binding energies E_b are read off from figure 5.3 associating $\langle r \rangle_{av}$ with cavity radius r_o. The experimental binding energies are taken from Table 5.1 and reference cited therein. For Mg, the experimental value is the one reported by Milnes. The binding energies are in eV.

IMPURITY	CORE RADIUS $\langle r \rangle_{av}$	E_b THEORETICAL	E_b EXPERIMENTAL
S	3.037	0.33 ($\pm$ 0.04)	0.32
Se	3.016	0.29 ($\pm$ 0.04)	0.31
Te	2.980	0.188	0.20
Mg	2.527	0.9092	0.11

REFERENCE

A.G.Milnes "Deep Impurities in Semiconductors" Wiley, N.Y. (1973).

FIGURE CAPTIONS

Figure 5.1: A typical plot of ground state binding energy per electron vs. the cavity radius r_o. The dielectric constant and the effective mass of the electron is taken as $10\epsilon_o$ and $0.5m_e$ respectively. This particular plot is for the product trial function described by equation 5.7. Note the steep rise of the binding energy for $r_o \geq 1.4$ a.u.

Figure 5.2: Similar to figure 5.1 except that the trial function in this case is described by a linear combination as described in equation 5.10. Note the steep rise in the binding energy for $r_o \geq 1.4$ a.u.

Figure 5.3: Plot of double donor level in silicon as a function of cavity radius. The cavity radius has been expressed in units of nearest neighbour distance of silicon ($r_{nn} = 4.43$ a.u). Note the sharp rise in the binding energy at around $0.665\ r_{nn}$.

Figure 5.4: Plot of a negatively charged donor level in $Ga_{0.7}Al_{0.3}As$ as a function of cavity radius r_o. The crossover behaviour occurs at different values of r_o for levels tied to the X and L bands. There is no crossover behaviour for the Γ band for reasonable values of r_o.

Figure 5.5: Similar to figure 5.4. The system in this case is

GaAs. The Γ band result remains parallel and is very close to the x axis.

Figure 5.6: Plot of binding energy per electron for a double donor defect level in GaAs. The level is for the Γ band. The crossover occurs for a large value of the cavity radius.

Figure 5.7: Similar to figure 5.6 for $Ga_{0.55}Al_{0.45}As$.

Figure 5.8: The shaded lines in the figure represent the conduction and the valence bands as the Al concentration is increased from 0% to 45%. The continuous line shows the plot of a typical defect level characterized by the cavity radius r_o = 10 a.u. Note that the level deepens as the Al concentration is increased.

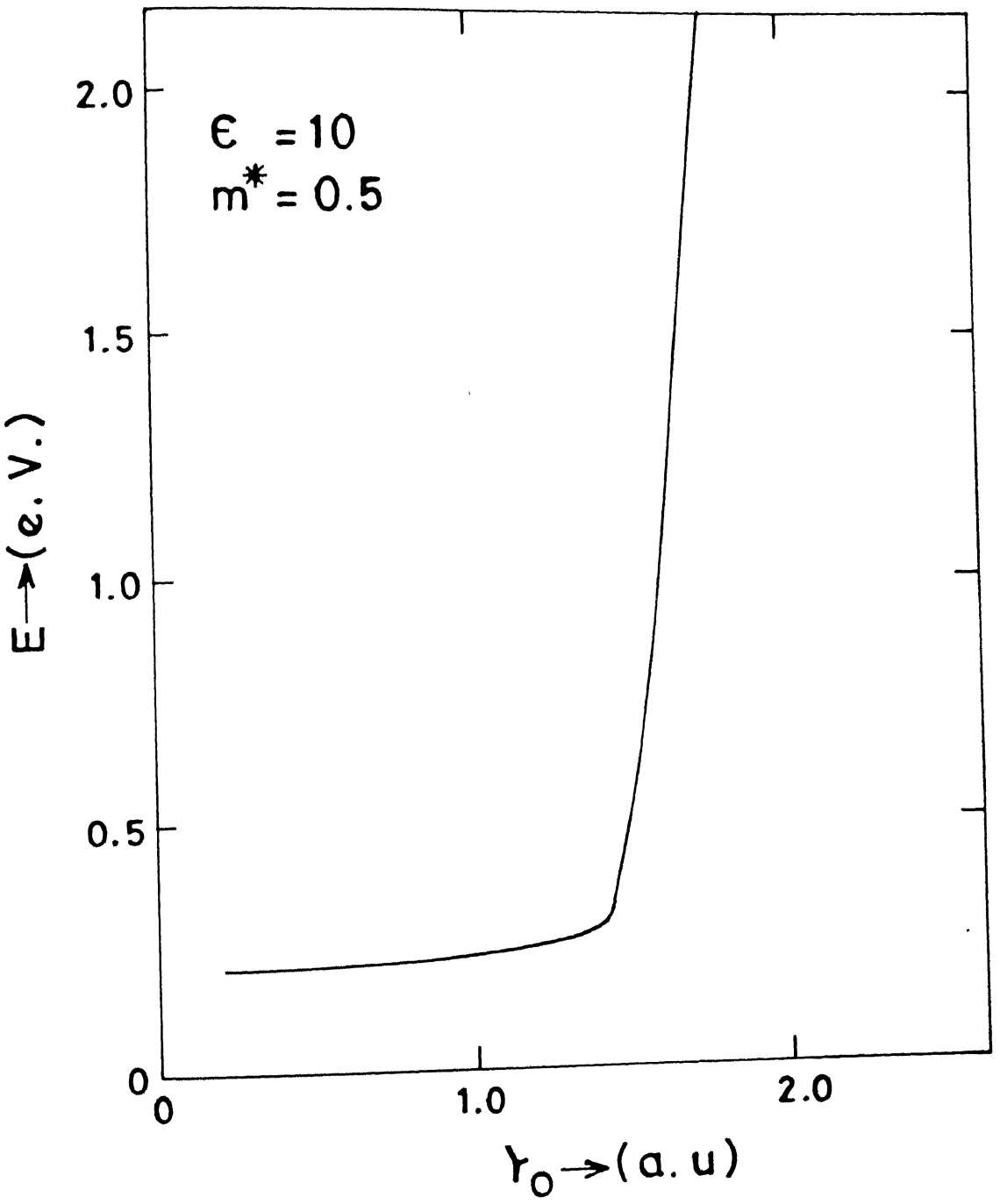

FIGURE 5.1

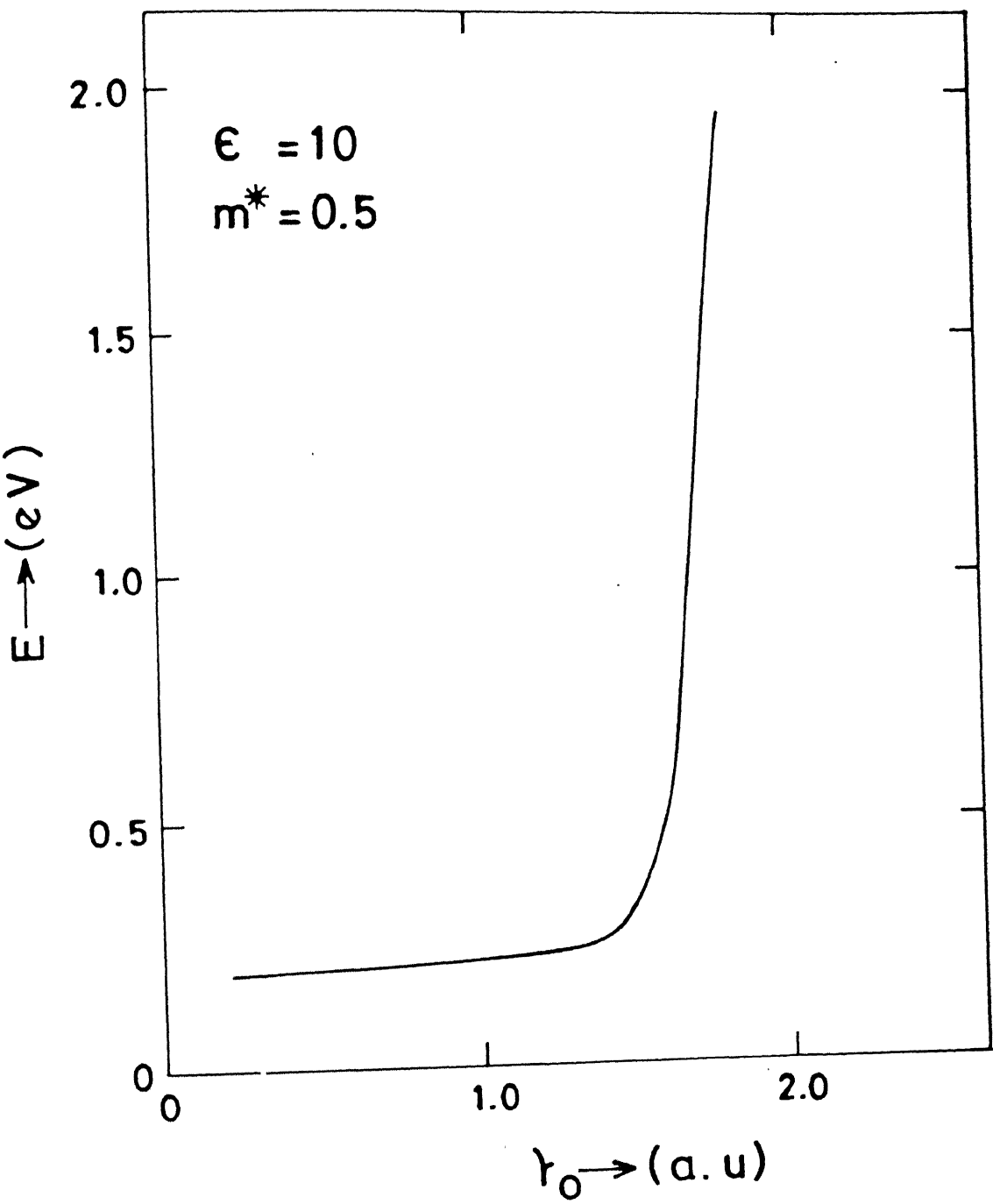

FIGURE 5.2

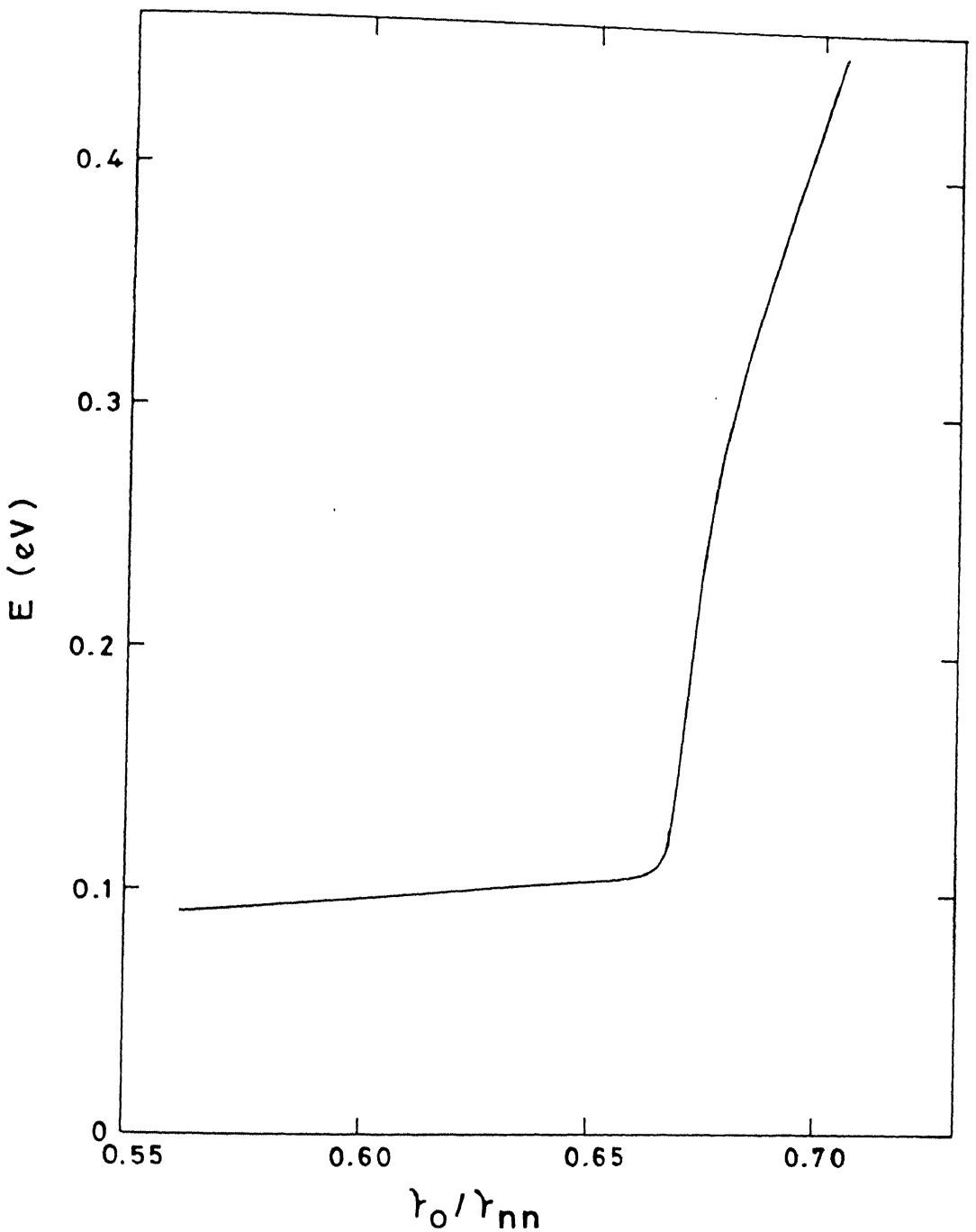

FIGURE 5.3

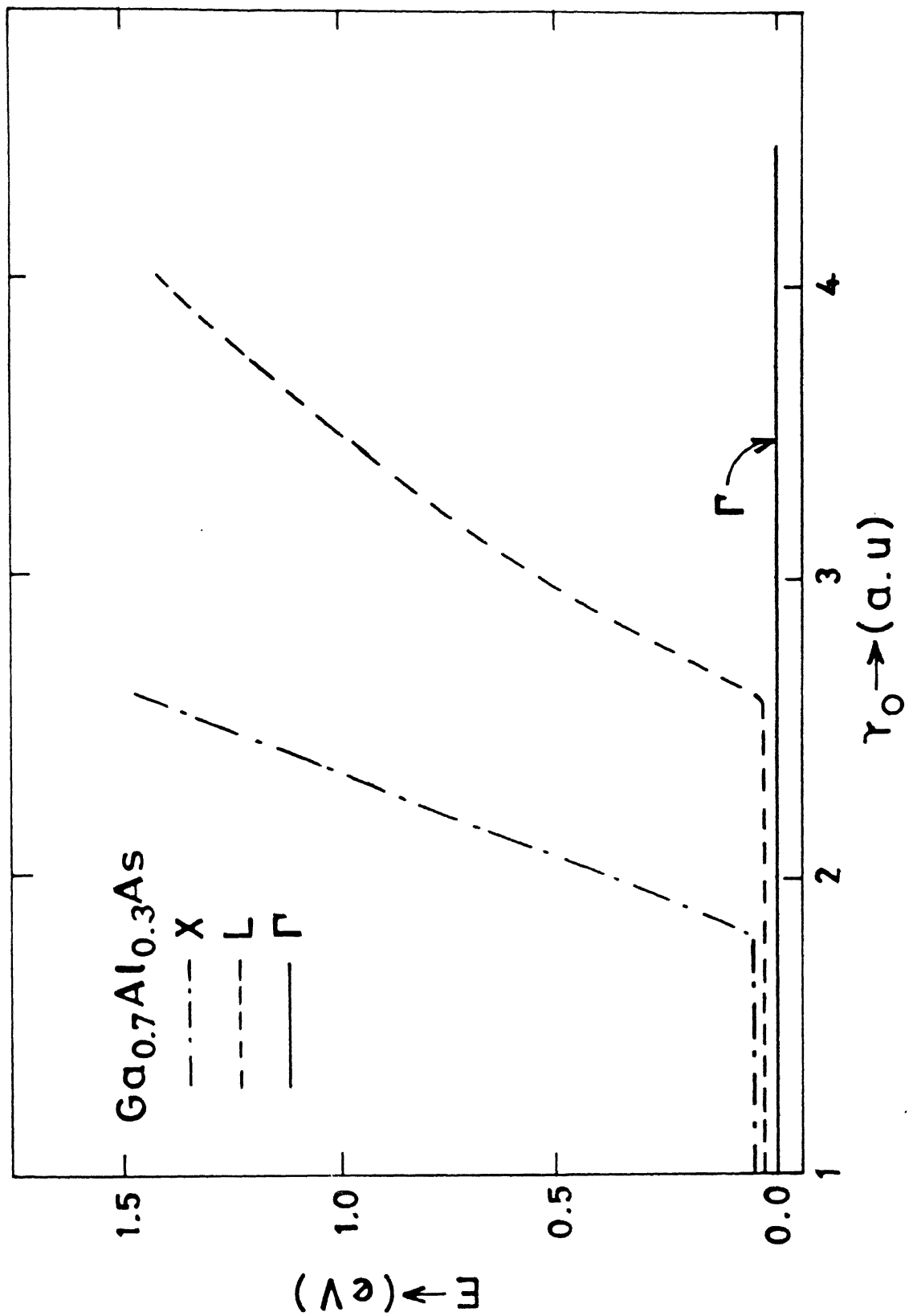

FIGURE 5.4

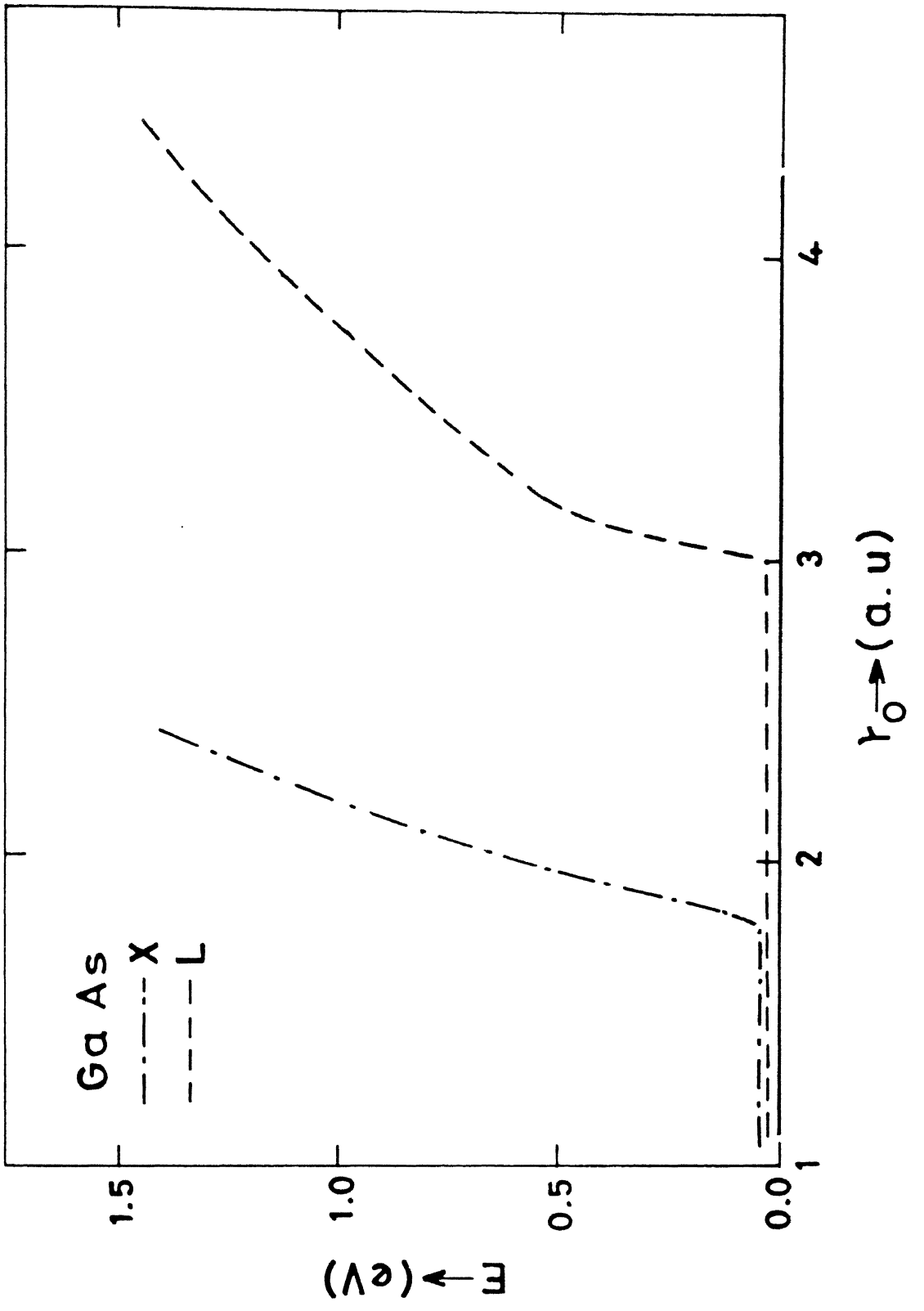

FIGURE 5.5

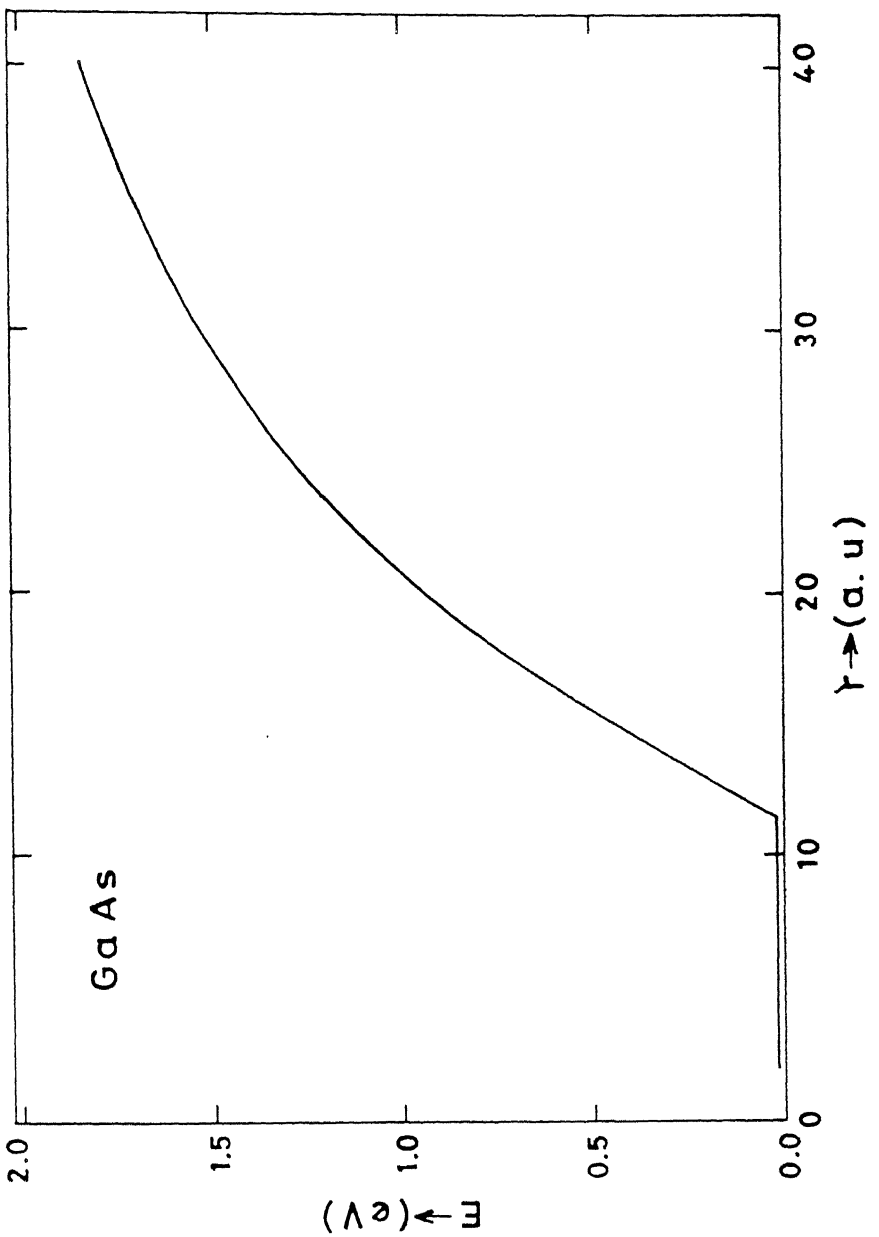

FIGURE 5.6

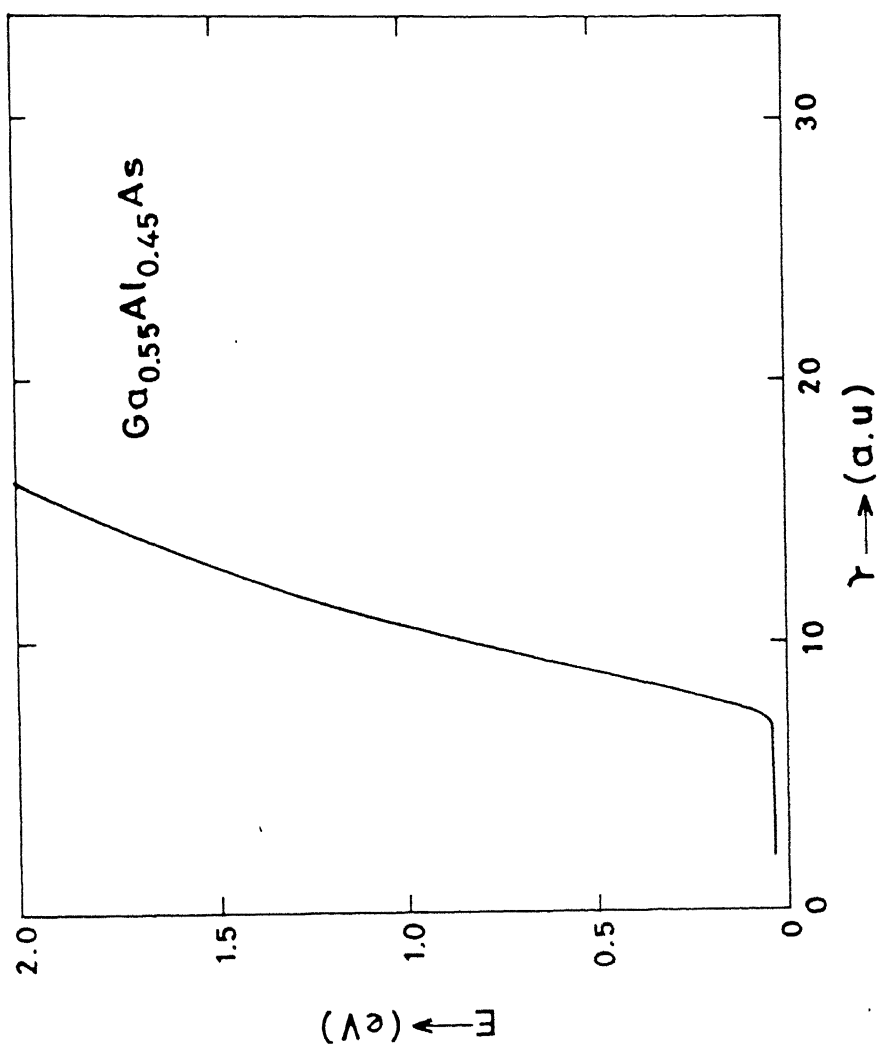

FIGURE 5.7

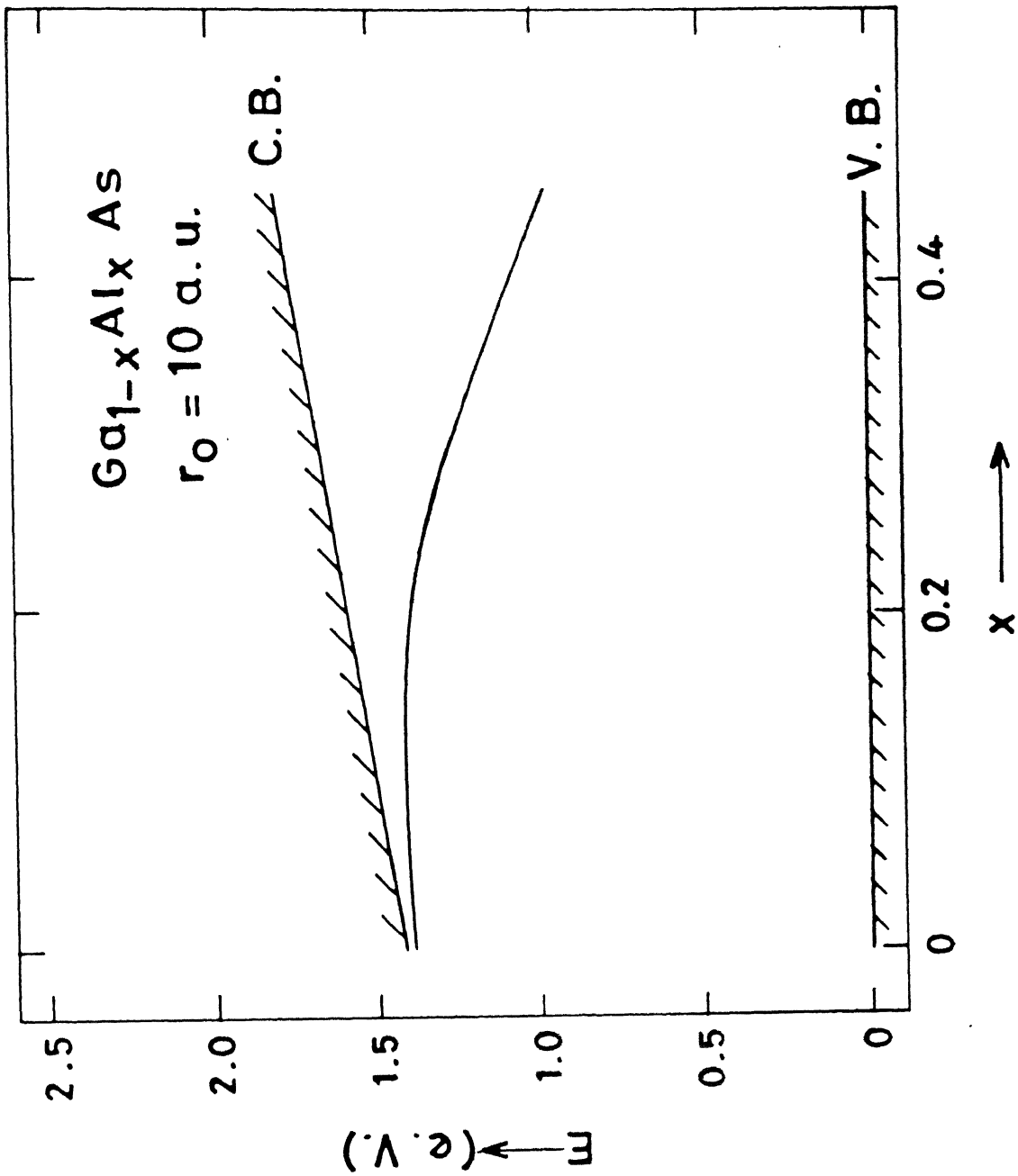

FIGURE 5.8

CHAPTER 6: EFFECT OF DISORDER IN THE ANALYSIS OF EXPERIMENTS

6.1: Introduction

Deep level transient spectroscopy (DLTS)[1] has been widely used over the past ten years as a tool to study deep levels in semiconductors. The context of the original proposal was that of defect states with well defined energy levels in crystalline host materials. In the past few years there has been considerable work on systems where either the host or the defect is disordered. In such cases the DLTS spectrum may be broadened and the underlying capacitance or current transient may be non-exponential. Nevertheless, in most cases, the standard DLTS expression derived for exponential transients is used to analyse the data. In this chapter we analyse the effect of gaussian broadening of a deep level energy spectrum on the DLTS signal. We show that in all cases except extreme broadening the standard DLTS analysis introduces negligible error. We shall also discuss the effect of disorder on techniques complementary to DLTS, in particular Paired Temperature Spectroscopy (PATS). Thr interplay between metastability and disorder in the interpretation of the above mentioned experimental techniques is also discussed.

A semiconductor alloy, e.g. $Ga_{1-x}Al_xAs$, may be considered to be a substitutionally disordered system. $Ga_{1-x}Al_xAs$ has a basic

zinc-blende structure where the cation site is occupied by Ga or Al atoms. The occupancy is essentially random if the probability that a given cation site is occupied by a Ga(Al) atom is 1-x(x). However, fluctuations from the mean occupancy are possible. These fluctuations arise due to a variety of causes. Some of them are: (i) the Pauling electronegativity difference between Ga and As is 0.4 while the difference between Al and As is 0.5, thus favouring Al as a neighbour of As. (ii) local inhomogeneities such as the presence of voids and anti-site defects. These can result in local deviations from the equilibrium concentration. A defect level in the fundamental gap of the semiconductor may be identified with its corresponding defect potential via the Koster-Slater equation as mentioned in earlier chapters. For the reasons discussed above, the defect potential in a semiconductor alloy has fluctuations which cause the delta function like gap level to be broadened.

There exists a growing body of experimental data on gap levels in semiconductor alloys. Some of these indicate the existence of potential fluctuations and consequent broadening of the gap level. In the present chapter we shall discuss this broadened gap level in the context of DLTS[1] and other complementary techniques. Let us mention briefly experimental work other than DLTS, which indicates the existence of broadening. Mooney and co-workers[2] have studied the kinetics of charge trapping in semiconductor alloys and have hypothesised a distribution of energy levels and capture cross sections. Raman

spectroscopy, too, suggests the importance of alloy potential fluctuations[3]. Samuelson et al[4] have attributed the splitting of photoluminescence lines of Cu in $GaAs_{1-x}P_x$ to alloy potential fluctuations.

Over the past few years there has been a growing body of literature on DLTS studies of disordered systems. Omling et al[5] have studied the broadened DLTS spectra in $GaAs_{1-x}P_x$. Murawala[6], Singh[7] and co-workers have discussed the broadening of the E3-like level in $GaAs_{1-x}Sb_x$. Kanieswka and Kanieswka[8] have similarly studied the main electron trap in $GaAs_{1-x}P_x$. Lang[9] and co-workers have studied the gap states in amorphous hydrogenated silicon (a-Si:H) where the disorder-induced broadening is expected to be more pronounced than in semiconductor alloys.

Under ideal conditions, the capacitance transient C(t) of deep level is a simple exponential[1,10]

$$C(t) = C_0 \exp(-t/\tau) \qquad (6.1a)$$

$$1/\tau = AT^2 \exp(-E/kT) \qquad (6.1b)$$

Here E is the activation energy and A is related to the capture cross section of the deep level under consideration. T is the temperature, k the Boltzmann constant and τ is referred to as the time constant. For the case of a broadened defect level the most general expression has been considered by Singh[7]

$$C(t) = \frac{C_o}{2\pi\sigma\sigma_1}\int_o^{E_g} dE \int_o^{\infty} dA \times \exp\left[-\frac{(E - E_o)}{2\sigma^2} - \frac{(A - A_o)}{2\sigma_1^2} - \frac{t}{\tau(A,E)}\right]$$

In the above expression the effect of the potential fluctuations on both the activation energy and the capture cross section has been taken into account. The broadening assumed is gaussian with a mean at E_o and A_o, and the half width at half maximum (HWHM) of approximately σ and σ_1 respectively. A detailed examination[7] has indicated that the broadening in the quantity related to the capture cross section may be ignored. We then obtain

$$C(t) = \frac{C_o}{(2\pi\sigma^2)^{1/2}}\int dE \exp\left\{-\frac{(E - E_o)}{2\sigma^2} - \frac{t}{\tau(E)}\right\} \qquad (6.2)$$

This expression has been widely employed in recent years[5-8]. In this chapter we first demonstrate how expression (6.2) implies a long lived and non-exponential capacitance transient. We demonstrate this by independent analytical and numerical work. Next, and more importantly, we show under what conditions the standard interpretation of DLTS data is valid for a broadened gap level. At this juncture we will define the term 'standard interpretation'. The time constant for the apparent peak of a DLTS signal was shown by Lang to be[1]

$$1/\tau_m = \frac{\ln(t_2/t_1)}{t_2 - t_1} \qquad (6.3)$$

This expression contains no information on the broadening or smearing factor σ. The use of this expression for extracting the defect parameters (activation energy and the pre-exponent A) will be deemed the standard interpretation.

We identify the natural scales in the problem:

$$\varepsilon = E_o/kT \qquad (6.4a)$$

$$s = \sigma/E_o \qquad (6.4b)$$

$$b = \sigma/kT \qquad (6.4c)$$

Unless the level is very shallow, we have $\varepsilon >> 1$ and this scale shall not concern us henceforth. If the potential fluctuations are small, then s and b in equation (6.4) will be small. We shall call the case { $b<1$, $s<0.1$ } the weak disorder case. The regime {$b\geq1$, $s\geq0.1$ } will be deemed the strong disorder case. We predict significantly different behaviour for these two cases.

A complementary technique for defect analysis based on capacitance transients was first proposed by Singh et al[11]. It is Paired Temperature Spectroscopy (PATS). In PATS the signal is defined as a function of time and its value is the difference between the transients at two temperatures. The major advantage of this technique is that it does not need a continuous thermal scan; two to three fixed temperature baths are sufficient for this purpose. The fixed temperature permits the use of signal averaging

and an enhanced signal to noise ratio can be achieved. The peak of the PATS signal occurs at a time

$$t_m = \frac{\ln(\tau_1/\tau_2)}{(1/\tau_1 - 1/\tau_2)}$$

In section 6.2 we treat the case of weak disorder {b<1, s< 0.01}. We show that the capacitance transient is weakly non-exponential. We validate the standard DLTS analysis based on equation(6.3). In section 6.3, where we treat the strong disorder case {b ≥ 1, s ≥ 0.1}, the transient capacitance is highly non-exponential, akin to glassy and spin-glass relaxation. Further, we demonstrate that the standard DLTS analysis will systematically overestimate the activation energy in cases of severe broadening. In section 6.4 we apply our experience of the previous two sections to two realistic cases: a-Si:H previously studied by Lang et al[9] and an E3 like level in $GaAs_{0.86}Sb_{0.14}$ previously studied by Murawala et al[6].

As noted in chapter 4 the DX center as well as several other defects are metastable. In section 6.5 we present a novel analysis of the DLTS peak heights for a metastable species in the presence of disorder. Section 6.6 encapsulates our conclusions on related phenomena.

6.2: Analysis for Weak Disorder

We first consider the weak disorder case {$b = \sigma/kT < 1$, $\sigma/E_o < 0.1$} in DLTS. As σ tends to zero the distribution approaches a delta function $\delta(E - E_o)$. We are then justified in expanding the exponential term in the integrand of equation (6.2)

$$\exp(-E/kT) = \exp(-E_o/kT)\exp(-(E-E_o)/kT)$$
$$\approx \exp(-E_o/kT)\times[1-(E-E_o)/kT + (E-E_o)^2/2(kT)^2]$$

Defining

$$1/\tau_o = AT^2 \exp(-E_o/kT) \qquad (6.5)$$

$$C(t) = C_o \exp(-t/\tau_o) \qquad (6.6)$$

equation (6.2) becomes

$$C(t) \approx C(t) \int_o^{Eg} \frac{dE}{(2\pi\sigma^2)^{1/2}} \exp\left[- \frac{1}{\sigma^2} \left\{ \frac{(E-E_o)^2}{2} - \frac{t(E-E_o)\sigma^2}{kT\ \tau_o} + \ldots \right\} \right]$$

We now apply the stationary point formula to the above integral. Given

$$I(\alpha) = \int \exp(-\alpha\phi(E))dE$$

the formula[12] states that for large α

$$I(\alpha) \approx (2\pi)^{1/2}\exp(- \alpha\phi(Ep))/| - \alpha\phi''(Ep) |^{1/2}$$

where Ep represents the minima of $\phi(E)$. Application of this prescription yields

$$C(t) = Co \exp \left[- \frac{t}{\tau o} + \frac{0.5(\sigma t/kT\tau o)}{1 +(\sigma/kT)^2 t/\tau o} \right] \Big/ [1+(\sigma/kT)^2 t/\tau o] \quad (6.7)$$

Equation (6.7) is our modified formula for the case of weak disorder. Note that for the case σ tends to zero we regain the exponential expression (6.6) for the ideal transient.

For a DLTS analysis we construct the signal

$$S(T) = (C(t_1) - C(t_2))/Co \quad (6.8)$$

and differentiate it with respect to the temperature to obtain (see Appendix) the equivalent of equation (6.3)

$$\frac{1}{\tau_m} = \frac{\ln(t_2/t_1)}{(t_2-t_1)[1 +(\sigma/kT_m)^2]} \quad (6.9)$$

The subscript m denotes the maximum DLTS signal. Expression (6.9) reduces smoothly to the standard DLTS expression (6.3) as σ/kT_m tends to zero. The implication is that the standard DLTS analysis may be in slight error and yield an incorrect activation energy.

For disordered systems the analysis of PATS is similar to that of DLTS. The maxima of PATS signal for weak disorder occurs at a time[11]

$$t_{max} = \ln(\tau_1/\tau_2)/[1/\tau_2(1 + (\sigma/kT_2)^2) - 1/\tau_1(1 + (\sigma/kT_1)^2)]$$

We see that the expression is identical to that of DLTS except for the interchange between the time and the inverse of the time constant. The inferences drawn in this case are the same as that of DLTS.

Figure 6.1 depicts the capacitance transient as calculated using the exact expression(6.2), our approximate equation(6.7) and the pure exponential equation(6.1). The three curves are nearly identical, though our approximate expression (6.7) and the exact (6.2) are in closer agreement. Further, the exponential expression decays faster than the other two, indicating the slowly decaying (non-exponential) character of the broadened gap level.

Figure 6.2 depicts the DLTS plot for the gap level discussed in section 6.1. The maxima of the signals are at identical temperatures for the three cases discussed in the previous paragraph. This implies that the modified expression (6.9) has little influence on the determination of the activation energy. For weak disorder the standard DLTS analysis based on equation (6.3) would yield accurate values of the activation energy and the pre-exponential factor. Thus we conclude that the standard

analysis is robust with respect to small disorder. We have indeed verified this for several values of the parameters b and σ/E_o.

6.3: Analysis for Strong Disorder

We now consider the case of strong disorder {$b = \sigma/kT > 1$, $s = \sigma/E_o > 0.1$}. Defining $x = (E-E_o)/\sigma$, and using the definitions (6.5) and (6.4), the capacitance transient of equation (6.2) may be cast in the form

$$C(t) = C_o \int_{-E_o/\sigma}^{\infty} \exp(-f(x))dx/(2\pi)^{1/2} \qquad (6.10)$$

where

$$f(x) = x^2/2 + (t \exp(-bx))/\tau_o \qquad (6.11)$$

On account of the nature of the gaussian, the upper limit E_g in the equation (6.10) has been replaced by infinity. This entails only negligible error. We next apply the stationary point formula in a manner similar to the previous section. Differentiating, we get

$$f'(x) = x - bt \exp(-bx)/\tau_o$$

For large b the solution of $f'(x_o) = 0$ is given by the recursive expression

$$x_o = \frac{1}{b} \ln \frac{tb^2/\tau_o}{\ln \frac{tb^2/\tau_o}{\ln(tb^2/\tau_o.....)}}$$

The above expression holds under the condition $tb^2/\tau_o > e$. We shall use a truncated form of the above expression, i.e. stop the recursion after the first denominator. A series of algebraic manipulations then yields

$$C(t) \approx C_o \exp\left\{ -\frac{1}{b^2}\left[\frac{1}{2}\left(\ln \frac{tb^2/\tau_o}{\ln tb^2/\tau_o}\right)^2 + \ln(tb^2/\tau_o)\right]\right\} \times \left[1 + \ln(tb^2/\tau_o)\right]^{-1/2} \qquad (6.12)$$

Equation (6.12) is a radical departure from the Debye relaxation (pure exponential) form. If the first term in the exponent is ignored, it reduces to

$$C(t) \propto 1/t^{\alpha} \qquad (6.13)$$

where $\alpha = 1/b^2$, a form of non-exponential relaxation currently popular in spin-glass and related areas.

Figure 6.3 depicts a typical capacitance transient encountered in a DLTS analysis of a-Si:H. Here $b = \sigma/kT$ is large (≈ 6). The transient is long lived and distinctly non-exponential.

The approximate expression (6.12) agrees moderately well with the exact one.

We have been unable to obtain a closed-form expression for the DLTS time constant extrema analogous to equation (6.3) or (6.9). The difficulty is due to the complicated character of equation (6.12). Hence, for further analysis of the strong disorder problem, we have to rely on the exact expression (6.2). The DLTS extrema can be located by differentiating equation (6.2)

$$\frac{\partial S}{\partial \tau} = \int dE \exp\left[1-(E-E_o)^2/2\sigma^2\right] \times \left[\exp(-t_1/\tau)/\tau^2 - \exp(-t_2/\tau)/\tau^2\right] = 0 \qquad (6.14)$$

and employing a non-linear numerical procedure such as Newton-Raphson to extract the three parameters E_o, A and σ.

A question of central importance is the error made if the standard analysis based on equation (6.3) is applied to the DLTS data for the strong disorder case. The analysis of the previous section indicates that the error made is almost neglible for the weak disorder case. We consider a typical deep level centred at E_o = 0.5eV, and $A = 10^9 s^{-1}K^{-2}$, and characterised by an increasing broadening σ = 0.1, 0.25 and 0.4eV, respectively. Using a rate window $t_2/t_1 = 4$, DLTS signals employing the exact broadened expression (6.2) were generated. From the maxima of these signals, T_m, we construct Arrhenius plots using the standard expression

(6.3). Figures 6.4 - 6.6 depict Arrhenius plots for the three distinct broadening considered (σ = 0.1, 0.25 and 0.4eV respectively). An examination of figures 6.4 - 6.6 leads us to conclude (i) there are no deviations from linearity over the four time decades considered in the DLTS simulations (0.1ms to 1s). Hence an examination of the Arrhenius plots provides little clue to the broadening of the gap level. (ii) The extracted gap level E_o' is invariably greater than E_o, the actual peak in broadened density of states. In fact as figure 6.6 depicts, for σ = 0.4eV, E_o' = 0.72eV, while E_o = 0.5eV, a 50% deviation! (iii)The extracted value of the pre-exponent A' is also larger than A. However no systematic trends were found for A.

Figure 6.7 displays the extracted value E_o' as a function of σ/E_o. It reinforces and encapsulates the conclusion based on figures 6.4 - 6.6. For $\sigma/E_o > 0.1$ there is a systematic overestimation of the activation energy. For $\sigma/E_o < 0.1$ this error is negligible.

An analysis for strong disorder in PATS has been carried by Singh et al[13].

6.4: Simulation on Real Systems

We shall apply our analysis to two experimental situations: (i) a-Si:H (ii) an E3 like level in $GaAs_{0.86}Sb_{0.14}$.

For the a-Si:H case[9] the disorder is large and a priori we expect σ to be large. Indeed, as figure 6.8 shows, the fit to the

experimental DLTS signal[9] is accomplished by using σ = 0.175eV, E_o = 0.82eV and A = 4×10^{8} $s^{-1}K^{-2}$ in equation (6.2). This implies that $\sigma/kT_m \approx 6$ and $\sigma/E_o \approx 0.2$. This fit was possible only after some trial and error. The corresponding Arrhenius plot is depicted in figure 6.9. Note that it is linear over five time decades. The value of the activation energy extracted from the slope of the data presented in figure 6.9 is E_o' = 0.87 eV. Recall that the fit in figure 6.8 used the input value of E_o = 0.82eV. Thus the standard DLTS analysis overestimates the activation energy in this case by 0.05eV. Lang et al[9] have done numerical analysis for the case of a-Si:H, taking into account both large trap densities and broadened energy spectra, and find similar results. Thus, our main thesis encapsulated in figure 6.7 that the standard DLTS overestimates the activation energy in the limit of severe broadening, is borne out.

The next case we consider is the E3 like level in $GaAs_{0.86}Sb_{0.14}$. This has been subjected to a DLTS study by Murawala and co-workers[6]. A close fit to the experimental DLTS plot is obtained by simulating equation (6.2) with E_o = 0.23eV, A = $2.31\times10^{4}s^{-1}K^{-2}$, and σ = 0.055eV. This corresponds to $\sigma/kT_m \approx 4$ and $\sigma/E_o \approx 0.24$. We have not reproduced the DLTS signal fit here since it is analogous to figure 6.8. However, we do show the Arrhenius plot in figure 6.10. The plot is again linear over five time decades . The extracted activation energy is 0.25 eV, in slight excess of the peak in the broadened gap level (E_o =

0.23eV).

6.5: Disorder and Metastability

Levinson has reported an analysis of the DLTS peak heights for a defect oscillating between two metastable states . In this section we examine the effect of disorder and present some new results.

In figure 6.11 we present an idealized model for a metastable defect set forth by Levinson[14]. The defect transforms from the state B to the state A during the forward (or zero) bias pulse of width t_p. It transforms from A to B during the reverse bias time of width t_i . Let the fraction of the species in states A and B at time t be $f_A(t)$ and $f_B(t)$ respectively. The normalization

$$f_A(t) + f_B(t) = 1 \qquad (6.15)$$

holds at each instance of time.Consider the time period $0 < t \leq t_i$ The transformation A —> B is described by a simple exponential in the absence of disorder

$$f_A(t_i) = f_A \exp(-t_i/\tau_{ab}) \qquad (6.16)$$

where τ_{ab} is the relevant time constant. Now let us examine the effect of disorder. Disorder dictates that the sharp delta

function like level characterizing a defect is broadened . This is indicated by the shaded regions around the A and B states in figure 6.11 . We assume without loss of generality that the relevant density of states (DOS) is rectangular.

$$n_A(E) = \delta(E - E_A) \xrightarrow{\text{disorder}} A \qquad 0<E<E_A \qquad (6.17a)$$

and similarly for $n_B(E)$. Normalization of DOS implies .

$$A\, E_A = 1 \qquad (6.17b)$$

We wish to state that the results of this section are independent of this particular choice of a rectangular DOS. Equation (6.16) must be averaged over disorder . Hence

$$\bar{f}_A(t_i) = \int n(E)\, f_A(t_i)\, dE = f_A^o \int n(E)\, \exp(-t_i/\tau_{ab})\, dE \qquad (6.18)$$

The time constant τ_{ab} is given by the barrier height formula

$$1/\tau_{ab} = \nu_{ab}\, \exp(-E/kT)$$

We define a new variable x

$$t_i/\tau(E) = \exp(-(E-x)/kT) \qquad (6.19)$$

This facilitates the reduction of the exponential in equation (6.18) to a step function

$$\exp(-t_i/\tau_{ab}) \simeq \theta(E - x)$$

where $\theta(E - x) = 1$ for $E > x$ and zero otherwise . Thus equation (6.18) reduces to

$$\begin{aligned} \bar{f}_A(t_i) &= f_A^o \int n(E)\ \theta(E - x)dE \\ &= f_A^o \int_x n(E)\ dE \\ &= f_A^o\ A\ (E_A - x) \end{aligned} \qquad (6.20)$$

where the last step employs equation (6.17). Using equation (6.19) for x we obtain

$$\bar{f}_A^o(t_i) = \theta_{AB}\ f_A^o \qquad (6.21a)$$

$$\begin{aligned} \theta_{AB} &= A\ (E_A - kT\ \ln\ (\nu_{ab} t_i)) \\ &= 1 - kT\ A\ \ln\ (\nu_{ab} t_i) \end{aligned} \qquad (6.21b)$$

Consider the time period $t_i < t < t_i + t_p$ when B $\longrightarrow$A . An analysis similar to above yields.

$$f_A(t_i + t_p) = 1 - \theta_{BA} + \theta_{AB}\theta_{BA}\, f_A^o \qquad (6.22a)$$

$$\theta_{BA} = 1 - kT\, B \ln(\nu_{ba} t_p) \qquad (6.22b)$$

The equations (6.21a) and (6.22a) possess a form similar to Levinson except that θ_{AB} and θ_{BA} are each different in content due to the effect of disorder .

Proceeding over further cycles of reverse and forward biases we obtain a generalized form

$$\bar{f}_A^{\infty} = C_1 + C_2 kT \ln(\nu_{ba} t_p) \qquad (6.23)$$

In equation (6.23) C_1 , C_2 and ν are constants . The dependence of the fractional species A on time and temperature is clearly displayed by this equation . An examination of the data on the MFe center in InP validates the above analysis. This can be seen from an examination of figures 6.12 and 6.13 which chart out the peak heights in the DLTS spectra of the A species at two different temperatures (T =175K and 195K).

6.6: Conclusion

In this section we first address ourselves to two issues :(i) What are the experimental signatures in the capacitance transient spectroscopy of a broadened gap level as opposed to a sharp delta function like gap level ? (ii) To what extent would a standard

DLTS analysis of a broadened defect level be in error ?

Regarding the first question, there are at least three indicators of the broadened gap level. First, if the system under study is patently inhomogeneous, then the qualitative arguments presented in section 6.1 indicate that the level should be broadened. Semiconductor alloys are typical suspect systems. An extreme example is GaAsSb since it is a semiconductor alloy with a large lattice constant mismatch between GaAs and GaSb. Amorphous semiconductors such as a-Si:H would be another set of suspect systems. Second, an examination of the capacitance transient is recommended. If it is non-exponential then one must presume broadening. In fact, it was this trait which led earlier workers to posit broadening[5-7]. What we have demonstrated in this work is an analytic proof of a long-lived non-exponential character of the capacitance transient both for weak disorder (equation (6.7) and figure 6.1) and strong disorder (equation (6.12) and (6.13) and figure 6.3). Third the DLTS signal is itself broadened over and above its normal value. Murawala et al[6] have proposed a phenomenological relationship connecting $\Delta T/T_m$ the full width at half maxima to

$$\sigma \, \Delta T/T_m = 0.1 + \sigma/E_o$$

This relation may help one to extract a rough value of σ. Lastly, the Arrhenius plot provides little clue to the existence of

broadening. As figures 6.4 - 6.6, 6.9 and 6.10 indicate, the Arrhenius plot is linear over four to five time decades, even in the presence of significant broadening.

Regarding the second question, the following conclusions may be gleaned from our work.

(i) The conventional DLTS analysis overestimates the activation energy for severely broadened levels. This overestimation is often quite small. It may, however, lead to small but systematic discrepancies between DLTS and other experimental probes such as optical studies, Hall effect etc. In the case of a-Si:H studied in section 6.4, the input value was E_o = 0.82eV while the extracted value was E_o' = 0.87eV. The precise factor responsible for this discrepancy can be traced to the expression for the time constant

$$\frac{1}{\tau_m} = \frac{\ln(t_2/t_1)\, F(\sigma/kT_m, \sigma/E_o)}{(t_2 - t_1)} \qquad (6.24)$$

$$F(\sigma/kT_m, \sigma/E_o) < 1. \qquad (6.25)$$

The functional form of F for small disorder is given by equation (6.9). For large disorder, the complicated form of the equation (6.12) prohibits a simple derivation. F, nevertheless, is always less than unity. This character of F is responsible for the overestimation.

(ii) The error involved in a standard DLTS analysis based on equation (6.3) is minor if (a) $\sigma/kT_m < 1$ and $\sigma/E_o < 0.1$, (b) $\sigma/kT_m > 1$ but $\sigma/E_o < 0.1$ and $A > 10^6 s^{-1}K^{-2}$. Thus, standard DLTS analysis is fairly robust with respect to disorder.

We would like to end with a few speculative remarks. The power law decay form in equation (6.13) was derived under the assumption of additive contributions embodied in equation (6.2). This implies that the carriers are emitted independently into the relevant band. Such a process is deemed parallel relaxation. Mutual correlations and subsequent modifications of the defect density of states during the emission process is ignored. Preliminary investigation in the relaxation of glassy phenomena indicate that non-exponential relaxation arises as a natural consequence of serial as opposed to parrallel relaxation[15]. Similar considerations in the study of capacitance transients may yield interesting results. The form of the defect density of states has been assumed to be gaussian (equation (6.3)). This form is premised on the central limit theorem. A microscopic theory for the defect density of states in semiconductor alloys should be pursued [16]. Finally, detailed analytical and numerical exercise similar to the current one must be carried out for other experimentally studied quantities of interest (e.g. Hall effect, thermally stimulated capacitance etc) to ensure that the conventional interpretation is valid for the disorder broadened case. The results of this chapter has been reported in references 11, 17 and 18.

Appendix

We will indicate the derivation of the modified DLTS expression (6.9). Differentiating equation (6.7)

$$\frac{1}{T}\frac{\partial C(t)}{\partial T} \approx \exp\,[-t/\tau_o + 0.5(\sigma t/kT\tau_o)^2] \times$$

$$\{[t/\tau_o - (\sigma t/kT\tau_o)^2]\partial\tau_o/\partial T - (\sigma t/kT\tau_o)^2/T\} \qquad (A.1)$$

If

$$|\partial\tau_o/\partial t| >> \tau_o/T \qquad (A.2)$$

then the last term on the RHS of (A.1) may be neglected. This condition translates to

$$2 + E_o/kT >> 1. \qquad (A.3)$$

Such a condition is easily met.

We then exponentiate the term in the curly brackets of (A.1) and expand the subsequent logarithm:

$$t/\tau_o - (\sigma t/kT\tau_o)^2 = t\,\exp\,[\ln(1-(\sigma/kT)^2 t/\tau_o]/\tau_o$$

$$\approx t\,\exp[-(\sigma/kT)^2 t/\tau_o] \qquad (A.4)$$

We obtain next the DLTS extrema by differentiating equation (6.8) and using equations (A.1) and (A.4) for the signal. This expression is trivially equation (6.9).

REFERENCES

1. D.V.Lang, J. Appl. Phys.45 3014 - 3023 (1974).

2. P.M.Mooney, N.S.Caswell, P.M.Solomon and S.L.Wright, Materials Research Society Meeting, San Francisco 15 -18 April (1985). T.N.Theis, T.F.Kuech, L.T.Palmateer and P.M.Mooney, Gallium Arsenide and Related Compounds, Inst. Phys.Conf. Ser. 74, Ch.4, p 241 (1984).

3. P.Parayanthal and F.H.Pollak, Phys. Rev. Lett. 52 1822 (1984).

4. L.Samuelson, S.Nilsson and H.G.Grimmeiss, Phys. Rev. Lett. 53 1501 (1984).

5. P.Omling, L.Samuelson and H.G.Grimmeiss J. Appl. Phys. 54 5117 (1984).

6. P.A.Murawala, Vijay A. Singh, S.Subramanian, S.S.Chandvanker and B.M.Arora, Phys. Rev. B 29 4807 (1984);Proc. 13th Int. Conf. on defects in semiconductors, ed. L.C. Kimerling and J.M.Parsey Jr (New York: AIME) p 1165 (1985).

7. Vijay A.Singh (unpublished).

8. M.Kanieswka and J.Kanieswka, Solid State Commun. 53 485 (1985).

9. D.V.Lang, J.D.Cohen and J.P.Harbison, Phys. Rev. B 25 109 (1982). J.D.Cohen, D.V.Lang, J.P.Harbison and A.M.Seregent Solar Cells 19 119 (1983).

10. M.Bleicher and E.Lange Solid State Electron. 16 375 (1973).

11. Raj K. Singh, Vijay A Singh, J.W.Corbett, and Amita Das, J.Phys.C 19 ,2177 (1986).

12. C.M.Bender and S.A.Orszag (ed.) Advanced Mathematical Methods for Scientists and Engineers (New York: McGraw-Hill) p 267 (1978).

13. Raj K. Singh, Vijay A.Singh and J.W.Corbett, Semiconductor Science and Technology, 2, 716-725 (1987); 2, 726-731 (1987).

14. M. Levinson, J. Appl. Phys 58, 2638 (1985); M. Levinson (private communication).

15. R.J.Palmer, D.L.Stein, E.Abrahams and P.W.Anderson, Phys. Rev. Lett. 53 958 (1984).

16. V.A.Singh in Elestronic Structure and its applications, Lecture notes in Physics, Springer Verlag, 283, 201 (1987).

17. Amita Das , Vijay A. Singh , and D.V.Lang, Semicond.Sci. and Tech.,3 1177-1183 (1988).

18. "Transient Spectroscopy and Disorder", Vijay A.Singh and Amita Das, Radiation Effects and Defects in Solids, (1989).

FIGURE CAPTIONS

Figure 6.1: Plot of the capacitance transient for small σ/kT ($\approx$ 0.2) and τ^{-1} = 3.4418 s^{-1}. Note the slower decay of the broadened gap level as opposed to the exponentially dictated form. T = 180K.———, exact (equation (6.2)); +++,aprroximate (equation (6.7)); ---,exponential (equation (6.6)).

Figure 6.2: Simulated DLTS signal for the parameters of figure 6.1and rate window t_2/t_1 = 4. The differences between the various expressions are very small, thus vindicating the standard DLTS analysis based on equation (6.3).———,exact(equation (6.2)); +++, approximate (equation (6.7)); ---, exponential (equation (6.6)).

Figure 6.3: Plot of the capacitance transient for E_o = 0.85eV, A = $4\times10^{8}s^{-1}K^{-2}$. The broadening factor σ = 0.175eV and T = 340K, leading to σ/kT = 6. The transient is long lived and distinctly non-exponential. The approximate expression (6.12) is in reasonable agreement with the exact one. The parameters selected for this plot are similar to ones encountered in a-Si:H^{o}. —·—·— , exact (equation(6.2)); +++, approximate (equation (6.12)); ——exponential (equation(6.6)).

Figure 6.4: The Arrhenius plot for a simulated DLTS signal with rate window t_2/t_1 = 4. A typical broadened deep level was considered and the parameters employed for the simulation of

equation (6.2) were E_o = 0.5eV, A = $10^9 s^{-1}K^{-2}$, and σ = 0.1eV. The Arrhenius plot is linear over four time decades (0.1 ms to 1 s). Note the difference between the extracted parameters (E_o,A). E_o' = 0.515eV, A' = $1.3\times10^9 s^{-1}K^{-2}$.

Figure 6.5: The Arrhenius plot for a typical broadened deep level with broadening σ = 0.25eV. The plot is linear over four time decades (0.1 ms to 1 s). Note the difference between the extracted activation energy E_o' = 0.607eV, and E_o = 0.5eV. A' = $2.5 \times 10^8 s^{-1}K^{-2}$. Other parameters employed are the same as figure 6.4.

Figure 6.6: The Arrhenius plot for a typical broadened deep level with broadening σ = 0.4eV. The plot is linear over four time decades (0.1 ms to 1s). Note the difference between the extracted activation energy E_o' = 0.72eV, and E_o = 0.5eV. A' = $2.4 \times 10^9 s^{-1}K^{-2}$. Other parameters employed are the same as figure 6.4.

Figure 6.7: Plot of the extracted activation energy E_o' against the dimensionless broadening σ/E_o. The parameters used are the same as figures 6.4 - 6.6. There is a systematic overestimation of the activation energy for $\sigma/E_o < 0.05$. The inset displays E_o' in the weak disorder limit ($\sigma/E_o > 0.1$).

Figure 6.8: Comparison of the experimental DLTS signal with the simulated one for a-Si:H. The parameters are identical to figure 6.3. The rate window t_2/t_1 = 4. ——, experiment; ----,simulated.

Figure 6.9: The Arrhenius plot for a-Si:H. The parameters are the same as in figure 6.3 and 6.8. The plot is linear over four time decades (0.1 ms to 1s). There is an overestimation of the extracted activation energy :E_o' = 0.87eV while E_o = 0.82eV. A' = $4.4 \times 10^8 s^{-1}K^{-2}$.

Figure 6.10: The Arrhenius plot for an E3-like level in $GaAs_{1-x}Sb_x$ (x = 0.14). The plot is linear over four time decades (0.1 ms to 1s). There is a negligible difference between the extracted activation energy E_o' = 0.25eV and E_o = 0.23eV. A' = 3.4×10^4 $s^{-1}K^{-2}$.

Figure 6.11: (2a) Generalized configuration coordinate diagram for a defect with two metastable states A and B . The shaded region around the coordinates Q_A and Q_B indicates the disorder induced broadening to a finite DOS from a sharp delta function like defect level . (2b) The forward (V_F) and reverse (V_R) bias during a DLTS experiment . The transformations of the defect between the A and B configurations are indicated.

Figure 6.12: The peak height in the DLTS spectra of the A species for the MFe center as a function of the logarithm of the filling pulse t_p for T = 175K .The experimental points are taken from reference 14.

Figure 6.13:The peak height in the DLTS spectra of the A species for the MFe center as a function of the logarithm of the filling pulse t_p for T = 195K .The experimental points are taken from reference 14.

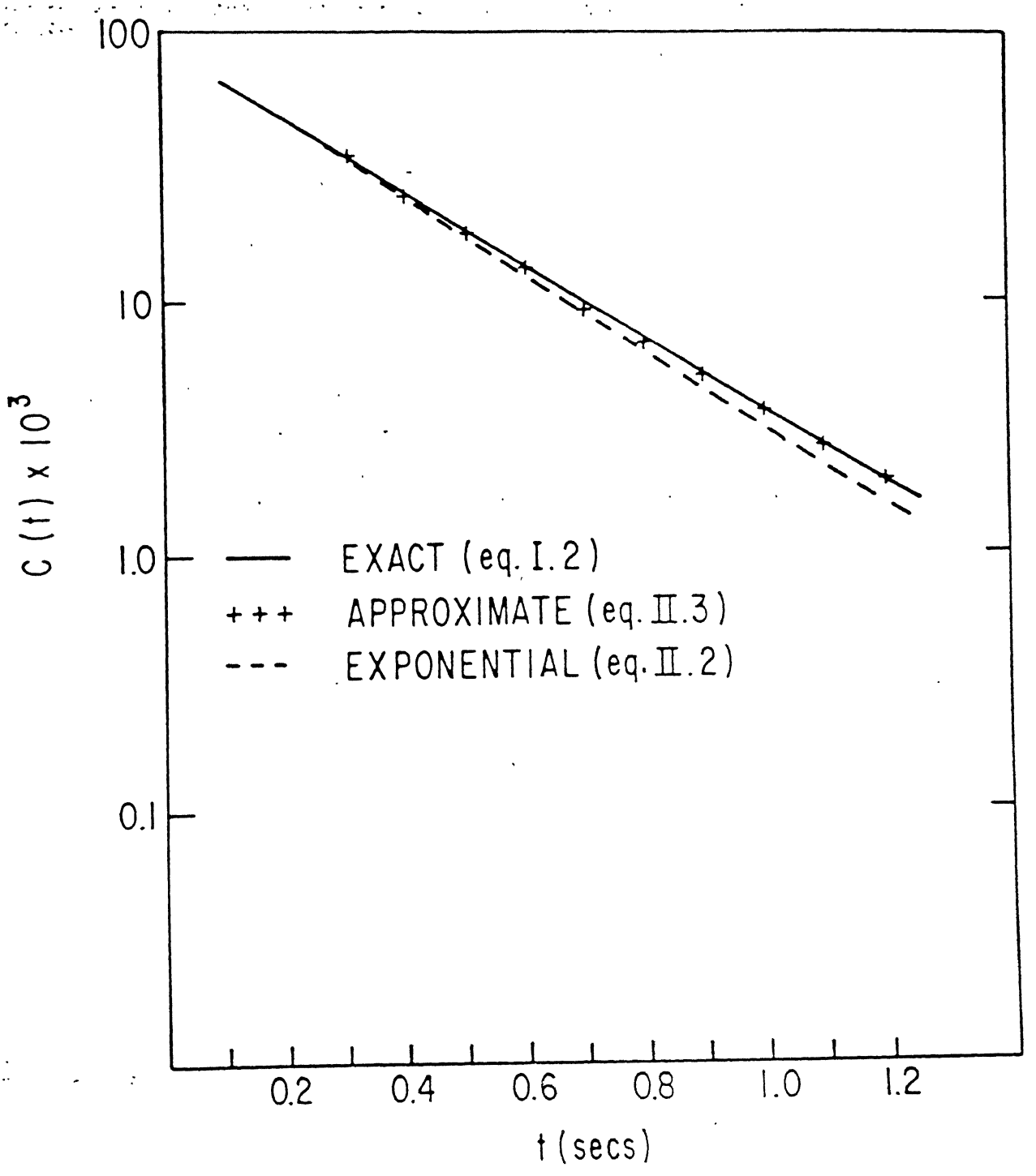
100
10
1.0
0.1
C (t) x 10^3
EXACT (eq. I.2)
+++ APPROXIMATE (eq. II.3)
--- EXPONENTIAL (eq. II.2)
0.2
0.4
0.6
0.8
1.0
1.2
t (secs)

FIGURE 6.1

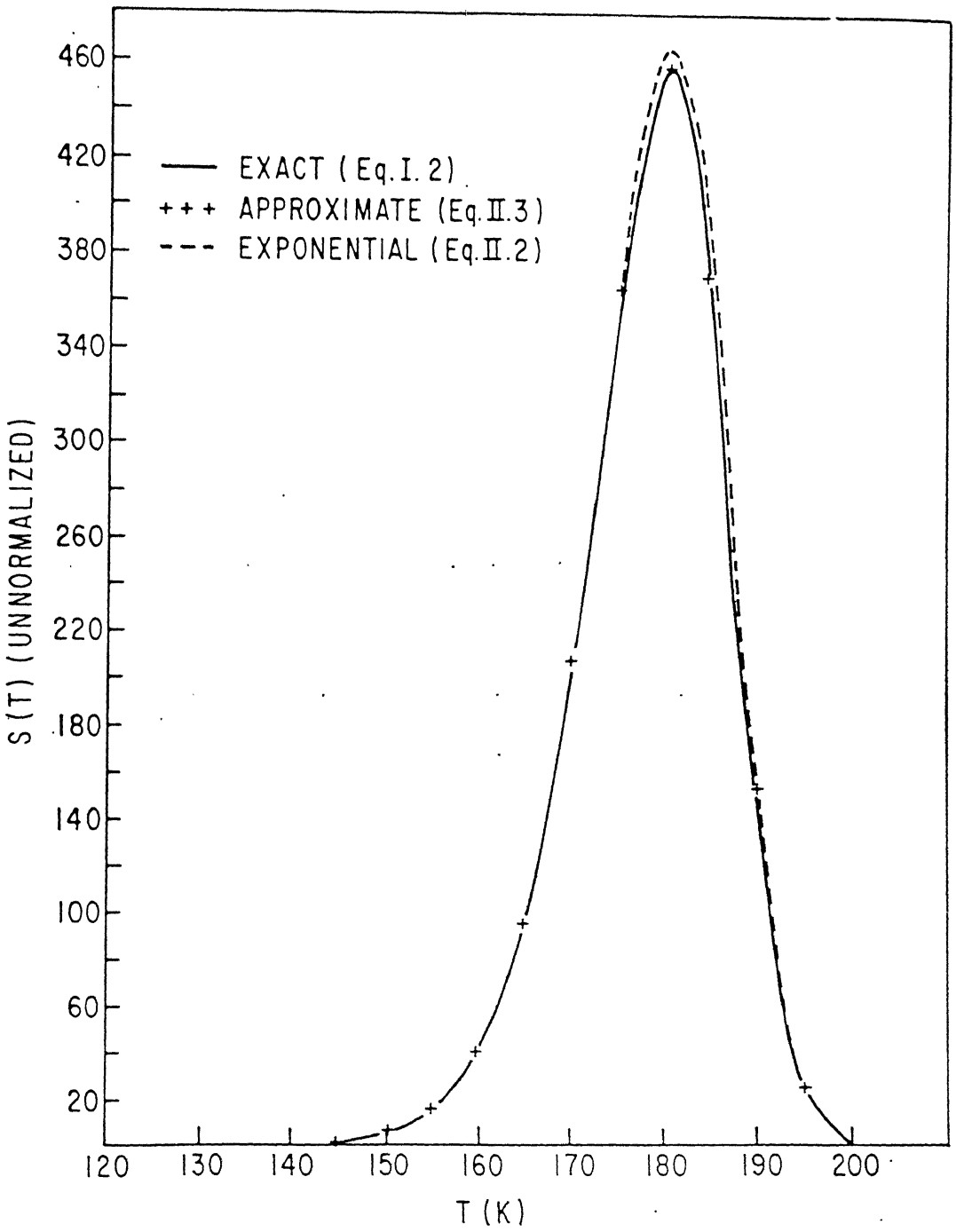
EXACT (Eq.I.2)
+++ APPROXIMATE (Eq.II.3)
--- EXPONENTIAL (Eq.II.2)
S(T) (UNNORMALIZED)
460
420
380
340
300
260
220
180
140
100
60
20
120
130
140
150
160
170
180
190
200
T (K)

FIGURE 6.2

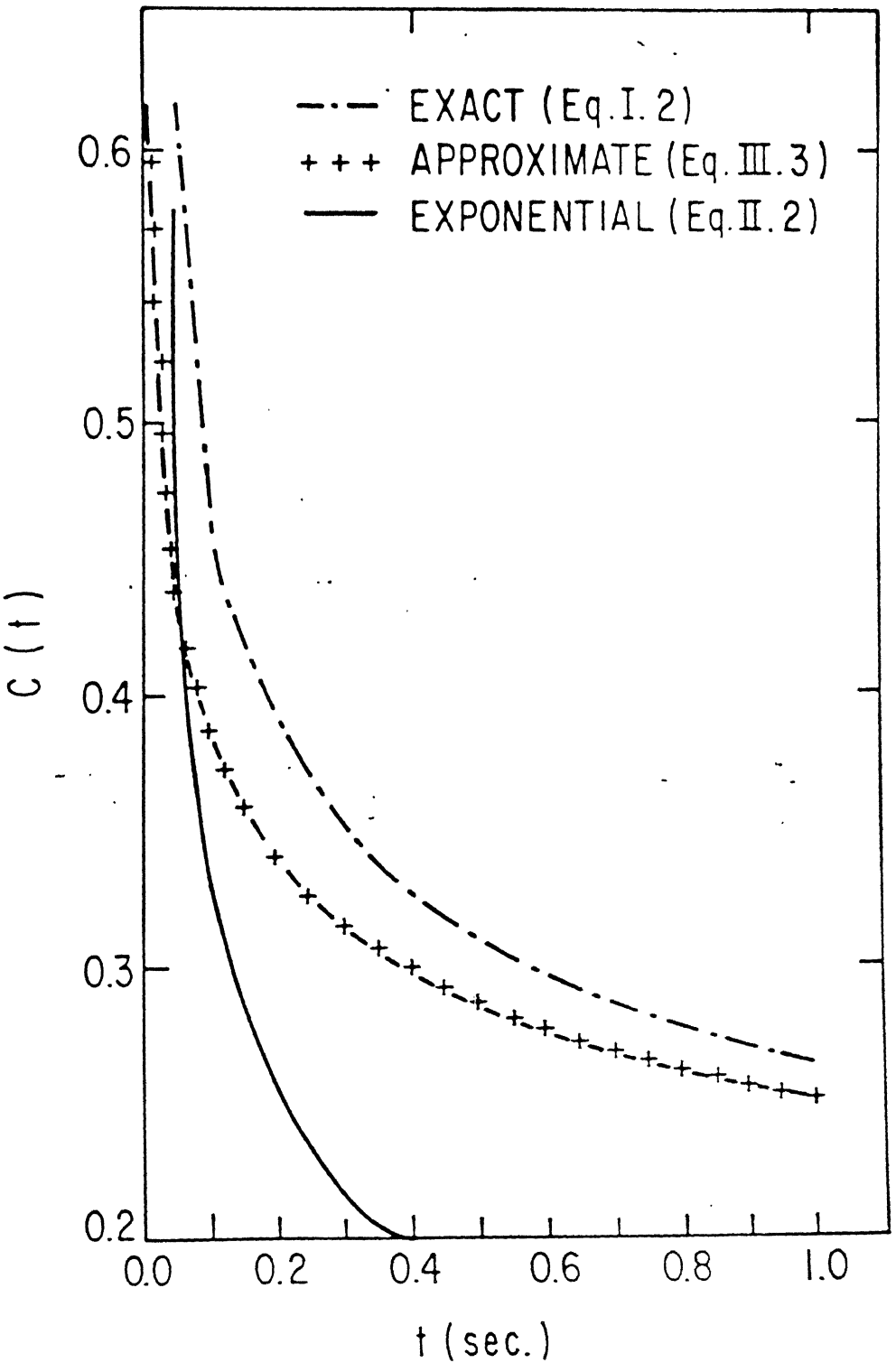
EXACT (Eq.I.2)
APPROXIMATE (Eq.III.3)
EXPONENTIAL (Eq.II.2)
C(t)
0.6
0.5
0.4
0.3
0.2
0.0
0.2
0.4
0.6
0.8
1.0
t (sec.)

FIGURE 6.3

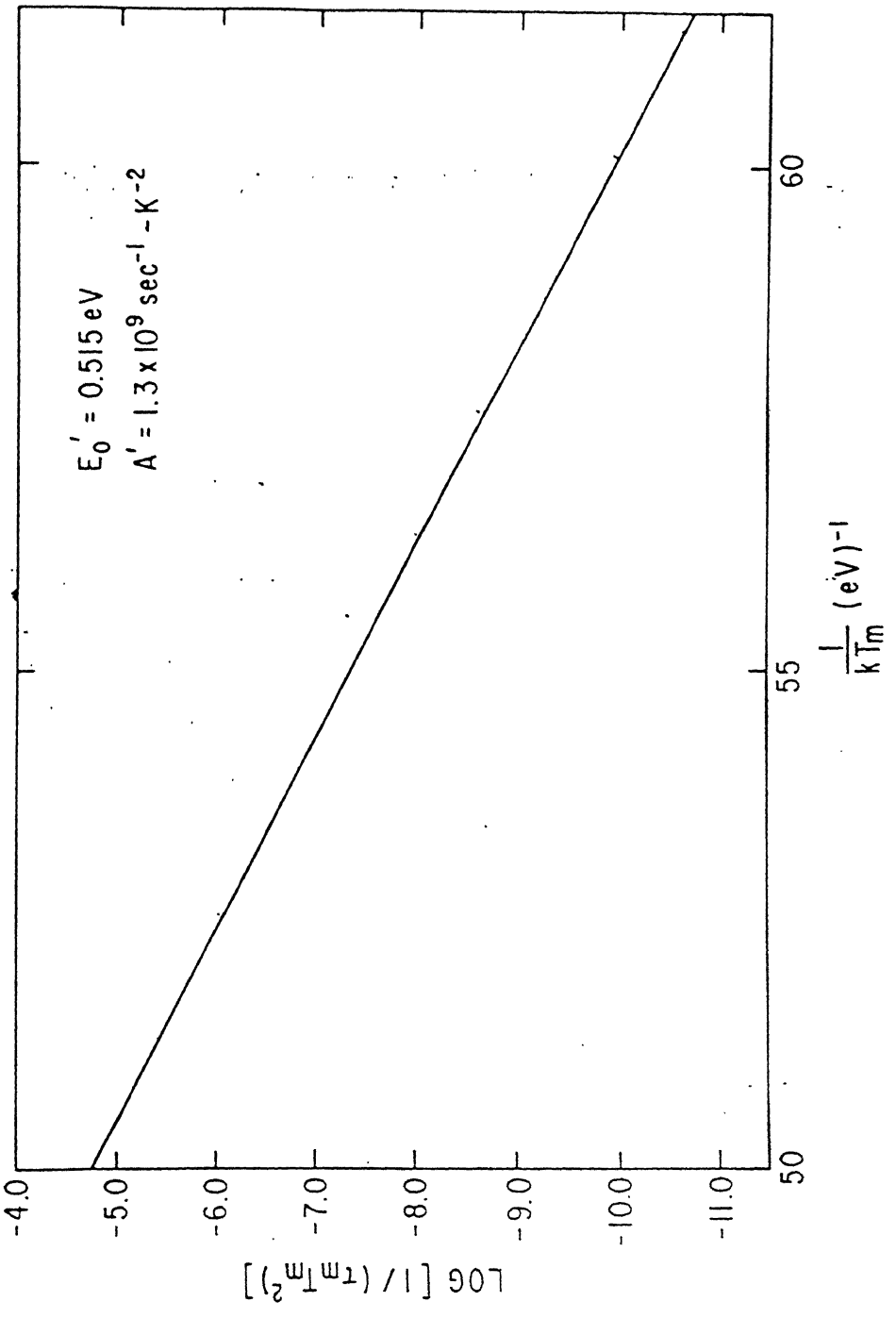
$E_o' = 0.515$ eV
$A' = 1.3 \times 10^9$ sec^{-1}-K^{-2}
-4.0
-5.0
-6.0
-7.0
-8.0
-9.0
-10.0
-11.0
Log [1/($\tau_m T_m^2$)]
50
55
60
$\frac{1}{kT_m}$ (eV)$^{-1}$

FIGURE 6.4

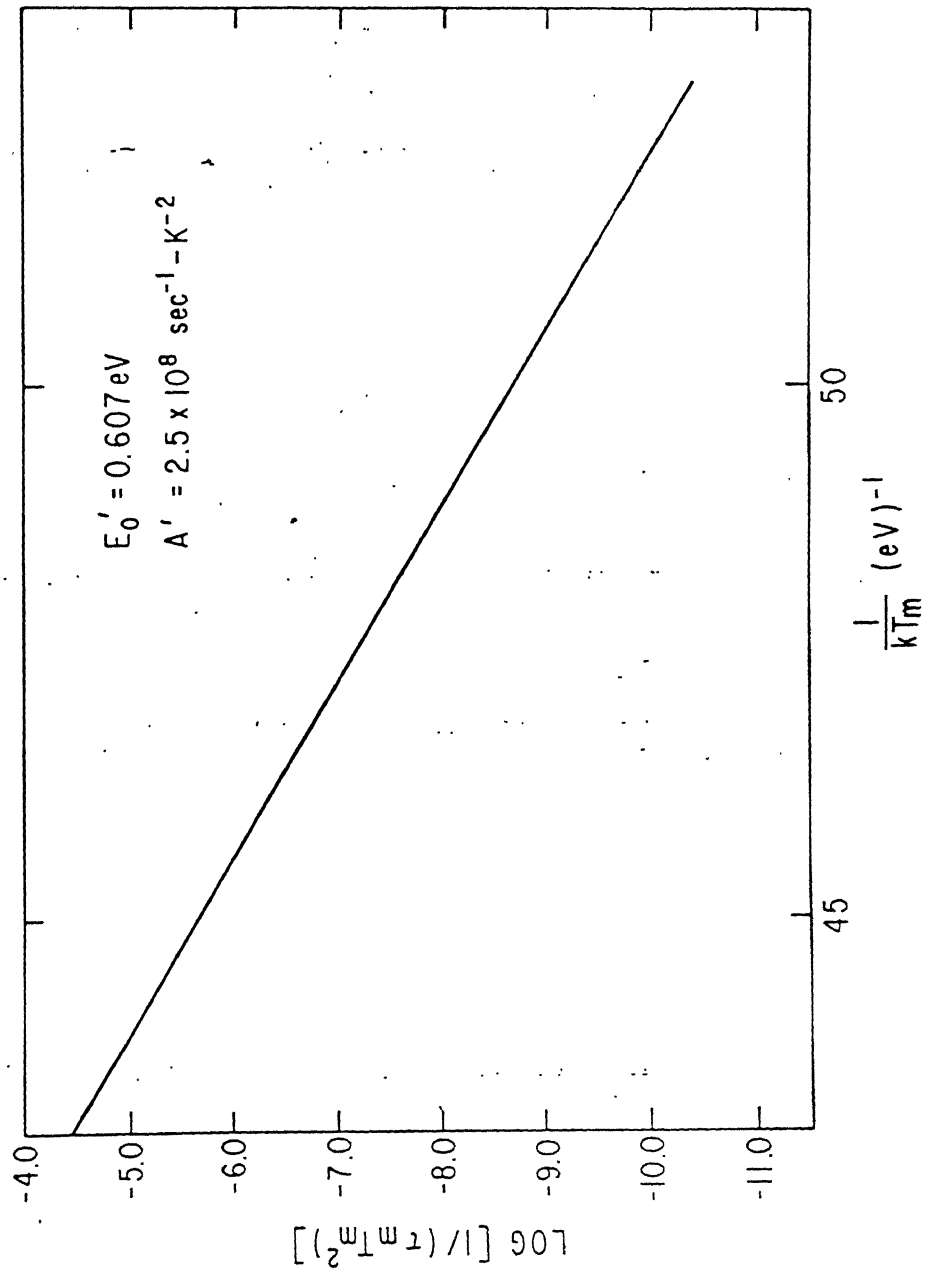
$E_0' = 0.607$ eV
$A' = 2.5 \times 10^8$ sec^{-1}-K^{-2}
-4.0
-5.0
-6.0
-7.0
-8.0
-9.0
-10.0
-11.0
Log $[1/(\tau_m T_m^2)]$
45
50
$\frac{1}{kT_m}$ (eV)$^{-1}$

FIGURE 6.5

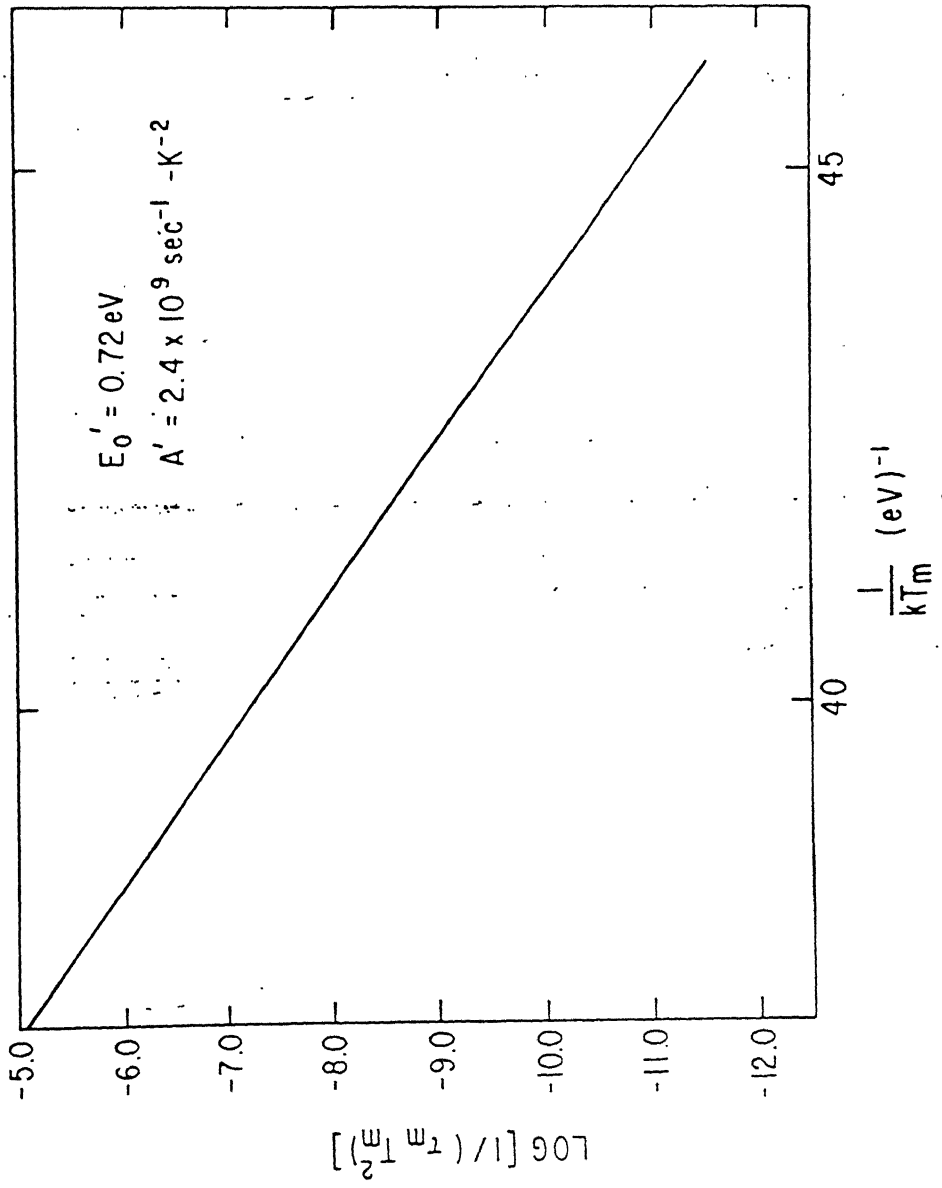
$E_o' = 0.72$ eV
$A' = 2.4 \times 10^9$ sec^{-1} -K^{-2}
-5.0
-6.0
-7.0
-8.0
-9.0
-10.0
-11.0
-12.0
40
45
$\frac{1}{kT_m}$ (eV)$^{-1}$
LOG [1/ (τ_m T_m^2)]

FIGURE 6.6

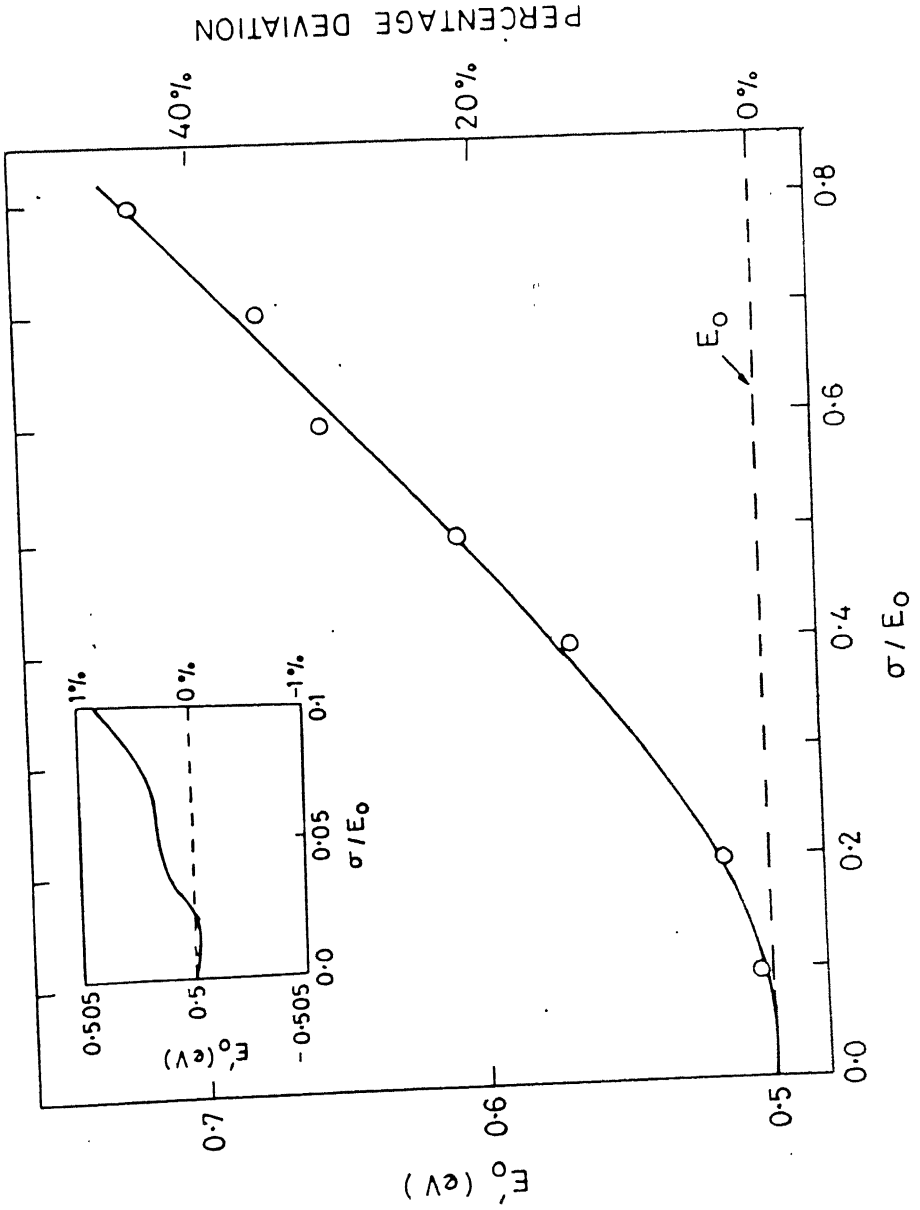
PERCENTAGE DEVIATION
40%
20%
0%
E'o (eV)
0·7
0·6
0·5
Eo
0·0
0·2
0·4
0·6
0·8
σ / Eo
1%
0%
-1%
0·1
0·05
0·0
σ / Eo
0·505
0·5
-0·505
E'o (eV)

FIGURE 6.7

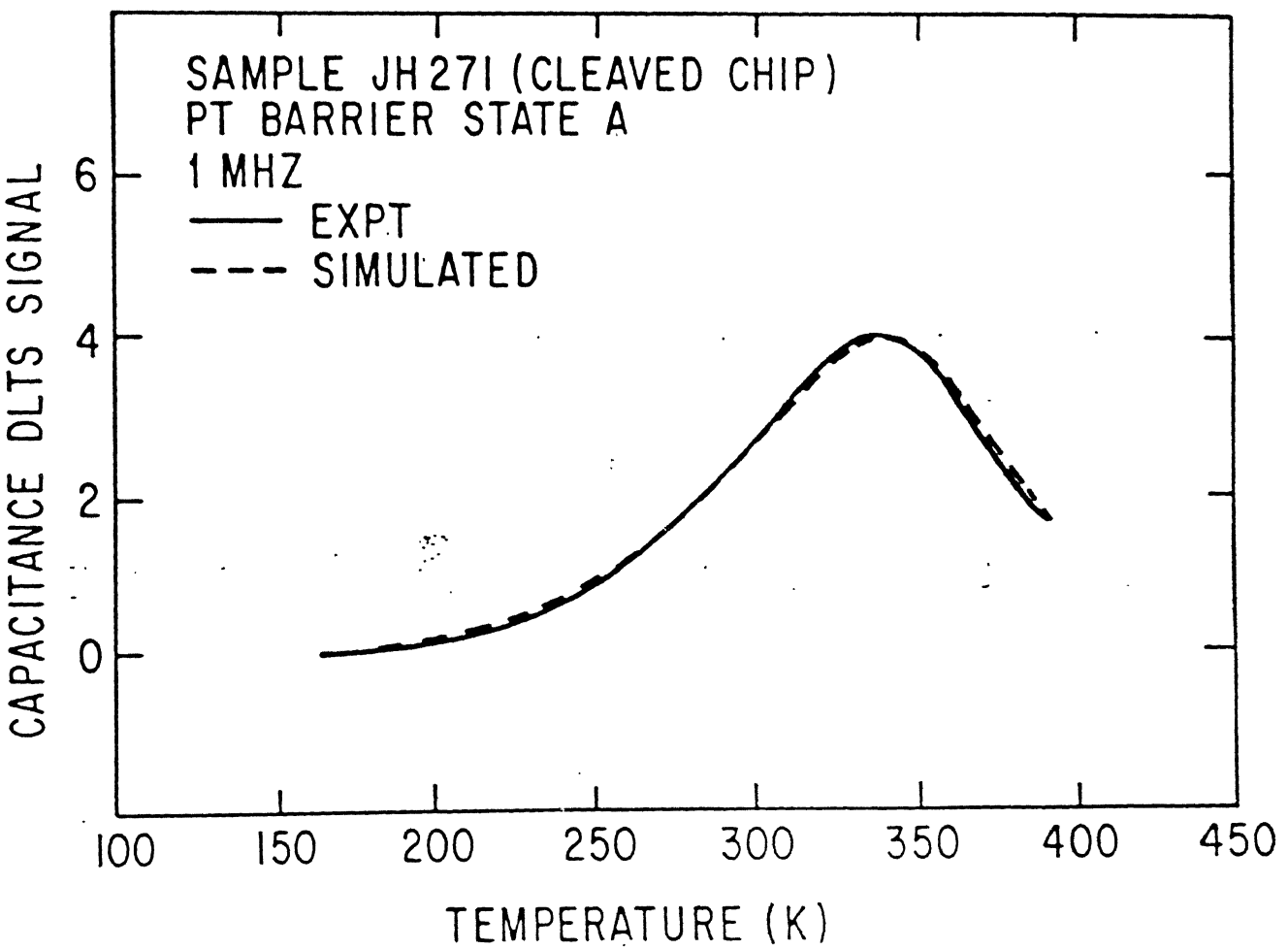
SAMPLE JH271 (CLEAVED CHIP)
PT BARRIER STATE A
1 MHZ
EXPT
SIMULATED
CAPACITANCE DLTS SIGNAL
0
2
4
6
100
150
200
250
300
350
400
450
TEMPERATURE (K)

FIGURE 6.8

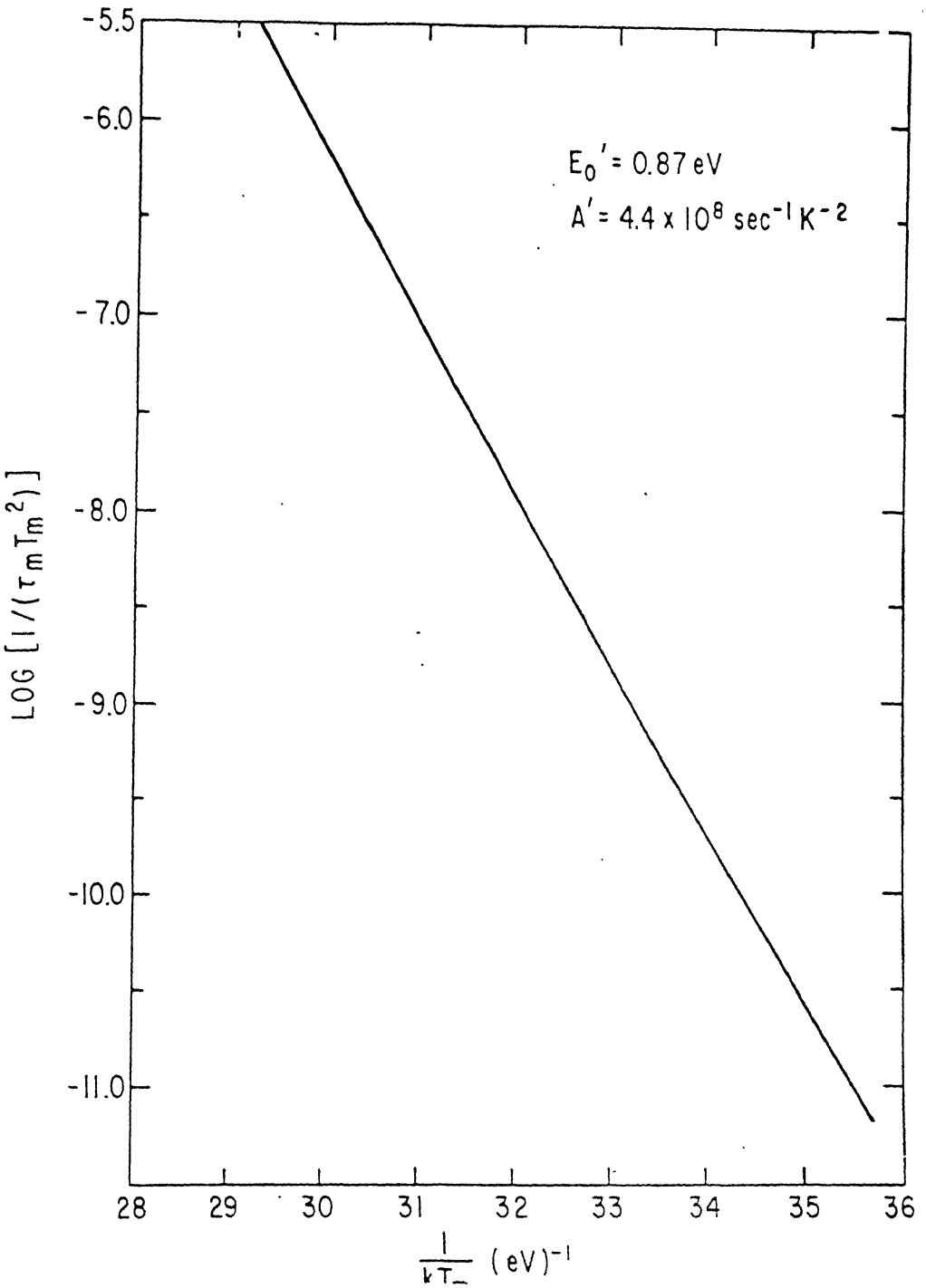
-5.5
-6.0
-7.0
-8.0
-9.0
-10.0
-11.0
LOG [1/(τm Tm²)]
E0' = 0.87 eV
A' = 4.4 x 10⁸ sec⁻¹ K⁻²
28
29
30
31
32
33
34
35
36
1/kT (eV)⁻¹

FIGURE 6.9

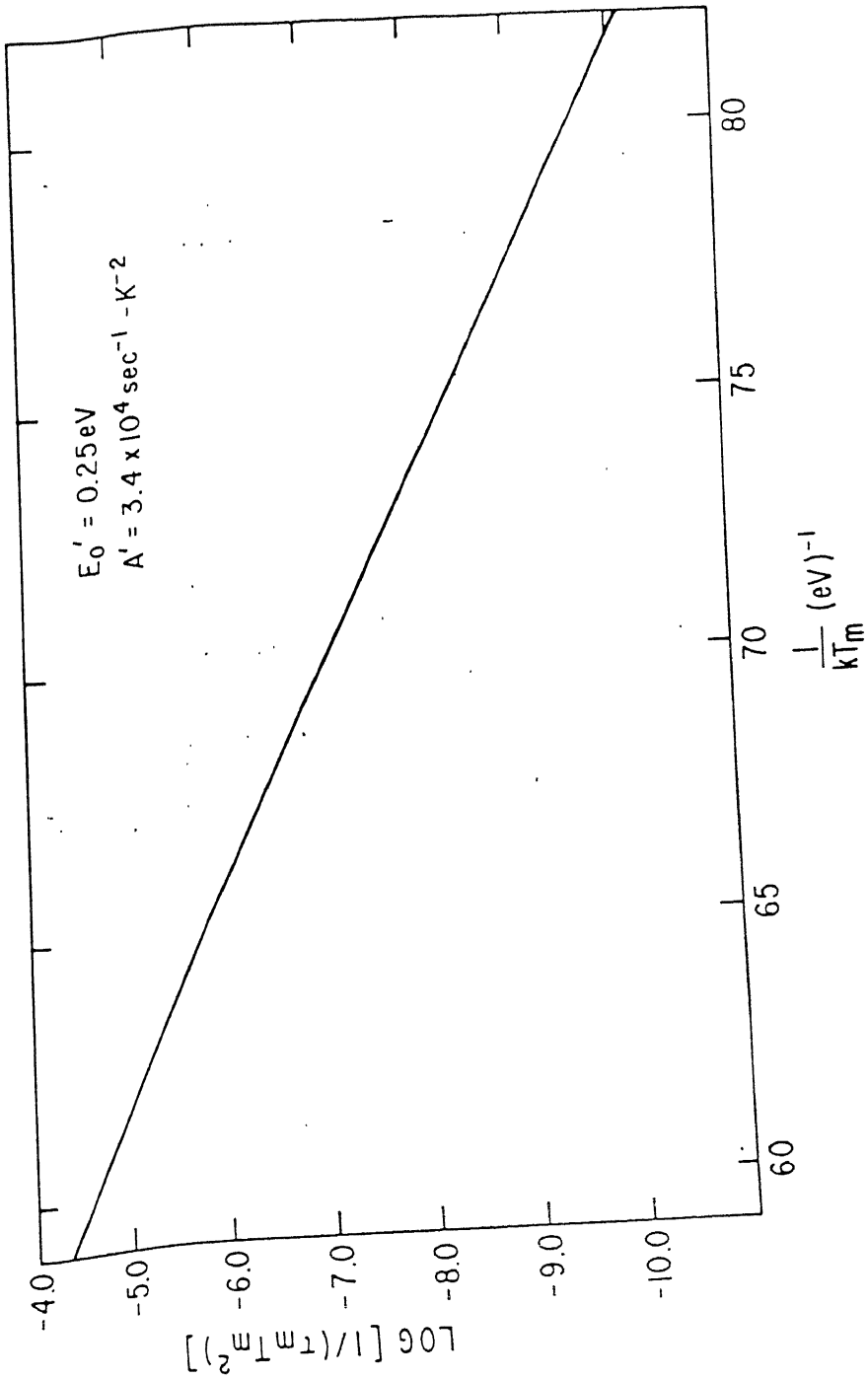
$E_o' = 0.25eV$
$A' = 3.4 \times 10^4 sec^{-1} - K^{-2}$
$\frac{1}{kT_m}$ (eV)$^{-1}$
60
65
70
75
80
-4.0
-5.0
-6.0
-7.0
-8.0
-9.0
-10.0
LOG [1/($\tau_m T_m^2$)]

FIGURE 6.10

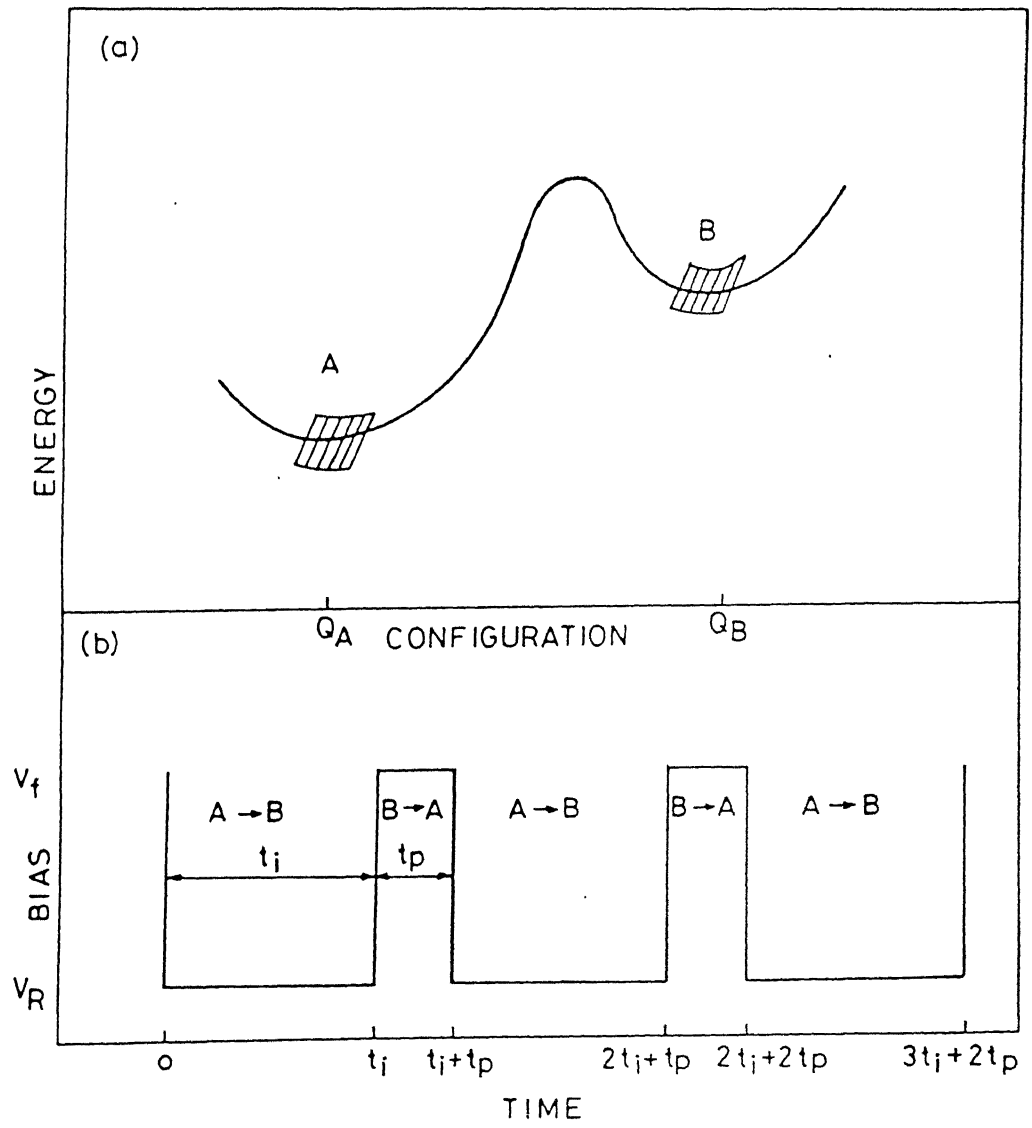
(a)
ENERGY
A
B
Q_A
CONFIGURATION
Q_B
(b)
V_f
BIAS
V_R
A → B
B → A
A → B
B → A
A → B
t_i
t_p
o
t_i
t_i+t_p
$2t_i+t_p$
$2t_i+2t_p$
$3t_i+2t_p$
TIME

FIGURE 6.11

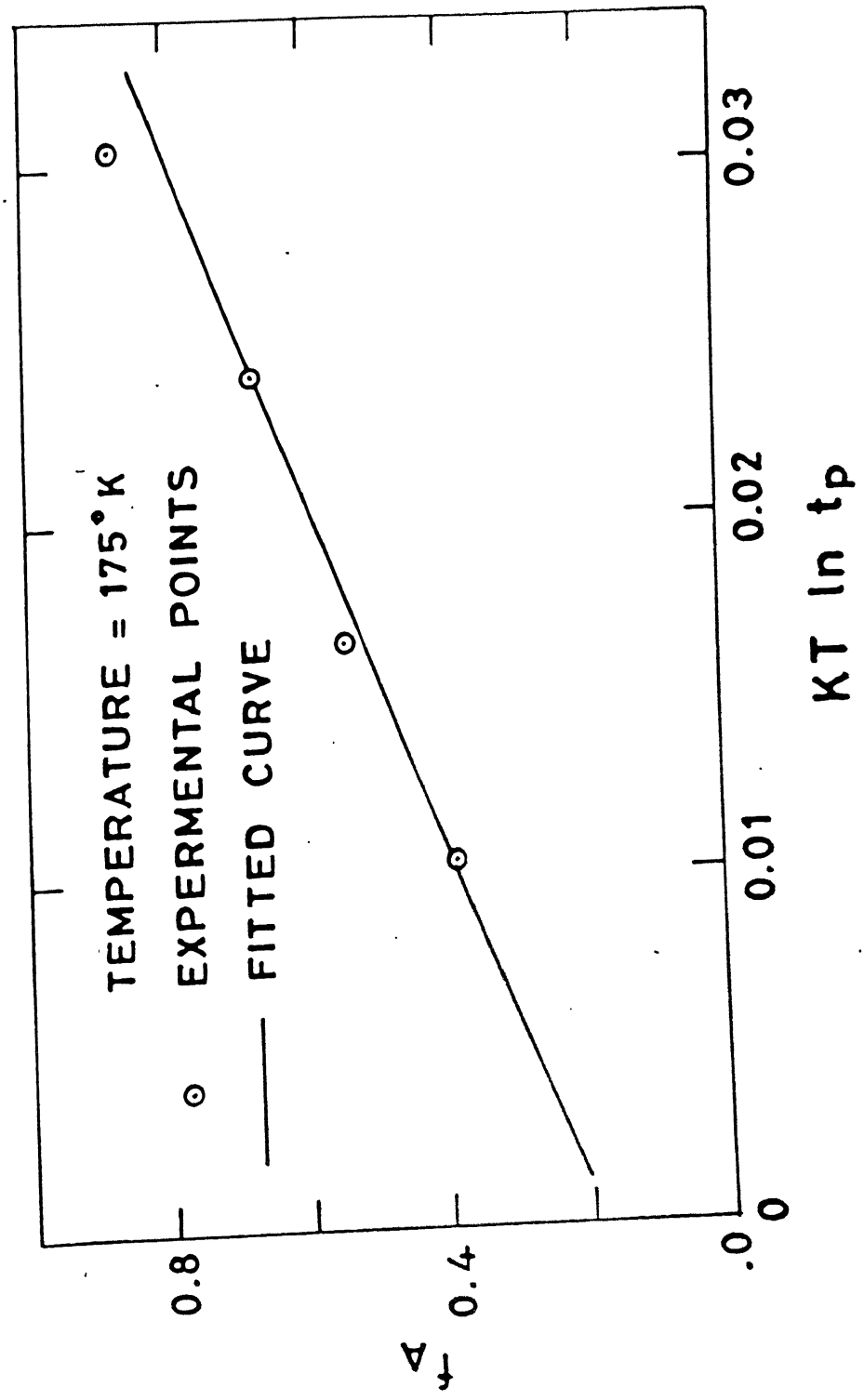
TEMPERATURE = 175° K
EXPERMENTAL POINTS
FITTED CURVE
0.8
0.4
0
0.01
0.02
0.03
KT ln tp

FIGURE 6.12

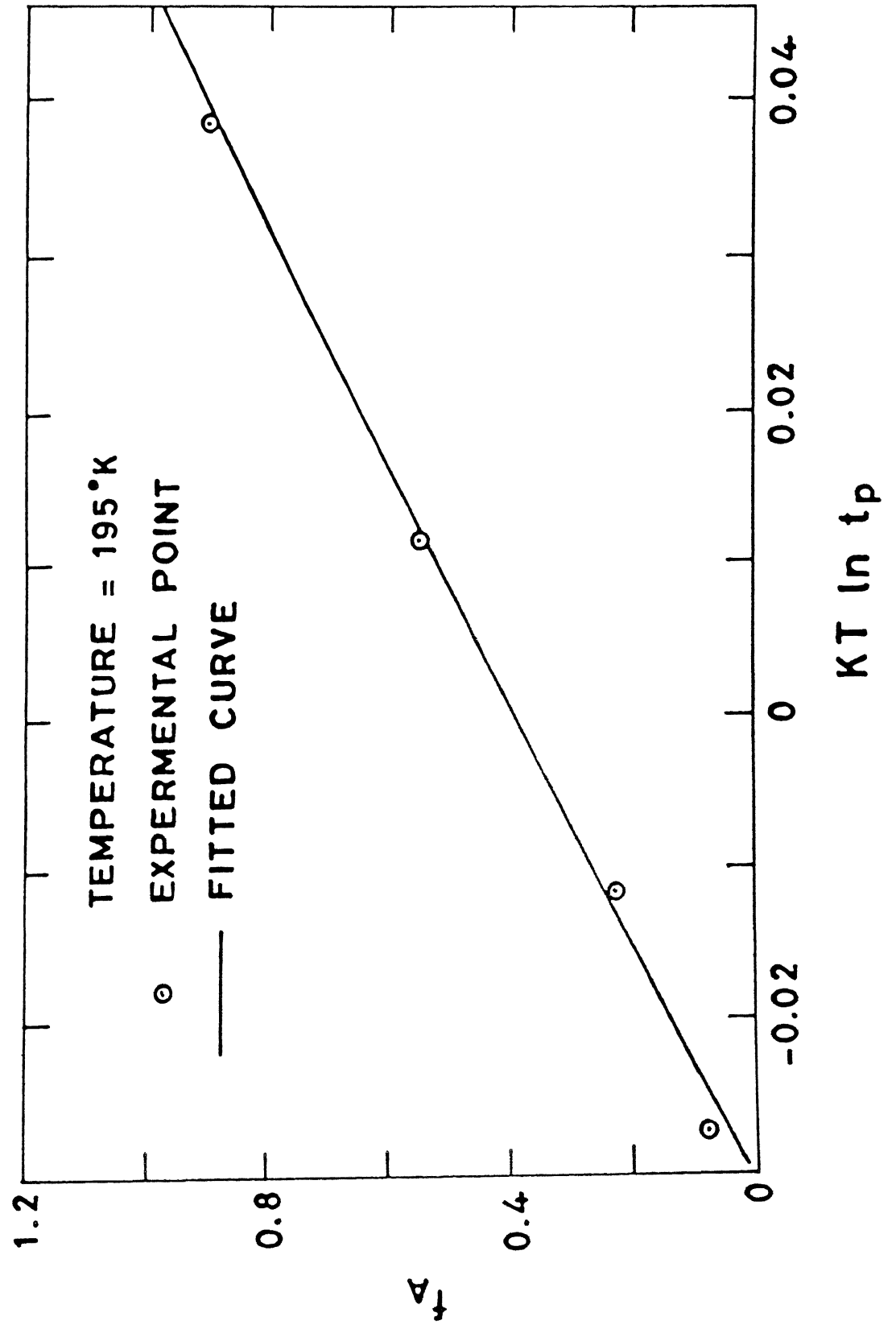
TEMPERATURE = 195°K
EXPERMENTAL POINT
FITTED CURVE
1.2
0.8
0.4
0
f_A
-0.02
0
0.02
0.04
KT ln t_p

CHAPTER 7 : CONCLUSION

In this thesis we have focussed on two issues involving disordered semiconductors. These are: (i) the presence of a gap level due to a point defect in a disordered medium and (ii) the effect of disorder on the analysis of experiments on the basis of expressions valid and derived for the ordered case, as is the usual practice.

In chapter 1 we have laid down the broad conceptual framework in which the thesis work was carried out. The Coherent Potential Approximation[1] (CPA) was described using a few well chosen examples[2]. The Koster-Slater[3] approach to a gap level was illustrated with a toy model for a semiconductor.

The problem of predicting a gap level in an alloy semiconductor may be partitioned as follows: (i) Determining the electronic structure of the host which is substitutionally disordered. The sophisticated CPA was employed to achieve this objective. (ii) Locating the gap level by recourse to a Koster-Slater equation. In chapter 2 we have illustrated the procedure with the single band model[4]. In chapter 3 we first develop the CPA formalism for a realistic multiband semiconductor. We next detail the application of the Koster-Slater equation. We have shown analytically as well as numerically that the prediction of the trap level by CPA and the simplest mean field theory VCA (Virtual Crystal Approximation) are identical for the vacancy.

This suggests that a perturbation approach to strong defect potentials may be gainfully employed. We call this the Deep Level Approximation (DLA). We have pointed out that since the VCA is basically a weak scattering theory, it agrees with the CPA only in the domain of weak scattering.

We have then concentrated on an archetypical defect in $Ga_{1-x}Al_xAs$: the DX center[5]. This has been widely discussed on account of its puzzling physical and chemical properties. We have reviewed some of its salient features. It is believed to be a donor related level in the alloy $Ga_{1-x}Al_xAs$. The shallow to deep instability of this particular defect when the Al concentration is increased beyond 20% led us to view the level as a simple donor which gets deepened due to disorder in the environment. We have self consistently accounted for disorder using CPA[6]. Our results for a simple substitutional donor in the disordered environment of $Ga_{1-x}Al_xAs$ agree well with the Hall effect measurements. The general trend of the level with the Al concentration 'x' also compares well with the experimental value. We have calculated the defect level for most of the group IV and group VI donors and have compared the theoretical values with those obtained from the experiments. Furthermore, our calculations reveal that the defect possesses an a_1 symmetry, which explains the phenomenon of persistent photoconductivity (ppc) associated with this defect.

The DX center has been identified in pure GaAs under pressures exceeding 20 kbar. We conjecture that when pressure is applied to a system, it results in a distortion of the lattice.

This is then the case of positional disorder. Thus, deepening of the level due to pressure can once again be attributed to disorder. This conjecture however needs to be explored. A cluster type calculation may be gainfully applied to this end.

The EPR invisibility of the DX center has led some authors to conjecture that this defect is a negatively charged donor. We have explored this viewpoint using Effective Mass Theory for helium like impurities[7]. The results of our calculations do not rule out such a possibility.

We would like to conclude with the following remarks for the DX center. Our calculations[7] reveal that disorder can result in deepening a level. We have shown it specifically for simple donor levels in $Ga_{1-x}Al_xAs$. The negatively charged donor, which explains EPR invisibility is not ruled out by an Effective Mass type approach. Similar effects of deepening of the level due to disorder in the host environment can be observed on negatively charged donors also. However, a firm statement in favour of the band model for the DX center cannot be made. This is because the cavity radius remains an empirical parameter in our EMT calculations. A simple self consistent procedure to delineate the dielectric screening $\epsilon(r)$ needs to be introduced. Further, the presence of slight lattice distortion can also explain the phenomenon of divergent optical and thermal activation energies.

The Effective Mass formalism for a helium like impurity has been extended to several other problems[7]. We have studied the chalcogen impurities in silicon, the anti-site defect in GaAs

(which is currently viewed as a popular model for the EL2 center in this semiconductor). Our results are in good agreement with the experimental values.

Finally, in chapter 6 we have concentrated on the analysis of some experiments. We have demonstrated analytically that a non exponential decay in a capacitance transient could be an experimental signature for a broadened gap level. We have further shown that in the conventional analysis of some experiments like DLTS and PATS, the expression employed have been derived for a sharp level. This results in an overestimation of the activation energy for severely broadened levels[8-10]. This may result in a systematic discrepancy between DLTS, PATS and other experimental probes. It could also result in serious disagreements between experiment and theory.

We would like to conclude that an attempt must be made to go beyond the Koster-Slater paradigm. Since several centers in the alloy semiconductors are metastable, total energy calculations are warranted. We have taken a step in this direction in chapter 2, where we use the Hellmann-Feynman theorem to calculate the total electronic energy for a single band tight binding Hamiltonian[4].

On the other hand an attempt ought to be made to go beyond the mean field descriptions of the disordered host. The Coherent Potential Approximation is a powerful approach. But localization effects are largely washed out by it. It would be a moot point to explore the interaction of a 'localized' defect wave function with the host eigenfunctions which are not extended Bloch states but are Anderson[11] localized.

REFERENCES

1. P.Soven, Phys. Rev. 156 809 (1967).

2. "Simple Illustrations of the Coherent Potential Approximation" Amita Das and Vijay A.Singh, Submitted Am.J.Phys (1990).

3. G.J.Koster and J.C.Slater, Phys. Rev.95 1167 (1954).

4. "Electronic Structure of Defects in the Alloy Semiconductors: The Weak Scattering Approximation". Amita Das, Kajoli Banerjee and Vijay A.Singh, Submitted J.Phys.: Condens. Matter (1990).

5. D.V.Lang, R.A.Logan and M.Jaros, Phys. Rev. B19 1015 (1979).

6. "DX Center: A Coherent Potential Approximation Based Approach". Amita Das and Vijay A.Singh, Submitted Phys. Rev. B (1990).

7. "Many Electron Effects in the Effective Mass Theory for Helium like Impurities". Amita Das and Vijay A.Singh, Submitted J.Appl. Phys. (1990).

8. "Paired Temperature Spectroscopy: A Novel Method to Characterize Traps in Semiconductors". Raj.K.Singh, Vijay A.Singh, James W.Corbett and Amita Das, J.Phys.C: Solid State Phys. 19 2177-2187 (1986).

9. "Deep Level Transient Spectroscopy (DLTS) Analysis of Defect Levels in Semiconductor Alloys". Amita Das, Vijay A.Singh and D.V.Lang, Semicond. Sci. Technol 3 1177-1183 (1988).

10. "Transient Spectroscopy and Disorder". Vijay A.Singh and Amita Das, Radiation Effects (1989).

11. P.W.Anderson, Phys.Rev.109, 1492 (1958).